Responses to the referees and changes to the manuscript

We wish to thank all three referees for their helpful and constructive reviews, which have greatly improved the ms. Below please find our responses to all of your points. The track-changes (latexdiff) version of the ms follows at the end of this pdf.

David Talmy

Thank you very much for your very positive and constructive review! Below please find our responses to all of your points. We think the changes have improved the ms and hope that it is now satisfactory.

Main points

Overall, the manuscript is extremely carefully prepared and quite straightforward to interpret. I haven't downloaded and used the code but they have provided access to online repositories and instructions for reproduction of the output. The model assumptions are firmly rooted in prior works. I anticipate this will be a useful tool for future investigations of marine ecosystem properties and the coupling with climate. I have a few queries regarding the solutions. Since this journal is focused on model development rather than specific modeling outcomes, I don't necessarily regard possible shortcomings as a barrier to publication. It might be nice, however, for the authors to respond to these major issues, clarifying whether they intend to investigate these issues here or in subsequent publications:

Reply: Thank you very much for this positive assessment.

1. *Phytoplankton biomass in the gyres seems a little high. This is most evident in Fig 9 comparing MODIS inferred Chl with model output. There are a few conspicuous patches especially in the South Pacific, which are clearly absent in the MODIS data. The patches in the south pacific look to me like they might be numerical artefacts. Can the authors comment on this? It sort of gets brushed over. There is more focus on the comparison of model vs. CbPM NPP (Fig 10). I'm not an expert on the CbPM but my understanding is that there is relatively low uncertainty on chl relative to carbon when inferred from satellites. Given the rather high estimates of global NPP in this study, it might be nice to be extremely clear about situations when the model over-estimates satellite inferred Chl, before moving on to other comparisons.*

Reply: It is not really clear to us which patches you refer to. The only numerical artefact in this area is the occurrence of negative Chl concentrations in a few grid cells in the original UVic. The band-like structures in the South Pacific probably result from the combination of UVic's ocean circulation pattern in this area and strong gradients in Fe supply from the atmosphere. The overestimated surface nitrate concentrations in the South Pacific gyre (Fig. 4) also point towards a problem in UVic's circulation, bringing too much nitrate to the surface. Nevertheless, we are very grateful for this comment, which has prompted use to re-evaluate the models' performance in terms of biomass and NPP. We now discuss more extensively the deficiencies in predicted Chl, biomass, and NPP. In the Abstract, we have added the sentence (p. 1, lines 16–18): "*The similarity in the overestimation of NPP and surface autotrophic POC could indicate deficiencies in the representation of top-down control or nutrient supply to the surface ocean.*" In the main text, we have

expanded the discussion of this topic on p. 16, lines 274–277, pp. 16–17, lines 285–297, and, p. 27, lines 458–461. We also show the overestimation of phytoplankton biomass in the new Fig. 11. Phytoplankton biomass is overestimated basically in proportion to NPP, as you can see in the comparison of NPP and surface autotrophic POC in Figs. 10 and 11. Thus, the model overestimates biomass not as severely as Chl. We attribute most of the overestimation of surface Chl to the occurrence of deep chlorophyll maxima (DCM) in oligotrophic areas, which the satellites cannot see and which the UVic model cannot resolve well. Since the surface layer of the UVic grid is 50 m thick, a DCM developing there is immediately spread throughout the surface layer, which might also partly explain the high NPP as mentioned below. We explain this now on pp. 13–15, lines 255–263. In addition, the similarity in the patterns of NPP and surface POC seems to indicate that the growth of primary producers might be relatively well represented, from which we conclude that improved formulations on top-down control may also be a promising avenue for future model development. We think these changes have improved the manuscript and hope that it is now satisfactory in this respect.

2. *I may have missed this, but I don't quite understand what aspect of the non-N fixing diazotrophs sets them apart from regular algae, from a trait perspective? Is it their high N:P ratio? Given that the high N:P of these groups appears to introduce artefacts in N*, is it really necessary to include this, instead of a functional representing, say, haptophytes? Apologies if I missed something very obvious here.*

Reply: The non-N_2 fixing diazotrophs in our model do indeed represent "*regular algae*", just with higher subsistence quotas and light affinity, and a lower nutrient affinity than the other (ordinary) phytoplankton group. The point here is that we have implemented facultative diazotrophs as one group of state variables (C, N, P) but they seem to represent two functional types: one diazotrophic and one non-diazotrophic type. As we discuss on p. 23, lines 377–386, the non-N_2 fixing diazotrophs in the Arctic probably do not provide a good representation of the phytoplankton community there. Adding another phytoplankton group is of course possible but not within the scope of our present study.

3. *Regarding the rather high C:N of detritus. I usually try to avoid doing this, but I wrote a paper on exactly this topic back in 2016 (Talmy et al., 2016). It looks like the mismatch in phyto and zoo C:N is largely being excreted directly into the detrital pool. Our conclusion with a model of microzooplankton respiration, was that much of the C may in fact be respired. This is a simple explanation for the overestimation of carbon in detrital pools.*

Reply: While that would be a simple explanation indeed, it does not apply here, as, according to Eq. (C15) for R^{C}_{zoo}, all the excess C is, in fact, respired. We are very sorry about the wrong explanation of the role of zooplankton with respect to the high detritus C:N:P on p. 22, lines 370–373 of the original manuscript, which referred to an earlier configuration of the model. We have corrected these statements (now on p. 25, lines 421–424). We have also added the statement (p. 8, lines 157–158): "*For example, all the excess ingested C is respired (see Eq. C15 in Appendix C2), as also suggested by Talmy et al. (2016).*" The higher-than-Redfield C:N of detritus in our model is due instead to the relatively high C:N of the phytoplankton. Also, please note that the detritus contribution to total POC in the surface layer of our model is relatively small, less than 10 % on average, with a range between 2.5 and 17 %. Please also note that there was a mistake in the left part of Eq. (C14) for E_{zoo}, which is now corrected.

Specific comments

Line 135 and Fig 2: *I got a bit confused here. The figure shows three temp responses but there are only two models. I get that the defining characteristic of OPEM-H is the contrasting temp response for N2 fixation. I just wonder if the fig. can be changed to more clearly group OPEM-H temp responses, e.g. with dashed lines, and by grouping them with an OPEM-H flag in the legend?*

Reply: Thanks for the suggestion. We have amended the figure and its caption and hope that it is clear now.

Line 146: *Take 'B18' out of parentheses?*

Reply: Done, now C18 on p. 8, line 142.

Line 165: *surely grazing is a form of mortality. Can you say 'background' mortality, or 'closure', or similar..? Also, might be nice to add a word or two on the quadratic closure*

Reply: Yes, we agree and have amended the statement on p. 8, lines 167–168 to read "*The background mortality is a quadratic closure term intended to represent losses due to viruses, predation by higher trophic levels, etc.*"

Line 178: *"C:N = 6.625 molC molN-1, as 1.45-2/6.625 = 1.15 mol O2 mol C-1." Apologies but I'm missing the reasoning for the 1.45–2/6.625. Can you add a word or two to explain?*

Reply: We have amended the text on p. 9, lines 176–180 and hope that it is clear now.

Line 179: *"Increases with depth" Why does sinking speed of detritus increase with depth? I understand this was reported elsewhere. Just might help to add a sentence or two about what underlies this physically / biologically.*

Reply: We have added the explanation that this reflects the disappearance of smaller particles during sinking (p. 9, lines 181–182): "*Detritus sinking speed v_{sink} increases with depth, reflecting the gradual disappearance of smaller particles during sinking, . . .*"

Line 187–188: *"400 parameter sets" I understand that the calibration was reported in the companion paper. Might help with the flow to give a little explanation. At least that the Latin Hypercube scheme was used. I had to look this up, but many readers will not.*

Reply: We now mention the Latin Hypercube method on p. 9, line 191.

Line 196–197: *"excess nitrate with respect to phosphate, termed N*" I thought the point of N* was to subtract out Redfield N:P, so that surpluses and deficits in N are evident. This wording feels a little off, perhaps rephrase?*

Reply: The difference between your formulation and ours is not entirely clear to us, but we have modified the wording to be closer to yours (p. 9, lines 201–202): ". . . *the Redfield N-equivalent of phosphate, termed* $N^* = NO_3^- - 16 \cdot PO_4^{3-} + 2.9\,\mathrm{mmol\,m^{-3}}$ . . . "

Line 238–239: *"require the combination of decoupled C, N, and P with a suitable parameter set" what is it about certain parameter sets that decouples C, N, and P? – this seems important*

Reply: The decoupling and the parameter set are two different things, sorry about the confusion. We have since learned that other models (without decoupled C:N:P) can also reproduce the direction of this gradient. We have clarified this statement (p. 13, lines 245–247) to read: "*Also, not all simulations in our OPEM and OPEM-H ensembles can reproduce this gradient, whereas other models without variable stoichiometry can (e.g., Kriest and Oschlies, 2015). Thus, reproducing the deep DIN:DIP distribution appears to require mostly a suitable model calibration.*"

Line 248: *why is your NPP so high? Apologies if I missed this. But perhaps it could be clarified more directly?*

Reply: We think that the high NPP results mostly from the high autotrophic POC estimate (see the new Fig. 11) in combination with enhanced nutrient supply due to the coarse vertical resolution. We have added an explanation on p. 16, lines 274–277.

Fig 13 and accompanying argument, specifically line 305 *"inverse relation between inorganic N:P and P". First, I find it really hard to grasp what is intended with Fig 13. There are a lot of data in the different panels and I find it hard to focus in on what's intended. Moreover, can the inverse relationship between N:P and P also be explained by preferential P remineralization? Given that the conclusion of this paragraph appears to be that "more investigation is warranted", and the main findings are somewhat obscure and difficult to grasp, I suggest either removing this figure or editing it / the accompanying text to make it clearer.*

Reply: We do not see how preferential P remineralisation could result in an inverse relation between DIN:DIP and DIP concentration, as this would just lower the DIN:DIP ratio irrespective of the actual concentrations. The inverse relation can be understood as the result of competition between coexisting diazotrophs and non-diazotrophs, however. We are sorry if this point was not sufficiently clear and have modified the paragraph on pp. 21–22, lines 339–352 to make it clearer.

Line 318: *"a higher values" check grammar*

Reply: Thanks, we have corrected it, now on p. 22, line 355.

Line 320: *"Phytoplankton is much more evenly distributed" in line with my comments above, the high phyto biomass in the gyres feels inconsistent with satellite estimates, and also frankly with our basic understanding of plankton biogeography.*

Reply: The distributions of Chl and autotrophic biomass (C) are very different in OPEM and OPEM-H, owing to the high variability in the Chl:C ratio (see Fig. 9 and the new Fig. 11). We have clarified this also on p. 22, lines 357–358: "*Phytoplankton biomass (not Chl, see Fig. 9) is much more evenly distributed and the integrated biomass is about 2.3 times as large as in the original UVic model.*"

Line 334: *"non-N2 fixing species adapted to low light and long periods of darkness" As per my main points above, surely this could apply to many phytos, why do they need to be diazotrophs?*

Reply: They are not diazotrophs (non-N_2 fixing species), as also explained above.

Line 375–378: *"The relatively low assimilation efficiencies…". I can't make sense of this sentence. Consider clarifying.*

Reply: We have clarified the sentence now, also explaining the relation between assimilation efficiency and ingestion (p. 25, lines 427–429): "*The relatively low assimilation efficiencies in the Arctic between 90°E and 120°W in OPEM-H compared to OPEM in Fig. 17 result from the availability of food, as OPEM-H is the only simulation with any appreciable NPP (Fig. 10) and hence biomass in this region (Fig. 15), and E_{zoo} is inversely related to ingestion in OPEM and OPEM-H.*"

Emily Zakem

Thank you very much for your helpful and constructive review! Below please find our responses to all of your points. We think the changes have improved the ms and hope that it is now satisfactory.

General comments

1. *Temperature function*

   Since this is a model development journal, the temperature implementation could be clarified in section 2.1 and in the abstract. In Fig. 2, the y axis label and the first sentence of the caption indicates that the plot shows the temperature function only for N2 fixation, but the rest of the caption and the in-text discussion (lines 135–139) suggests a different configuration. My take-away understanding is:

   a. *Original UVic: All diazotrophic rates (uptake, growth, and N2 fixation) are multiplied by a factor of 0 at 15C and a factor of 2 at 30C.*

   b. OPEM: same

   c. *OPEM-H: The Eppley curve is used for uptake and growth for diazotrophs as well as ordinary phytoplankton. The Houlton curve is used for N2 fixation alone.*

   Is this correct? If so, what is the temperature function for ordinary phytoplankton in UVic and OPEM? Did that also change between OPEM and OPEM-H, so that ordinary phytoplankton metabolic rates are also higher at lower temperatures and lower at higher temperatures?

Reply: Yes, this is correct. The temperature function for ordinary phytoplankton in OPEM is the Eppley curve, i.e., it is unchanged from the original Uvic, but since the maximum, temperature-dependent rates are multiplied with 0.4 for diazotrophs in the original UVic only, they remain below those of ordinary phytoplankton throughout the temperature range shown in Fig. 2 in the original UVic. We explain this now in the caption of the modified Fig. 2 and on p. 7, lines 129–135

2. *Denitrification and cost function*

   Could the global water column denitrification rates for the three models be summarized somewhere? They are referred to multiple times. A realistic denitrification rate effectively served as a second cost function for assessing the simulations, in addition to the cost function itself (l. 190). Since denitrification rates are stated to be lower in OPEM and OPEM-H (l. 231), this implies that the cost function was also different. How did denitrification weigh against the actual cost function? With effectively two cost functions to minimize in this way, how does this result in an objective determination of one parameter set? Since the same optimized parameter set emerged for both OPEM and OPEM-H, does that mean that they have the same denitrification rate? Did the geography of denitrification change (the OMZs themselves or the anoxic portions of them), or was it just lower everywhere? It would be helpful for the interpretation of the results to have a bit more information about denitrification.

Reply: Since we have run the models into steady state, the global (water-column) denitrification rates are the same as the global rates of N_2 fixation, which are summarised in the caption of Fig. 13. We have now added the distribution of denitrification to Fig. 13 (bottom 3 panels) and explicitly mention in the caption that, in each of the spun-up steady-state simulations, global denitrification is the same as global N_2 fixation. The total rates differ slightly between OPEM and OPEM-H because of the different temperature dependencies of diazotrophy (p. 20, lines 329–330).

We did not include denitrification in the cost function, precisely because we could not find a way to do this in an objective manner. Instead, we applied a minimally-required global denitrification of 60 Tg N year^{-1}, which is the lower end of the plausible range for water-column denitrification estimated by DeVries et al. (2012), as a threshold and excluded all simulations with less denitrification from the selection of the reference simulations (trade-off solutions in Part II, Chien et al., 2020). We have modified the description in the ms, now stating explicitly (on p. 9, lines 193–195) that the reference simulations were selected "*... according to two objectives: (1) We minimise a cost function under the condition that (2) we obtain realistic levels of global water-column denitrification, i.e. at least* 60 Tg N yr^{-1} *(DeVries et al., 2012). Thus, no weighting had to be applied to our objectives.*" For a detailed description of this topic, please refer to Part II (Chien et al., 2020).

3. *Discussion of the new grazing model?*

The results and discussion are nearly exclusively focused on the variable stoichiometry of the phytoplankton and its effects. Yet the model also includes a new grazing parameterization: the optimal current feeding model. As a suggestion (within the authors' discretion), it would be more comprehensive to at least include a few sentences evaluating the impacts of this portion of the implementation on the simulations. Perhaps the discussion of the coexistence of ordinary phytoplankton with the non-N2 fixing diazotrophs (l. 335–338) or the presentation of the more evenly distributed phytoplankton biomass would be good segues for this.

Reply: Thank you for this comment. We agree that the new zooplankton formulation has not been discussed in sufficient detail. We have now added comparisons of autotrophic and total food availability relative to the zooplankton feeding threshold in the new Fig. 11 and Fig. 17, and discuss these on p. 17, lines 288–297 and p. 25, lines 424–430. However, in our view the coexistence of ordinary and diazotrophic phytoplankton follows directly from the optimality-based formulation of phytoplankton and diazotrophy in OPEM because autotrophic POC is well above the feeding threshold in the regions of coexistence and hence the feeding threshold could not prevent extinction of a weak competitor there.

Specific comments

l. 94–95: *To what degree is the tracer not conserved as a result of these schemes?*

Reply: These schemes only reduce fluxes between neighbouring cells, so that tracer conservation is not affected. We have added the statement (p. 28, line 516): "*This flux limitation does not affect tracer conservation.*"

l. 76–99: *These paragraphs include quite technical detail about how to deal with negative concentrations in the model. For readability purposes, it would be more engaging to have the model descriptions first (starting with section 2.1), and move these two paragraphs either to after 2.3, with their own section heading, or (better yet) even moving them into Appendix A. In either case, it would also be helpful to address why it is that negative concentrations are "one of the main problems for implementing variable stoichiometry" (l. 76).*

Reply: Thank you, we agree that the appendix is a much better place for this. The main reason why OPEM is much more affected by negative concentrations is that it creates steeper vertical gradients close to the ocean surface. We explain this now in the new Appendix B on pp. 28–29, lines 493–520, where we have moved these two paragraphs.

l. 136: *"the same temperature dependence (Eppley, 1972)" – does this mean the same as in OPEM? Or just that it is the same for both ordinary phytoplankton and diazotrophic uptake and growth?*

Reply: We intended to say the latter and have clarified this now in the caption of Fig. 2 and on p. 7, lines 129–135.

l. 157–158: *"mostly in dissolved form (as inorganic nutrients)". This is consistent with Chi in Table 1 described as "dissolved N, P loss". However, Chi then shows up in Eqn. 6 as a source for sinking detritus. Could the fate of Chi be clarified? It would also be helpful to describe Chi in words after it is introduced in Eqn. 6.*

Reply: We are sorry for this mistake and thank you for spotting it. R^n_{zoo} is dissolved (respiration, excretion) loss and X^n_{zoo} particulate egestion. We have corrected this in Table 1.

l. 238: *"reproducing the deep DIN:DIP distribution appears to require . . . a suitable parameter set". Could you qualify what is suitable? Any information about what parameter space works better than another?*

Reply: After submitting the ms, we have learned that other models without variable stoichiometry can also reproduce these deep N:P gradients. Thus, this ability may be more related to the model calibration than the decoupling of C, N, P. We have changed this statement now on p. 13, lines 245–247: "*Thus, reproducing the deep DIN:DIP distribution appears to require mostly a suitable model calibration.*"

l. 231: *Since C export is the same, N export must be lower. Could the lower O2 consumption from lower rates of nitrification partially explain the lower denitrification?*

Reply: As shown in the three new panels at the bottom of Fig. 13, denitrification in the Indian Ocean occurs only in the original UVic, where C export is in fact lower in OPEM than in the original UVic (Fig. 12), which we see as the main reason for this difference. We have clarified this now on p. 12, lines 239–241: "*. . . the C:N ratio, which determines the O_2 demand for the remineralisation of sinking detritus, remains above the original UVic value of* 6.625 mol C (mol N)$^{-1}$. *Rather, the lack of denitrification in the Indian Ocean in OPEM and OPEM-H (Fig. 13 bottom) appears to result simply from the reduced C export in this area compared to the original UVic (Fig. 12).*"

l. 235–240: *The fact that only OPEM-H is able to capture the Pac vs. Atl basin differences in N* seems key, if this is separate from the gradient within the Atl. Could this be emphasized and explained?*

Reply: We are not sure this is the case. We refer to the deep-water formation region in the northern North Atlantic here, where N* is higher in OPEM-H than in OPEM, but still lower than in the original UVic. The surface N* in all other parts of the Atlantic is more a consequence than a cause of the deep-ocean nutrient distributions, and this applies also to the Pacific Ocean. We have added a corresponding statement on p. 13, lines 249–250: "*We interpret the surface N* distribution outside the deep-water formation regions as a consequence, rather than a cause the of deep-ocean nutrient distributions, however.*"

l. 248 and on: *If NPP is $\sim 2\times$ as high, and the export is the same, why is the export efficiency so much lower?*

Reply: We think that the low export efficiency, which we calculate as the ratio of net community production (NCP) over NPP, is actually a consequence of the release of the excess C as CO_2 by the zooplankton in the surface layer of the UVic grid, as it removes this C from the particulate pools, and hence reduces NCP in the UVic model. We have added a paragraph describing this on p. 24, lines 408–420.

l. 256: *Perhaps somehow the much higher NPP is simply evidence that the optimized growth is indeed optimizing the pp growth in the model, and so the well-matched UVic estimate might be close to the observations for the wrong reason?*

Reply: Yes, this is indeed our view.

l. 290: *"a wider geographical range" in OPEM-H. Does the fact that the temperature function is lower at higher temperatures have any impact?*

Reply: From Fig. 13 it is clear that the distribution of N_2 fixation in OPEM and OPEM-H is very similar, so the effect of the lower temperature function at higher temperatures in OPEM-H must be rather small. Nevertheless, we think that it could well explain the slightly lower global estimate in OPEM-H compared to OPEM, as explained now on p. 20, lines 328–330: "*The effect of the lower temperature function of Houlton et al. (2008) compered to the UVic temperature function for diazotrophs at high temperatures appears to be rather small, but may be the main reason for the slightly lower global N_2 fixation in OPEM-H compared to OPEM.*"

l. 317–318: *Does the higher kFe for diazotrophy impact its resulting biogeography?*

Reply: We are sorry, but we cannot answer this question satisfactorily. While this parameter clearly affects diazotrophy, so do most of the other parameters of biotic processes (see Fig. 1 of Part II). An analysis of the effects of individual parameters on the biogeography of diazotrophy is beyond the scope of our study.

l. 335–338: *Could top-down control also play a role in supporting the non-N2 fixing "diazotrophs", suppressing the ordinary phytoplankton?*

Reply: We consider this rather unlikely because the food preference for diazotrophs is almost twice that for ordinary phytoplankton. See the modified statement on p. 23, lines 365–367: "*The main reason why the facultative diazotrophs can populate the high latitudes in OPEM-H is their higher α (0.5 compared to 0.4 m^2 mol C W^{-1} (g Chl)$^{-1}$ d^{-1} for ordinary phytoplankton), which can overwhelm the effect of the much higher food preference for diazotrophs (compare ϕ_{dia} and ϕ_{phy}, Table 2) under light-limited conditions.*"

l. 350 and Table 3 caption: *Do you mean the average of the log-transformed values? Then write as the "log-average" or the geometric mean (not "log-normally averaged"). Also, by particulate, do you mean both the biomass and the sinking detritus?*

Reply: We have changed "*log-normally averaged*" to "*log-averaged*" throughout the ms. Indeed, particulate refers to all particulate tracers, i.e., phytoplankton, diazotrophs, zooplankton, and detritus. We have clarified this now on p. 23, line 388.

l. 364–370: *Is it appropriate to have the matching of the model with data as a goal when preferential remineralization is not included? (I.e. Letscher and Moore 2015 as you've already cited). Perhaps discussion could be tweaked to acknowledge that only part of the story is included. Also, Talmy et al 2016 GBC showed that zooplankton respiring the extra C, rather than returning it in organic form, might be more mechanistic and would have the effect of dampening the non-living surface ratios.*

Reply: Preferential remineralisation is obviously not the only process missing in the UVic versions considered in this study, benthic denitrification being the one most prominently described in the ms. So, while we agree that only part of the story is included, we think that we always have to aim for calibration of any (necessarily imperfect) model before we can learn from the remaining model-data differences. We stated this in the Abstract as (p. 1, lines 13–14) "*Deficiencies of our calibrated OPEM configurations may serve as a magnifying glass for shortcomings in global biogeochemical models and hence guide future model development.*" Comparison with data is the only technique known to us for doing this kind of analysis, however, so it is unclear to us what the alternative could be. As we also write in our response to reviewer David Talmy, zooplankton do in fact respire all the extra C in their food (see Eq. C15), so that it does not contribute to the organic pools. We apologise for the misleading explanation on p. 22, lines 370–373 of the original manuscript, which has been corrected (now on p. 25, lines 421–424). We state now also more clearly on p. 8, lines 157–158 that "*. . . all the excess ingested C is respired . . .* " In fact, this may, as explained above, largely explain the relatively low export efficiency in OPEM and OPEM-H.

Fig. 15: *The two captions should be one caption that is the same for both plots.*

Reply: Fig. 15 (now Fig. 16) has only one caption, but you are probably referring to the legend, which we had spread across the two panels for better readability. We have now reformatted the legend and placed it in the right panel.

Anonymous referee #3

In this manuscript, the authors take as a reference an existing global biogechemical model, which they improve in several ways (e.g. better parametrizations, different phytoplankton temperature response curves. . .). One of the main focus is to move from fixed to flexible phytoplankton stoichiometry (C:N:P), as well as the implementation of optimal phytoplankton nutrient uptake and zooplankton grazing. The manuscript is devoted to comparing versions of the global model, with special emphasis on reproducing key patterns for N and P, including patterns of nitrogen fixation.

The manuscript is overall well written, and most of the different components are understandable. Although I have some experience with global models, most of my expertise focuses on more localized microbial models and, in spite of this, I think I could understand most of the model explanation and results. Still, I think my comments below can help improve the accessibility of the manuscript to a broader modeler audience.

Reply: Thank you for this overall positive assessment.

1. *In general, I got the feeling that the authors tried so many different versions of the UVic model (e.g. several parametrizations) that it is difficult to trace back why the improved OPEM models show the behavior they show. Also, the authors emphasize the move from fixed to flexible stoichiometry as the main selling point of their improvement, but they do alter and discuss other many aspects and for the same reasons it is difficult to understand what part of the observed behavior results from that improvement versus just a more suitable parametrization. The authors somehow touch on this same issue by the end of the manuscript, but I do not think they suggest any way to fix it. In models with so many moving pieces, I would have suggested choosing one single "best" UVic version/parametrization, and change one aspect at a time. I understand that given the rigidity of the model there won't be a single good parametrization that works globally, but then it may make sense to focus on the comparison of specific regions using the best version for each region. That would mean move from global to semi-regional maps, but at least it would be easier to identify which details of the OPEM models make a difference with the UVic model.*

Reply: We disagree with the statement that we compare "*many different versions of the UVic model.*" In fact, we compare exactly three versions of it, (1) the original UVic, (2) OPEM and (3) OPEM-H, whereby OPEM and OPEM-H differ only in one aspect, namely the temperature dependence of diazotrophs. We have clarified that we use this small set of model versions in the revised manuscript on p. 3, lines 75–80.

The emphasis on variable stoichiometry has also been mentioned by the other referees. We did not introduce variable stoichiometry merely for its own sake, however. Rather, our main motivation was the introduction of realistic organism behaviour, in the sense that it reflects observed behaviour in the lab, into an Earth system model, and variable stoichiometry of primary producers is only one aspect of the mechanistic foundation of OPEM, which also encompasses an improved description of zooplankton behaviour. The only other changed aspect of the model, aside from bug fixes, is the prevention of negative concentrations, which turned out to be a precondition for stable simulations with OPEM and OPEM-H. It was simply not possible to implement and calibrate OPEM without preventing negative concentrations, as we explain now in the new Appendix B on p. 28, lines 494–498 and p. 28, lines 506–510. We do indeed consider OPEM-H a more suitable parametrisation than OPEM but we do not understand the statement "*what part of the observed*

behavior results from that improvement versus just a more suitable parametrization."

It is not clear to us what "*so many moving pieces*" refers to, as we see only two: OPEM and the temperature dependence of diazotrophs, so we think that we did, in fact, change only one aspect at a time. Indeed, we view this strategy as a prerequisite for a meaningful comparison of the three model versions. The parameters of OPEM had to be calibrated as described in Part II (Chien et al., 2020), and also outlined in Section 2.4, because most of them have a very different meaning to those of the original UVic.

Regarding the regional behaviour, we do present a regional model sensitivity analysis for 17 biomes in our Part II (see its Fig. 9 and associated discussion there). However, the resolution of the UVic grid is in our view not suitable for a dedicated regional analysis, which we thus consider very much beyond the scope of our study.

2. *I found Fig1, which is supposed to schematically show how the OPEM model works, quite uninformative. It describes the links between the different components of an improved NPZD model, but I don't see any detail that makes it specific of the optimality model (other than the caption stating that some of those components are described with optimality functions). I think some additional panels describing how optimality works for those components would go a long way in convincing the reader that this is a significantly different version of the model of reference.*

Reply: Thank you. We agree that this figure was not informative enough and have amended it by adding panels illustrating the optimality-based phytoplankton and zooplankton formulations, as you suggested.

Actually, I think the authors could improve the justification as to why the optimality assumption is needed or is expected to describe the system more closely. Would other forms of variability play the same role? Would a non-optimal description of plasticity for uptake and grazing play the same role? Given the expected variability for planktonic organisms, why would them all follow an optimal strategy? And why would nutrient uptake follow an optimal strategy and not, e.g. temperature acclimation?

Reply: The optimality assumption is based on the expectation that evolution leads to optimally-adapted organisms. We attribute the ability of the optimality-based formulations underlying OPEM to describe the behaviour of a wide range of phytoplankton and zooplankton organisms for spatially and temporally varying environmental conditions, without increasing the number of parameters, to the appropriateness of this concept for modelling plankton organisms. While we do not want to repeat these arguments in depth in the current ms, we have added a corresponding statement and a reference to Smith et al. (2011) on p. 3, lines 57–60. We do not see any conflict between an optimal strategy and temperature acclimation. If sufficient observations were available on the process of temperature acclimation in several phytoplankton species, we believe that an optimal strategy for temperature acclimation could be developed.

And regarding the optimality description, why does the N-related maximum uptake go to zero when Q->Q0? Isn't that behavior exactly opposite to what has been re- ported experimentally (see e.g. S.Dyhrman's work or, from a theoretical point of view, F. Morel's work)? Why is there no flexible P-related maximum uptake (even though it's been shown experimentally that regulation of P transporters occurs)? And why is r_DIC multiplicative? All these are modeling choices and therefore need to be well justified and put in context.

Reply: The N-related maximum uptake does not go to zero but in fact approaches its maximum for $Q^{\mathrm{N}} \to Q_0^{\mathrm{N}}$ (see Pahlow et al., 2013). This follows directly from Eq. (C4), saying that f_{V} is maximal for $Q^{\mathrm{N}} = Q_0^{\mathrm{N}}$. It is not clear to us where this

misunderstanding originates. Eq. (C8) (right) does in fact describe a "*flexible P-related maximum uptake*" rate, denoted by V^{N}_{max} in the ms, as a function of the P cell quota (Q^{P}). As explained in Appendix C1.2, the r_{DIC} is needed to prevent outgrowing the P subsistence quota and that it is an arbitrary measure to stabilise the optimal growth model, i.e., the form of Eq. (C10) has no clear physiological interpretation. We have added an explanation of the two terms involved on p. 31, lines 573–575.

Finally, can the authors explain whether this (instantaneous) optimal acclimation entails any type of metabolic cost in the model?

Reply: The optimal acclimation is not instantaneous but drives the temporal evolution of the N and P cell quotas as defined and explained in Eqs. (1) to (3). The metabolic costs are defined as respiration losses in Eqs. (C1) and (C2) for phytoplankton and diazotrophs and in Eq. (C15) for zooplankton. We indicate these now also in the new panels B and C in Fig. 1.

3. *Although I understand this is a quite standard way to present the information, I find Figs4-12 not very helpful when it comes to assessing which model does a better job where. Unless there is a very obvious divergence with observations, it's difficult to see clearly which model works better at each region/feature. The authors mentioned a cost function to compare models (which I guess acts as indicators such as the AIC, and hopefully also takes into account the number of parameters). I think that maps that show instead the difference in that or another way to quantify closeness to the specific pattern they want to show would help hugely the discussion, because it'd be much easier to spot which model diverges less from observations and where.*

Reply: We agree that Figs. 4–12 do not show which model works better where compared to observations, but that is not the purpose of these figures. The model-data comparison is the subject of Part II. Here we just want to provide an overview of the behaviour of the three different model parameterisations (original UVic, OPEM, OPEM-H). This is all clearly stated in the last two sentences of the introduction (p. 3, lines 75–80). Please note also that we did not increase the number of tuneable parameters in OPEM and OPEM-H compared to the original UVic (p. 5, lines 105–109 and p. 8, lines 145–147).

4. *I would also suggest for the authors to state more clearly/emphasize what assumptions/parametrizations are based on published experimental observations, which ones in existing model results that have been validated, and which ones are just the result of observing that including them brings the model closer to general observations.*

Reply: We now state on p. 3, lines 64–65, that "*All of the new assumptions in OPEM are based on published experimental observations used to validate the optimality-based formulations.*" This is also clearly stated and explained in Sections 2.1 and 2.2 (with references to the Appendix). We did not introduce any assumptions for the sake of bringing the model closer to general observations. We present references for the ranges of all parameters involved in the calibration in Table 1 of Part II.

Also, I think it'd be also reassuring if the authors commented on whether some of the "moving pieces" introduced here (e.g. Vmax for nitrogen, gmax) remain within realistic ranges. I can envision several compensating factors leading to e.g. realistic overall uptake through highly unrealistic Vmax values. For example, gmax in the OPEM model is 4x the one reached with UVic, and the authors don't seem bothered about it because the overall total grazing remains under

acceptable levels, but it would be reassuring if the authors commented on whether such high gmax values are still within reasonable levels themselves.

Reply: $V_{\max}$ has an upper limit below the value of V_0^{N} (because it also depends on the P quota, see Eq. C8) at the reference temperature, which has been validated for a wide range of phytoplankton species in Pahlow et al. (2013), so we believe that it is realistic. Note that although $V_{\max}^{\mathrm{N}}$ has a clear physiological interpretation (the maximum uptake rate relative to the nutrient-uptake compartment), it would be very difficult to observe directly. Our calibrated value for $g_{\max}$ for OPEM and OPEM-H is well within the range of observations for several zooplankton groups as reported by Pahlow & Prowe (2010). Since the model calibration is the subject of Part II, we have added a corresponding statement there, on p. 4, lines 105–107, and references in its Table 1 (p. 5).

5. *Did the authors track how close each version of the model is to observations at particular times of the year (e.g. around blooms, winter…)? That exercise may help narrow down when and why one version works better than another for a particular feature.*

Reply: Yes, we did consider monthly and regional variability in the cost function, but as stated above, the model-data comparison and calibration are the subjects of Part II (Chien et al., 2020).

6. *I strongly recommend that the authors structure the subsections by key findings, i.e. introduce sub-subsections with titles that summarize the main finding. This would help/guide the reader to discern better what the main messages from each studied feature is. Although the individual subsections read well, the fact that a model does well in a particular region for a particular feature but not another, etc makes the flow a bit lost/erratic, and thus it is difficult to know what the take-home message for each section.*

Reply: We are sorry, but we do not understand this comment. We think that our section and subsection titles do exactly what you suggest here.

7. *Finally, given how large the potential for grazing gets, I think it'd be very interesting for the authors to comment on how other sources of top-down regulation that are not present (e.g. viruses, or even fish targeting grazers) would affect their results. After all, one of the main goals of the manuscript is to identify the deficiencies of this and similar models, and the lack of a realistic representation for such a key player in the microbial loop is one of the main shortcomings of current global models.*

Reply: Yes, we agree. We have added a corresponding statement on p. 8, lines 167–168: "*The background mortality is a quadratic closure term intended to represent losses due to viruses, predation by higher trophic levels, etc.*"

L50: *Plasticity has a very specific meaning for these organisms, and is not necessarily the same as variability (the latter can come from other sources and not only plasticity).*

Reply: We use the term plasticity to describe the variability of the cellular elemental stoichiometry and the allocation of cellular resources among competing requirements. We now explain this explicitly on pp. 2–3, lines 54–57: "*Plasticity here refers to the variability of elemental composition and allocation of resources among competing requirements for light harvesting and nutrient acquisition in phytoplankton and for foraging and digestion in zooplankton, implying variable*

Chl:C:N:P stoichiometry, half-saturation concentrations for nutrient uptake, and ability to fix nitrogen in phytoplankton, and zooplankton feeding thresholds and variable assimilation efficiency."

L86–99: *Please be explicit as to whether all these improvements are also implemented in the UVic reference version.*

Reply: We state now explicitly that the prevention of negative concentrations is applied only to OPEM on p. 28, lines 506–510: "*We have addressed the problem in OPEM by limiting the biological tracer fluxes of the sub-cycled biological time step at every grid box . . .* "

L119: *Has FTC been defined before in the text?*

Reply: No, we are sorry. FCT is explained now on p. 6, line 114

L122: *Just for PON and POP, right?*

Reply: Yes, as stated in Eq. (1).

Page 6: *I think "balance equation" is easier to understand (and more standard) than "sources-minus-sinks terms".*

Reply: We use "*sources-minus-sinks terms*" because that is the established term in Earth system models.

130–133: *Why is leakage not a nutrient-specific parameter/process?*

Reply: The leakage terms are not nutrient-specific because we do not have sufficient information from laboratory experiments which would allow us to justify different parameters for C, N, and P.

L137: *Replace "phy" and "dia" for their complete word.*

Reply: Yes, we do now, thank you.

L152: *A figure similar to Fig2 explaining how the optimal uptake/grazing terms differ from the ones used for the UVic model would be very illustrative.*

Reply: We agree, in principle, that this may be so. However, the nutrient uptake depends on the interaction of nutrient concentration and the current acclimation state (stoichiometry) of the cell, so it would need several figures, and the same problem applies to zooplankton grazing. Also, we would just repeat figures already published in Pahlow & Prowe (2010) and Pahlow et al. (2013). Therefore, we think that those interested in the details of the optimality-based formulations should refer to these references.

Table 2 (page 9): *Does the lack of values for the original model mean that the OPEM versions are incorporating 13 new parameters to describe zooplankton? If so, it should be noted in the main text (the same way it is discussed the fact that the phytoplankton improved component does not increase the number of parameters).*

Reply: No, the OPEM zooplankton has only two more parameters than the original UVic. The prey capture coefficients (ϕ) have a similar role as the food preferences in the original UVic, but because they have different units, the numbers cannot be compared directly. This is why we do not list values for the original UVic in Table 2. Also, please note that two of the zooplankton parameters in OPEM can be considered constant, so that the number of parameters to be calibrated is actually the same. We state this now explicitly on p. 8, lines 145–147.

L197: *I think N* should have been defined like this much earlier (the definition in the abstract is not as clear as this one).*

Reply: We provide only the mathematical definition in the abstract in order to keep the abstract short.

Eq.8: *It'd be good to translate each term into its ecological meaning as it's done with other equations, so the reader understands how NPP is exactly defined here.*

Reply: Yes, we do this now below Eq. (8), (p. 15, lines 266–269), thank you.

Optimality-Based Non-Redfield Plankton-Ecosystem Model (OPEM v1.0) in the UVic-ESCM 2.9. Part I: Implementation and Model Behaviour

Markus Pahlow[1], Chia-Te Chien[1], Lionel Alejandro Arteaga[2], and Andreas Oschlies[1]

[1]GEOMAR Helmholtz Centre for Ocean Research Kiel, Düsternbrooker Weg 20, 24105 Kiel, Germany
[2]Princeton University, Princeton, NJ, USA

Correspondence: M. Pahlow (mpahlow@geomar.de)

Abstract.

Uncertainties in projections of marine biogeochemistry from Earth system models (ESMs) are associated to a large degree with the imperfect representation of the marine plankton ecosystem, in particular the physiology of primary and secondary producers. Here we describe the implementation of an optimality-based plankton-ecosystem model (OPEM) version 1.0 with variable C:N:P stoichiometry in the University of Victoria ESM ~~(UVic)~~ (UVic, Eby et al., 2009; Weaver et al., 2001) and the behaviour of two calibrated reference configurations, which differ in the assumed temperature dependence of diazotrophs.

Predicted tracer distributions of oxygen and dissolved inorganic nutrients are similar to those of an earlier fixed-stoichiometry ~~model (Keller et al., 2012)~~formulation in UVic (Nickelsen et al., 2015). Compared to the classic fixed-stoichiometry UVic model, OPEM is closer to recent satellite-based estimates of net community production (NCP), despite overestimating net primary production (NPP), can better reproduce deep-ocean gradients in the NO_3^-:PO_4^{3-} ratio, and partially explains observed patterns of particulate C:N:P in the surface ocean. Allowing diazotrophs to grow (but not necessarily fix N_2) at similar temperatures as other phytoplankton results in a better representation of surface Chl and NPP in the Arctic and Antarctic Oceans.

Deficiencies of our calibrated OPEM configurations may serve as a magnifying glass for shortcomings in global biogeochemical models and hence guide future model development. The overestimation of NPP at low latitudes indicates the need for improved representations of temperature effects on biotic processes, as well as phytoplankton community composition, which may be represented by locally-varying parameters based on suitable trade-offs. The similarity in the overestimation of NPP and surface autotrophic POC could indicate deficiencies in the representation of top-down control or nutrient supply to the surface ocean. Discrepancies between observed and predicted vertical gradients in particulate C:N:P ratios suggest the need to include preferential P remineralisation, which could also benefit the representation of N_2 fixation. While OPEM yields a much improved distribution of surface N* ($NO_3^- - 16 \cdot PO_4^{3-} + 2.9\,\mathrm{mmol\,m^{-3}}$), it still fails to reproduce observed N* in the Arctic, possibly related to a mis-representation of the phytoplankton community there and the lack of benthic denitrification in the model. Coexisting ordinary and diazotrophic phytoplankton can exert strong control on N* in our simulations, which questions the interpretation of N* as reflecting the balance of N_2 fixation and denitrification.

Copyright statement.

1 Introduction

Earth system models (ESMs) are routinely used for simulating both the possible future development and the past of our climate system ~~(e.g. IPCC, 2013; Hülse et al., 2017; Keller et al., 2018; Park et al., 2019)~~ (e.g., IPCC, 2013; Hülse et al., 2017; Keller et al., 2018; Park et al., 2019). While different ESMs agree to some extent in their predictions, they usually also encompass a rather wide range, e.g., in the predicted temperature increase until the end of the current century (IPCC, 2013). Some predictions do not even agree in the sign of the projected changes, e.g., of marine net primary production, particularly in low latitudes, varying between −25 % and 40 % across current models (Laufkötter et al., 2015; see also Taucher and Oschlies, 2011). But even where many ESMs agree, their predictions are sometimes counter to observations, e.g., in the case of oceanic O_2 patterns and trends (Oschlies et al., 2017). These problems are likely rooted in uncertainties in parameter estimates (Löptien and Dietze, 2017) but also inherent model deficiencies, such as limited spatio-temporal resolution or inaccurate representation of physical and biotic processes (Keller et al., 2012; Getzlaff and Dietze, 2013).

In our view, a major limitation of the biogeochemical modules of current ESMs is that the formulations used to describe the plankton compartments are at odds with organism behaviour as observed in the laboratory. While the variability of the chlorophyll:carbon (Chl:C) ratio is considered in recent ESMs (e.g., Park et al., 2019), the carbon:nitrogen:phosphorus (C:N:P) stoichiometry of phytoplankton is ~~usually~~ still often represented by static (Redfield) ratios, entirely ignoring its highly variable nature (Klausmeier et al., 2008), which can affect model sensitivity to climate change (Kwiatkowski et al., 2018). The only model with variable C:N:P in phytoplankton in CMIP5 (Bopp et al., 2013) and CMIP6 (Arora et al., 2019) is PELAGOS (Vichi et al., 2007), which has no diazotrophs. Other models consider only variable N:P (TOPAZ2, Dunne et al., 2012) or C:P (MARBL (CESM2), Danabasoglu et al., 2020). The problem extends also to the representation of fundamental biotic processes, such as nutrient uptake or zooplankton foraging. For example, Smith et al. (2009) showed that the half-saturation concentration of nitrate use varies systematically with nitrate concentration and suggested that optimal uptake kinetics (Pahlow, 2005) may be more appropriate than the commonly-used Michaelis-Menten kinetics for simulating phytoplankton nutrient uptake. Zooplankton foraging behaviour can be characterized by a significant feeding threshold followed by a steep increase in ingestion (e.g., Kiørboe et al., 1985; Strom, 1991; Gismervik, 2005), which has also been demonstrated for a natural plankton community in the Sargasso Sea (Lessard and Murrell, 1998). This kind of feeding behaviour may be important for capturing the distribution of primary production in large ocean areas (Strom et al., 2000), but it is not represented by the Holling type II and III models (Holling and Buckingham, 1976) used in current biogeochemical models.

We have recently developed optimality-based formulations for phytoplankton and zooplankton (Pahlow and Prowe, 2010; Pahlow et al., 2013), which can describe observed plasticity of ~~organism composition and function, including phytoplankton~~ plankton organisms, yet are sufficiently simple for implementation in global biogeochemical models. Plasticity here refers to the variability of elemental composition and allocation of resources among competing requirements for light harvesting and

nutrient acquisition in phytoplankton and for foraging and digestion in zooplankton, implying variable Chl:C:N:P stoichiometry, ~~the~~ half-saturation concentrations for nutrient uptake, and ability to fix nitrogen in phytoplankton, and zooplankton feeding thresholds ~~, yet are sufficiently simple for implementation in global biogeochemical models~~and variable assimilation efficiency. The optimality concept is based on the "assumption that natural selection should tend to produce organisms optimally adapted to their environments" (Smith et al., 2011) which is particularly applicable to marine plankton, where intense mixing and the absence of physical boundaries ensure strong competition, and short generation times allow for rapid evolution. These formulations have shown their ability to describe ecosystem behaviour in 0D and 1D modelling studies (e.g., Fernández-Castro et al., 2016; Su et al., 2018), and to predict patterns of phytoplankton nutrient and light colimitation based on satellite and in situ observations (Arteaga et al., 2014). In this contribution, we describe the implementation of our new optimality-based plankton-ecosystem model (OPEM) into a global 3D ocean model component of an ESM of intermediate complexity. ~~The model~~ All of the new assumptions in OPEM are based on published experimental observations used to validate the optimality-based formulations. We view the implementation of OPEM as one step towards the ultimate goal of reconciling plankton-organism behaviour as observed in the laboratory with global marine biogeochemistry. Therefore, the variable stoichiometry of primary producers should be considered but one, albeit central, aspect of the mechanistic foundation of OPEM. The ESM employed is the University-of-Victoria Earth System Climate model (UVic in the following, Eby et al., 2009; Weaver et al., 2001). Owing to its coarse spatiotemporal resolution, UVic is a practical choice when working on long time scales (e.g., Niemeyer et al., 2017) and/or when many simulations are needed. Computational efficiency is also one of the main impediments to introducing more mechanistic formulations of biotic processes (Chen and Smith, 2018), as, e.g., the representation of variable C:N:P stoichiometry requires additional tracers, which must be mixed and advected as well. UVic has been used extensively with typical state-of-the-art fixed-stoichiometry NPZD (nutrients-phytoplankton-zooplankton-detritus)-type marine ecosystem and biogeochemistry models (e.g., Keller et al., 2012; Niemeyer et al., 2017; Oschlies et al., 2017). Here we compare the behaviour of the OPEM with that of a previous UVic configuration, described in Nickelsen et al. (2015), modified with several improvements and bug fixes as described below. An empirically founded temperature dependence of diazotrophy is introduced in a second configuration, OPEM-H, in order to distinguish between effects of the optimality-based physiological regulation and the temperature formulation. Since the calibration of ~~the OPEM~~ OPEM and OPEM-H embedded in UVic presents a major challenge, it is dealt with in ~~the companion paper (Chien et al., 2019)~~Part II (Chien et al., 2020).

2 Optimality-based plankton in the UVic model

The UVic model version 2.9 (Weaver et al., 2001; Eby et al., 2013) in the configuration of Nickelsen et al. (2015) with the isopycnal diffusivity modifications by Getzlaff and Dietze (2013), vertically increasing sinking velocity of detritus (Kriest, 2017), and several bug-fixes (some of which were already introduced by Kvale et al., 2017, see Appendix A for the new bug fixes applied here) is referred to as the original UVic in the following. We base our new configurations on this original UVic, except that we use constant half-saturation iron concentrations and omit the upper temperature limit in the zooplankton temperature dependence. For OPEM, we replace the formulations for phytoplankton, diazotrophs and zooplankton in the original UVic

model with an optimality-based model (Pahlow et al., 2013) for phytoplankton and diazotrophs, and the optimal current-feeding model (Pahlow and Prowe, 2010) for zooplankton (Fig. 1). Negative concentrations have always occurred in the UVic model, but they have usually been confined to small negative numbers in a few places. However, negative concentrations turned out to be a major problem for OPEM, which had to be dealt with in order to stabilise our optimality-based variable-stoichiometry implementation (see Appendix B).

One of the main problems for implementing variable stoichiometry in UVic's finite-difference code is the occurrence of negative concentrations in UVic, predominantly owing to its semi-implicit vertical mixing scheme (with smaller contributions arising from advection, the explicit isopycnal mixing scheme, and high-latitude filtering), as revealed by detailed inspection of the model's behaviour. Inside its biogeochemical module, UVic deals with negative concentrations by preventing, at every time step and in every grid box, any fluxes out of negative tracer compartments, although several bugs in the original code previously rendered this mechanism partly ineffective. UVic also applies a flux-corrected central-differencing scheme for tracer advection (flux-corrected transport, FCT, applied here also in the vertical) in order to prevent generation of negative concentrations. Negative concentrations are also generated in the main biogeochemical module of UVic (subroutine npzd_src), owing to the long time-steps (we use 0.5 times the physical time step of and, if this would generate negative tracer concentrations, subcycle with 0.25 times the physical time step) and the Euler scheme used for calculating the sources-minus-sinks terms.

For many cases (parameter settings), phytoplankton and/or diazotrophs can end up negative everywhere, compromising our calibration procedure, which depends on the reliability of simultaneous evaluation of simulation ensembles (see Section 2.4 below and Chien et al., 2019). We have addressed the problem by limiting the biological tracer fluxes of the sub-cycled biological time step at every grid box, so that not more than of any tracer is removed within any grid box during one time step. In order to counter the generation of negative concentrations by advection and vertical mixing, we also modify the physical transport of all particulate tracers and dissolved iron as follows: The sources-minus-sinks terms of the biogeochemical module are applied before calculating advective and diffusive fluxes, so that diffusion is the only remaining source of negative concentrations. In all cases where the sum of all diffusive fluxes ($\mathcal{D}$) would remove more of a tracer than is present in a grid cell after applying advective fluxes ($\mathcal{T}$), we calculate a correction factor, $f_D = -\mathcal{T}/(\mathcal{D} \times \Delta t)$, where Δt is the time step, which is then multiplied with all outward diffusive fluxes to ensure a non-negative tracer concentration. Since limiting the flux out of one grid cell reduces the flux into the neighbouring cell, this procedure is applied recursively until non-negative concentrations are guaranteed everywhere. Whenever high-latitude filtering (Kvale et al., 2017) results in negative concentrations, we multiply positive changes $\Delta\mathcal{T}^+$ by a factor $f_{\text{filt}} = \sum_{\mathcal{T}_{\text{filt}}<0.1\mathcal{T}}(0.1\mathcal{T} - \mathcal{T}_{\text{filt}})/\sum\Delta\mathcal{T}^+$ and hence allow filtering-induced reductions by at most , where $\mathcal{T}_{\text{filt}}$ is the (possibly negative) result of the high-latitude filter.

2.1 Phytoplankton and diazotrophs

Ordinary and diazotrophic phytoplankton are described by the optimal-growth model (OGM) of Pahlow et al. (2013), modified to account for the coarse spatio-temporal resolution of UVic and augmented with temperature and iron effects (see equations provided below). Owing to the relatively long time step, the model does not resolve the dynamics of photo-acclimation and we therefore describe the Chl:C ratio of the chloroplast by its balanced-growth optimum. Hence we do not need state variables for

~~Optimality-based plankton-ecosystem model (OPEM). Ordinary phytoplankton, diazotrophs, and zooplankton are represented by optimality-based physiological regulatory formulations.~~

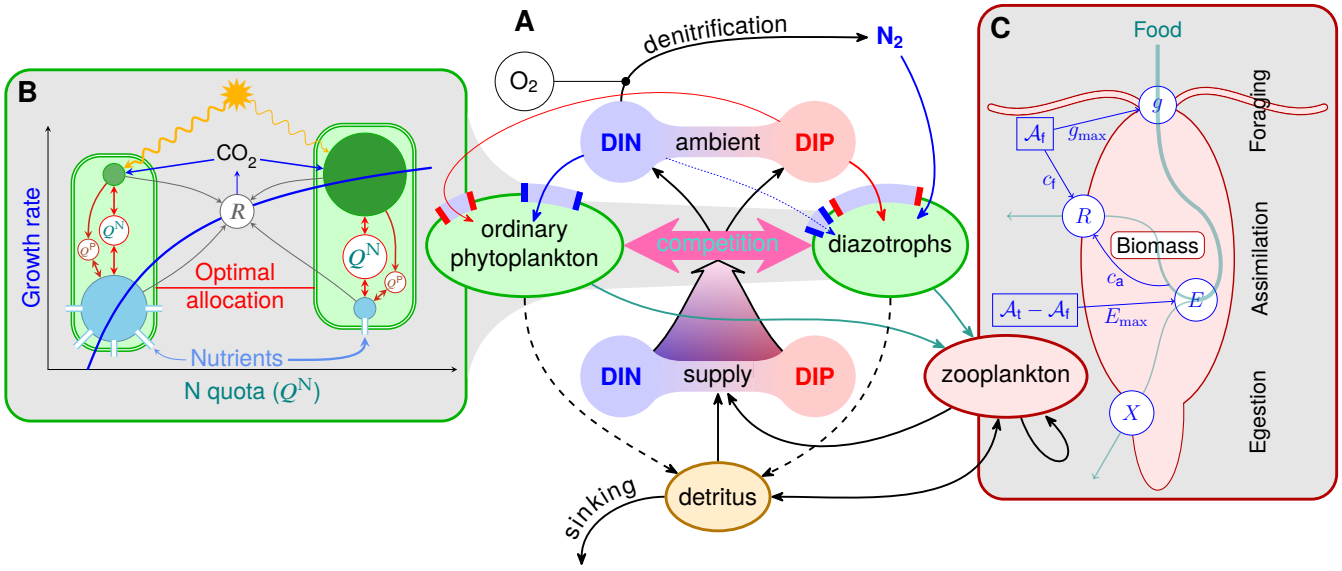

Figure 1. Optimality-based plankton-ecosystem model (OPEM, panel A). Ordinary phytoplankton, diazotrophs, and zooplankton are represented by optimality-based physiological regulatory formulations. Ordinary phytoplankton and diazotrophs are driven by optimal allocation of cellular resources (panel B), balancing the benefits of nutrient assimilation and light harvesting against allocation and energetic costs (respiration, R) of these processes. The optimal allocation trades off, e.g., cellular N as defined by Q^N, between the requirements for photosynthesis (green) and nutrient acquisition (blue), with an additional compartment for N_2 fixation in diazotrophs (not shown). The phosphorus quota (Q^P) controls N assimilation (see Appendix C1.2) but only Q^N affects the growth rate directly (see Appendix C1.1). Zooplankton foraging (panel C) is optimised by balancing costs and benefits of allocating total activity ($\mathcal{A}_t$) between foraging activity ($\mathcal{A}_f$) and assimilation activity ($\mathcal{A}_t - \mathcal{A}_f$). Both foraging and assimilation incur energy costs (c_f and c_a, respectively) fuelled by respiration (R). Increasing ingestion (g) reduces assimilation efficiency ($E \leq E_{max}$), causing more particulate egestion (X).

Chl. Simulating variable Chl:C:N:P stoichiometry in phytoplankton then requires three state variables, representing particulate organic C, N, P (POC, PON, POP) for each phytoplankton group and for detritus.

The OGM is a cell-quota model comprising several levels of physiological regulation. At the whole-cell level, resources are optimally allocated between nutrient acquisition and CO_2 fixation, Chl synthesis is optimised within the chloroplast, and optimal uptake kinetics (Pahlow, 2005; Smith et al., 2009) drives nutrient uptake and assimilation inside the protoplast. For all trade-offs, we define optimal as yielding maximum balanced growth of the cell. For facultative diazotrophs, N_2 fixation is switched on whenever this enhances growth. The biological model parameters of the OGM are different from the original UVic configuration. In spite of its ability to describe two additional tracers (phytoplankton C and P) and the Chl:C ratio, the OGM has only 8 parameters (maximum rate V_0, nutrient affinity A_0, costs of N assimilation ζ^N and Chl synthesis ζ^{Chl} and

maintenance $R_{\mathrm{M}}^{\mathrm{Chl}}$, subsistence quotas Q_0^{N} and Q_0^{P}, and the light-absorption coefficient α), i.e., the same as the phytoplankton parameters of the original UVic configuration (Nickelsen et al., 2015). In addition, two of these (V_0 and ζ^{Chl}) can be considered constant (Pahlow et al., 2013), leaving 6 parameters to be calibrated.

~~None of the measures against negative concentrations are effective if the minimum required concentration of a tracer is greater than zero, which is the case for our phytoplankton PON and POP tracers, whose minimum (subsistence) concentrations are given by the product of POC and the N and P subsistence quotas Q_0^{N} and Q_0^{P}, respectively, which can be thought of as the subsistence PON and POP of phytoplankton. In order to circumvent this problem and also be able to benefit from the FCT technique, we define δ-tracers as the differences between actual and subsistence phytoplankton PON and POP concentrations. The lower limit of the δ-tracers is 0, the δ-tracers can be transported with the positive transport schemes, and subsistence PON and POP are implicitly advected and mixed in proportion to phytoplankton POC and added back onto the δ-tracers where required:~~

$$\delta n_p = n_p - \mathrm{C}_p \cdot Q_{0,p}^n \quad \Leftrightarrow \quad n_p = \delta n_p + \mathrm{C}_p \cdot Q_{0,p}^n, \qquad n \in \{\mathrm{N}, \mathrm{P}\}, \qquad p \in \{\mathrm{phy}, \mathrm{dia}\}$$

~~where C_p, N_p, P_p are POC, PON, POP, respectively, of phytoplankton group p (phytoplankton or diazotrophs).~~

Table 1. Parameters and variables of the optimality-based plankton compartments.

Symbol(s)	Units	Description
DIN, DIP	$\mathrm{mol\,m^{-3}}$	dissolved inorganic N, P
ϵ	$\mathrm{m^{-1}}$	light-attenuation coefficient
T	°C	temperature
phytoplankton and diazotrophs		
A_0	$\mathrm{m^3\,(mol\,C)^{-1}\,d^{-1}}$	potential nutrient affinity
α	$\mathrm{m^2\,W^{-1}\,mol\,C\,(g\,Chl)^{-1}\,d^{-1}}$	potential light affinity
ζ^{Chl}	$\mathrm{mol\,C\,(g\,Chl)^{-1}}$	cost of chlorophyll synthesis
ζ^{N}	$\mathrm{mol\,C\,(mol\,N)^{-1}}$	cost of N assimilation
δN, δP	$\mathrm{mol\,m^{-3}}$	$\mathrm{N} - \mathrm{C} \cdot Q_0^{\mathrm{N}}$, $\mathrm{P} - \mathrm{C} \cdot Q_0^{\mathrm{P}}$
F_0, F_0^{N}	$\mathrm{mol\,(mol\,C)^{-1}\,d^{-1}}$	potential, temperature-dependent rate of $\mathrm{N_2}$ fixation
f_{C}, f_{F}, f_{V}	—	allocation for $\mathrm{CO_2}$ fixation, $\mathrm{N_2}$ fixation, nutrient uptake
f_{N}	—	relative (to f_{V}) allocation for N uptake
$f(T)$	—	temperature dependence
k_{Fe}	$\mathrm{mmol\,m^{-3}}$	half-saturation Fe concentration
L_{day}	—	day length
I, I_{min}	$\mathrm{W\,m^{-2}}$	actual, minimum irradiance
λ, M	$\mathrm{d^{-1}}$	leakage, mortality
μ	$\mathrm{d^{-1}}$	net relative growth rate
Q^{N}, Q^{P}	$\mathrm{mol\,(mol\,C)^{-1}}$	N:C, P:C ratios (N, P cell quotas)
Q_0^{N}, Q_0^{P}	$\mathrm{mol\,(mol\,C)^{-1}}$	N, P subsistence quotas

Table 1. (continued)

Symbol(s)	Units	Description
R	d^{-1}	respiration
R^{Chl}, $R^{\mathrm{Chl}}_{\mathrm{M}}$	d^{-1}	total, maintenance cost of chlorophyll
r_{DIC}	d^{-1}	extra DIC release
S_{Fe}, S_{I}	—	degree of iron, light saturation
θ	$\mathrm{g\,Chl\,(mol\,C)^{-1}}$	Chl:C ratio*
V_0	$\mathrm{mol\,(mol\,C)^{-1}\,d^{-1}}$	potential-rate parameter
V^{C}	d^{-1}	rate of C fixation
V^{N}, V^{P}	$\mathrm{mol\,(mol\,C)^{-1}\,d^{-1}}$	rates of N, P uptake*
V_0^{C}, V_0^{N}, V_0^{P}	$\mathrm{mol\,(mol\,C)^{-1}\,d^{-1}}$	temperature-dep. pot. rates of C, N, P acquisition
zooplankton and detritus		
$\mathcal{A}_{\mathrm{f}}$, $\mathcal{A}_{\mathrm{t}}$	d^{-1}	foraging, total activity
β	—	digestion-efficiency coefficient
c_{a}, c_{f}	—	cost of assimilation, foraging
E_{max}, E_{zoo}	—	max., actual assimilation efficiency
$f_{\mathrm{det}}(T)$, $f_{\mathrm{zoo}}(T)$	—	detritus, zooplankton temperature dependence
G^{C}_{prey}, G^{N}_{prey}, G^{P}_{prey}	$\mathrm{mol\,m^{-3}\,d^{-1}}$	prey-specific rate of C, N, P ingestion
g_{max}, g_{zoo}	d^{-1}	reference, actual relative rate of total ingestion
M_{zoo}	$\mathrm{m^3\,(mol\,C)^{-1}\,d^{-1}}$	zooplankton mortality
μ_{zoo}	d^{-1}	net relative growth rate
ν_{det}	d^{-1}	detritus reference decay rate
Π^{C}, Π^{N}, Π^{P}	$\mathrm{mol\,m^{-3}}$	effective prey C, N, P concentration
ϕ_p	$\mathrm{m^3\,(mol\,C)^{-1}}$	prey-capture coefficients, $p \in \{\mathrm{phy, dia, det, zoo}\}$
$Q^{\mathrm{N}}_{\mathrm{zoo}}$, $Q^{\mathrm{P}}_{\mathrm{zoo}}$	$\mathrm{mol\,(mol\,C)^{-1}}$	zooplankton N:C, P:C ratio
$R^{\mathrm{C}}_{\mathrm{zoo}}$, ~~$X^{\mathrm{N}}_{\mathrm{zoo}}$, $X^{\mathrm{P}}_{\mathrm{zoo}}$~~ $R^{\mathrm{N}}_{\mathrm{zoo}}$, $R^{\mathrm{P}}_{\mathrm{zoo}}$	$\mathrm{mol\,m^{-3}\,d^{-1}}$	respiration, dissolved N, P loss
r_{Q}	—	stoichiometric reduction factor
S_{g}	—	degree of ingestion saturation
$X^{\mathrm{C}}_{\mathrm{zoo}}$, $X^{\mathrm{N}}_{\mathrm{zoo}}$, $X^{\mathrm{P}}_{\mathrm{zoo}}$	$\mathrm{mol\,m^{-3}\,d^{-1}}$	particulate C, N, P loss (egestion)

*variants with hat (ˆ) accents are relative to the chloroplast or protoplast

None of the measures against negative concentrations (Appendix B) are effective if the minimum required concentration of a tracer is greater than zero, which is the case for our phytoplankton PON and POP tracers, whose minimum (subsistence) concentrations are given by the product of POC and the N and P subsistence quotas Q_0^{N} and Q_0^{P}, respectively, which can be thought of as the subsistence PON and POP of phytoplankton. In order to circumvent this problem and also be able to benefit from the FCT technique (flux-corrected transport, see Appendix B), we define δ-tracers as the differences between actual and

subsistence phytoplankton PON and POP concentrations. As the lower limit of the δ-tracers is 0, they can be transported with the positive transport schemes, and subsistence PON and POP are implicitly advected and mixed in proportion to phytoplankton POC and added back onto the δ-tracers where required:

$$\delta n_p = n_p - \mathrm{C}_p \cdot Q^n_{0,p} \quad \Leftrightarrow \quad n_p = \delta n_p + \mathrm{C}_p \cdot Q^n_{0,p}, \qquad n \in \{\mathrm{N}, \mathrm{P}\}, \qquad p \in \{\text{phy, dia}\} \tag{1}$$

where C_p, N_p, P_p are POC, PON, POP, respectively, of phytoplankton group p (phytoplankton or diazotrophs).

The local rates of change of the phytoplankton tracers are then defined by sources-minus-sinks terms ($\mathcal{S}$):

$$\mathcal{S}(\mathrm{C}_p) = (\mu_p - \lambda_p - M_p) \cdot \mathrm{C}_p - G^{\mathrm{C}}_p, \qquad p \in \{\text{phy, dia}\} \tag{2}$$

$$\mathcal{S}(\delta n_p) = V^n_p \cdot \mathrm{C}_p - (\lambda_p + M_p) \cdot n_p - G^n_p - \mathcal{S}(\mathrm{C}_p) \cdot Q^n_{0,p}, \qquad n \in \{\mathrm{N}, \mathrm{P}\} \tag{3}$$

where μ_p is net relative (C-specific) growth rate (C fixation minus the sum of respiration and release of dissolved organic carbon by phytoplankton, immediately respired to DIC here), λ_p leakage, M_p mortality, G^n_p grazing by zooplankton, V^{N}_p and V^{P}_p DIN and DIP uptake, and Q^{N}_p and Q^{P}_p biomass-normalised N and P cell quotas (N:C and P:C ratios). The last term in (3) accounts for the subsistence amounts of N and P implicitly contained in C_p and subtracted from δn_p via (1). Leakage is the fast-recycling term parametrising the microbial loop (Keller et al., 2012). Definitions for all terms in Eqs. (2) and (3) are provided in Appendix C1.

We set up configurations with two representations of temperature dependence for diazotrophs, (1) configuration OPEM with the same temperature dependence as in the original UVic, and (2) configuration OPEM-H with the ~~same temperature dependence (Eppley, 1972) applied to phy and dia~~ Eppley (1972) temperature dependence applied to both phytoplankton (subscript phy) and diazotroph (subscript dia) growth and nutrient uptake, and the temperature function from Houlton et al. (2008) for N_2 fixation (Fig. 2, see Appendix C1.3). The maximum, temperature-dependent rates for diazotrophs are multiplied with 0.4 in the original UVic but not in OPEM, so that they remain below those of ordinary phytoplankton for the whole temperature range in Fig. 2. All other temperature dependencies are unchanged from the original UVic, i.e., they follow the Eppley (1972) curve (dashed red line in Fig. 2).

2.2 Zooplankton

Zooplankton foraging is described by the model of optimal current feeding (OCF, Pahlow and Prowe, 2010). The OCF is based on the idea that the animal has a certain inherent maximum total activity ($\mathcal{A}_\mathrm{t}$), which can be allocated between foraging activity ($\mathcal{A}_\mathrm{f}$) and activity for the assimilation of food ($\mathcal{A}_\mathrm{t} - \mathcal{A}_\mathrm{f}$), so that the net relative growth rate is maximised, considering the costs of foraging and assimilation (represented by the coefficients c_f and c_a, respectively). While $\mathcal{A}_\mathrm{t}$ is a rather abstract quantity, it can be expressed as a function of the maximal ingestion rate, which is routinely determined in feeding experiments, and temperature (see Eq. C18 in Appendix C2). The OCF can represent different foraging strategies via its prey-capture coefficient (ϕ) and c_f. Very low ϕ and $c_\mathrm{f} \approx 0$ represent ambush feeding, whereas $c_\mathrm{f} \approx c_\mathrm{a}$ is representative of current feeding for intermediate ϕ and cruise feeding for high ϕ. The parameter values in OPEM and OPEM-H (Table 2) are between values determined for cruise and current feeders by Pahlow and Prowe (2010). The OCF has two more parameters the original UVic, but since two

~~Temperature functions ($f_{dia}(T)$) for N_2 fixation. The UVic function is the one employed by the original and OPEM configurations. The OPEM-H configuration applies the Eppley (1972) function to nutrient uptake and CO_2 fixation to both ordinary and diazotrophic phytoplankton and the Houlton et al. (2008) function to N_2 fixation.~~

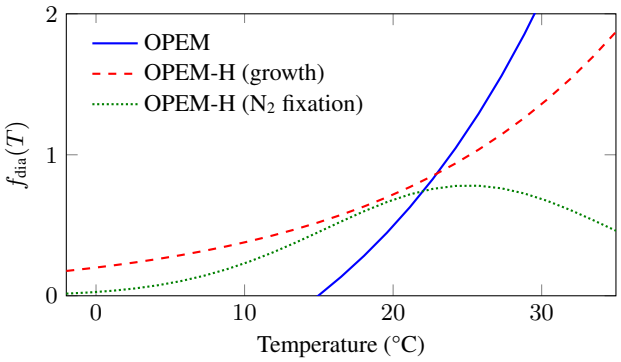

Figure 2. Temperature functions ($f_{dia}(T)$) for diazotrophs. The OPEM function (solid blue line) is the one employed by the original and OPEM configurations for both diazotroph growth and N_2 fixation. The OPEM-H configuration applies the Eppley (1972) function (dashed red line) to nutrient uptake and CO_2 fixation to both ordinary and diazotrophic phytoplankton and the Houlton et al. (2008) function (dotted green line) to N_2 fixation.

of them can be considered constant ($\beta = 0.2$ and $E_{max} = 1$, Pahlow and Prowe, 2010), the number of parameters which have to be calibrated is the same as in the original UVic.

Besides its mechanistic foundation, the main advantages over the Holling-II formulation in the original UVic model are the predicted feeding threshold and variable assimilation efficiency. Assimilation efficiency is constant and a feeding threshold does not exist in the original UVic model. Temperature dependence is accounted for by multiplying the maximum ingestion rate and maintenance respiration with the temperature function as described in Keller et al. (2012) but here without the cap at 20 °C. The cap on the increase of maximum ingestion rate with grazing in the original version was deemed necessary in order to avoid inordinately high grazing in the tropics (Keller et al., 2012). It is noteworthy that this does not appear to be a problem in OPEM even though maximum ingestion rates g_{max} are about 4-fold higher than in the original UVic version (Table 2). We attribute this to the feeding threshold in the OCF, which reduces grazing in oligotrophic regions. Since zooplankton stoichiometry is fixed (constant Q^{N}_{zoo} and Q^{P}_{zoo}) but that of the food is variable, any excess C, N, or P must be released, assumed here in mostly dissolved form (as inorganic nutrients). For example, all the excess ingested C is respired (see Eq. C15 in Appendix C2), as also suggested by Talmy et al. (2016). To this end we define a stoichiometric reduction factor r_Q that reduces net uptake and growth of zooplankton to the uptake of the most limiting nutrient of the ingested food,

$$r_Q = \min\left(\frac{\Pi^N}{\Pi^C \cdot Q^N_{zoo}}, \frac{\Pi^P}{\Pi^C \cdot Q^P_{zoo}}, 1\right), \qquad \Pi^n = \sum_{p\in\{phy,\, dia,\, det,\, zoo\}} \phi_p n_p, \qquad n \in \{C, N, P\} \tag{4}$$

where Π^n is the effective prey concentration for nutrient element n and ϕ_p are the prey-specific capture coefficients. The relations among the ϕ_p effectively determine the (relative) food preferences. The sources-minus-sinks term for zooplankton biomass $\mathcal{S}(N_{zoo})$ is expressed here in terms of nitrogen, which can easily be converted to P and C via the zooplankton's fixed stoichiometry. $\mathcal{S}(N_{zoo})$ is the difference between net growth (μ_{zoo}), which is corrected for r_Q (Appendix C2), and losses due to

intra-guild predation ($G^{\mathrm{N}}_{\mathrm{zoo}}$) and background mortality (M_{zoo}):

$$\mathcal{S}(\mathrm{N_{zoo}}) = \mu_{\mathrm{zoo}} \cdot \mathrm{N_{zoo}} - G^{\mathrm{N}}_{\mathrm{zoo}} - M_{\mathrm{zoo}} \frac{N^2_{\mathrm{zoo}}}{Q^{\mathrm{N}}_{\mathrm{zoo}}} \tag{5}$$

Equations for μ_{zoo} and $G^{\mathrm{N}}_{\mathrm{zoo}}$ are given in Appendix C2. The background mortality is a quadratic closure term intended to represent losses due to viruses, predation by higher trophic levels, etc.

2.3 Detritus and dissolved pools

Mortality terms and egestion of faecal particles by zooplankton produce detritus, which is itself subject to grazing and temperature-dependent remineralisation. We consider separate C, N, and P tracers for detritus:

$$\mathcal{S}(n_{\mathrm{det}}) = M_{\mathrm{phy}} \cdot n_{\mathrm{phy}} + M_{\mathrm{dia}} \cdot n_{\mathrm{dia}} + M_{\mathrm{zoo}} \cdot \frac{n^2_{\mathrm{zoo}}}{Q^n_{\mathrm{zoo}}} + X^n_{\mathrm{zoo}} - G^n_{\mathrm{det}} - f_{\mathrm{det}}(T) \cdot \nu_{\mathrm{det}} \cdot n_{\mathrm{det}}, \qquad n \in \{\mathrm{C, N, P}\} \tag{6}$$

where ν_{det} is the detritus remineralization rate at 0 °C. Hence, the export and remineralisation fluxes are also traced individually for C, N, and P. This applies also to alkalinity, where we assume a sulfur-to-carbon ratio of 0.023 mol S mol C^{-1} for organic C (Matrai and Keller, 1994). For $\mathrm{O_2}$ consumption during remineralisation, we consider contributions from C and N separately. We assume $-\mathrm{O_2{:}N} = 2$ (the N contribution to $\mathrm{O_2}$ consumption) during nitrification and calculate the respiratory quotient for C based on an $\mathrm{O_2{:}C}$ ratio of $170{:}117 = 1.45$ mol $\mathrm{O_2}$ mol C^{-1} (Anderson and Sarmiento, 1994), corrected for the contribution of nitrification, ~~assuming~~ and an average C:N = 6.625 mol C mol N^{-1}~~, as $1.45 - 2/6.625 = 1.15$ mol $\mathrm{O_2}$ mol C^{-1}~~. Thus, we obtain the respiratory quotient for C (the C contribution) as the difference between the average $\mathrm{O_2{:}C}$ ratio and the N contribution to $\mathrm{O_2}$ consumption, i.e., 1.45 mol $\mathrm{O_2}$ mol C^{-1} − 2 mol $\mathrm{O_2}$ mol N^{-1} / 6.625 mol C mol N^{-1} = 1.15 mol $\mathrm{O_2}$ mol C^{-1}. Eq. (6) does not include gains and losses from sinking detritus particles. Detritus sinking speed v_{sink} increases with depth~~according to~~, reflecting the gradual disappearance of smaller particles during sinking, according to

$$v_{\mathrm{sink}} = v_0 + a_{\mathrm{v}} \cdot z \tag{7}$$

where $v_0 = 6\,\mathrm{m\,d^{-1}}$ is the sinking velocity at the surface, z is depth and $a_{\mathrm{v}} = 0.06\,\mathrm{d^{-1}}$ the rate of increase in v_{sink} with depth (Kriest, 2017).

Dissolved inorganic C and nutrients are utilised by phytoplankton and released by phytoplankton leakage, zooplankton respiration and excretion and detritus remineralisation, as well as via rejection of surplus elements via grazing of organic matter with elemental stoichiometries differing from that of zooplankton.

2.4 Model reference simulations

We first did a preliminary sensitivity analysis to identify sensitive model parameters. Then we set up an ensemble of 400 parameter sets, using a Latin-Hypercube method, and ran both of our model configurations into steady state for all parameter sets. We select two reference simulations (trade-off solutions in Part II, Chien et al., 2020), one each from the OPEM and OPEM-H ensembles, ~~according to~~ according to two objectives: (1) We minimise a cost function ~~and the ability to predict~~ under the

Table 2. Parameter settings for the original and our reference OPEM and OPEM-H configurations. Parameters in **bold** vary within the ensembles of simulations ~~(Chien et al~~(Chien et al., 2020). ~~, 2019).~~ Symbol descriptions are given in Table 1.

Parameter	Original	OPEM/OPEM-H	
$\boldsymbol{A_{0,\mathrm{dia}}}$	—	$0.75 \times A_{0,\mathrm{phy}}$[a]	$\mathrm{m^3\ (mol\ C)^{-1}\ d^{-1}}$
$\boldsymbol{A_{0,\mathrm{phy}}}$	—	229	$\mathrm{m^3\ (mol\ C)^{-1}\ d^{-1}}$
α_{dia}	0.13–0.53[b]	0.5[c]	$\mathrm{W\ m^{-2}\ mol\ C\ (g\ Chl)^{-1}\ d^{-1}}$
α_{phy}	0.13–0.53[b]	0.4[c]	$\mathrm{W\ m^{-2}\ mol\ C\ (g\ Chl)^{-1}\ d^{-1}}$
β	—	0.2	
$c_{\mathrm{a}} = c_{\mathrm{f}}$	—	0.1	
E_{max}	—	1	
$\boldsymbol{g_{\mathrm{max}}}$	0.4	1.75	$\mathrm{d^{-1}}$
$\boldsymbol{k_{\mathrm{Fe,\ dia}}}$	0.10×10^{-3}	$2 \times k_{\mathrm{Fe,\ phy}}$[d]	$\mathrm{mmol\ m^{-3}}$
$\boldsymbol{k_{\mathrm{Fe,\ phy}}}$	0.12×10^{-3}	0.066×10^{-3}	$\mathrm{mmol\ m^{-3}}$
$\boldsymbol{\lambda_{0,\mathrm{phy}} = M_{0,\mathrm{dia}}}$	0.015	0.018	$\mathrm{d^{-1}}$
$\lambda_{0,\mathrm{dia}}$	0	0	$\mathrm{d^{-1}}$
$M_{0,\mathrm{phy}}$	0.03	0.03	$\mathrm{d^{-1}}$
$\boldsymbol{\nu_{\mathrm{det}}}$	0.07	0.087	$\mathrm{d^{-1}}$
$\boldsymbol{\phi_{\mathrm{dia}}}$	—	232	$\mathrm{m^3\ (mol\ C)^{-1}}$
$\boldsymbol{\phi_{\mathrm{phy}}}$	—	118	$\mathrm{m^3\ (mol\ C)^{-1}}$
$\boldsymbol{\phi_{\mathrm{det}}}$	—	94	$\mathrm{m^3\ (mol\ C)^{-1}}$
$\boldsymbol{\phi_{\mathrm{zoo}}}$	—	118	$\mathrm{m^3\ (mol\ C)^{-1}}$
$\boldsymbol{Q^{\mathrm{N}}_{0,\mathrm{dia}}}$	—	0.067	$\mathrm{mol\ (mol\ C)^{-1}}$
$\boldsymbol{Q^{\mathrm{N}}_{0,\mathrm{phy}}}$	—	0.041 28	$\mathrm{mol\ (mol\ C)^{-1}}$
$\boldsymbol{Q^{\mathrm{P}}_{0,\mathrm{dia}}}$	—	0.002 71	$\mathrm{mol\ (mol\ C)^{-1}}$
$\boldsymbol{Q^{\mathrm{P}}_{0,\mathrm{phy}}}$	—	0.0022	$\mathrm{mol\ (mol\ C)^{-1}}$

[a] $A_{0,\mathrm{dia}} < A_{0,\mathrm{phy}}$ according to Pahlow et al. (2013)

[b] minimum and maximum, see Nickelsen et al. (2015)

[c] $\alpha_{\mathrm{dia}} > \alpha_{\mathrm{phy}}$ according to Pahlow et al. (2013)

[d] the higher $k_{\mathrm{Fe,\ dia}}$ represents the larger Fe requirement of diazotrophs

condition that (2) we obtain realistic levels of global water-column denitrification~~(Chien et al., 2019)~~, i.e. at least 60 Tg N $\mathrm{yr^{-1}}$ (DeVries et al., 2012). Thus, no weighting had to be applied to our objectives. The cost function quantifies the model-data misfit by a measure of the discrepancies between observed and simulated O_2, $NO_3{}^-$, $PO_4{}^{3-}$, and Chl, considering also correlations and covariances ~~(Chien et al., 2019).~~ (see Part II, Chien et al., 2020).

In the following we describe and discuss the behaviour of the two reference simulations, which turned out to have same parameter set (Table 2). While this may be a coincidence, it has the advantage that all differences between OPEM and OPEM-

H can be ascribed unequivocally to the difference in the temperature dependence of the diazotrophs. We specifically consider the models' ability to reproduce features not included in the cost function, ~~namely the excess~~ namely the surplus nitrate with respect to the Redfield N-equivalent of phosphate, termed $N^* = NO_3^- - 16 \cdot PO_4^{3-} + 2.9\,\mathrm{mmol\,m^{-3}}$ (Gruber and Sarmiento, 1997; Mills et al., 2015), and global N_2-fixation rates and distributions within current observational ranges. All our UVic-model results are shown as annual averages at the end of the spin-up (i.e. after at least 10,000 years), when a seasonally cycling steady state has been reached.

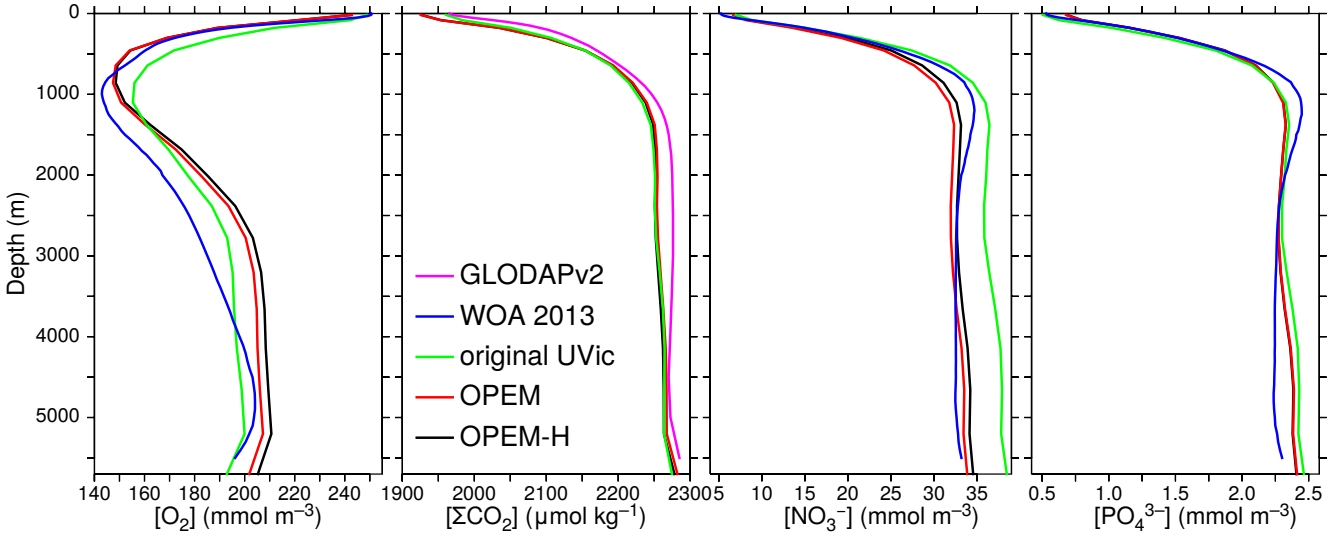

Figure 3. Globally-averaged vertical profiles of O_2, DIC (ΣCO_2), NO_3^-, and PO_4^{3-} concentrations. Oxygen, nitrate, phosphate, but not DIC are considered in the cost function. O_2, NO_3^-, and PO_4^{3-} data from the World Ocean Atlas 2013 (WOA 2013, Garcia et al., 2013a, b) and ΣCO_2 data from GLODAPv2 (Key et al., 2015; Lauvset et al., 2016) are compared to our original, OPEM, and OPEM-H UVic configurations (Section 2.4). Note that the PO_4^{3-} profiles coincide for OPEM and OPEM-H.

We compare the predictions of our reference simulations with data from these sources: NO_3^-, PO_4^{3-}, and O_2 data are from the World Ocean Atlas 2013 annual objectively analysed mean fields (WOA 2013, Garcia et al., 2013a, b). Dissolved inorganic C (DIC) data are from GLODAPv2 (Key et al., 2015; Lauvset et al., 2016). Estimates of Chl (MODIS Aqua, level 3, https://oceancolor.gsfc.nasa.gov/l3, Hu et al., 2012), particulate organic carbon and net primary and community production ~~(NPP and NCP, Westberry et al., 2008; Li and Cassar, 2016)~~ (POC, NPP and NCP, Westberry et al., 2008; Li and Cassar, 2016) are based on satellite data. In situ N_2 fixation data are from MAREDAT (Luo et al., 2012).

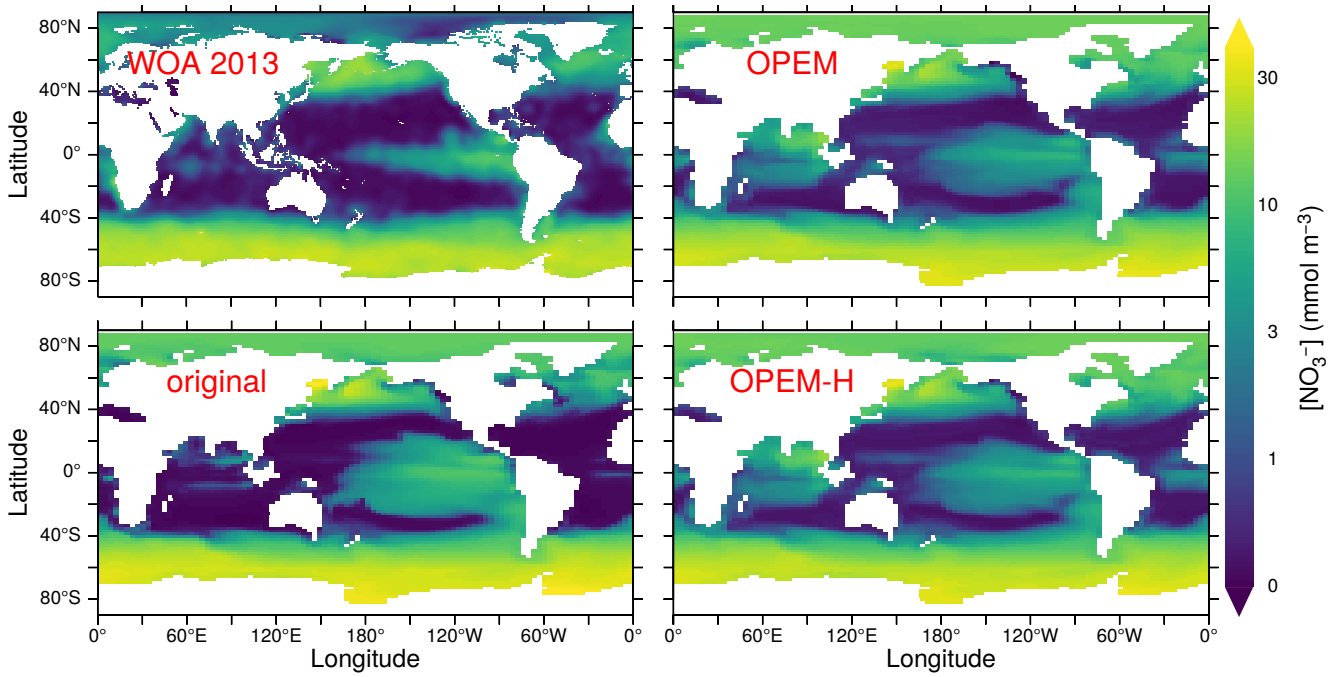

Figure 4. Annually-averaged distribution of NO_3^- in the upper 50 m in the WOA 2013 climatology, and predicted from the original, OPEM, and OPEM-H UVic simulations.

3 Model behaviour

3.1 Vertical and horizontal nutrient distributions

Horizontally-averaged vertical profiles of O_2 in the OPEM and OPEM-H simulations are closer to the WOA 2013 data in the upper 1500 m than in the original UVic model. At intermediate depths, all model versions overestimate O_2 concentrations, OPEM and OPEM-H slightly more so than the original UVic (Fig. 3). The original UVic better reproduces the NO_3^- profile above 1000 m than OPEM and OPEM-H but overestimates NO_3^- below 2000 m. The DIC and PO_4^{3-} profiles from our reference simulations are very similar to those of the original UVic model (Fig. 3).

Surface nitrate concentrations are generally slightly higher and more evenly distributed in OPEM and OPEM-H than in the original UVic model (Fig. 4). For most of the Atlantic, OPEM and OPEM-H are closer to the WOA 2013 data. Surface NO_3^- in the Indian Ocean ~~are~~ is underestimated by the original UVic and overestimated by OPEM and OPEM-H. Surface patterns of N* are much closer to observations in both OPEM and OPEM-H than in the original UVic configuration (Fig. 5). However, while N* in the northern North Pacific and Arctic Oceans is lower in OPEM and OPEM-H than in the original UVic, all UVic configurations still fail to reproduce the very low N* in large parts of the North Pacific and Arctic Oceans (Fig. 5). While N_2 fixation is not limited to temperatures higher than 15 °C in OPEM-H, only very little N_2 fixation occurs in the high northern and southern latitudes and thus cannot explain the higher surface N* values in OPEM-H there (see Section 3.3 below). In our

model simulations, low N* in the eastern tropical Pacific and South Atlantic result from denitrification in underlying oxygen-minimum zones (OMZs) (Landolfi et al., 2013). The original UVic configuration also displays very low N* in the Andaman Sea, whereas results of OPEM and OPEM-H are somewhat closer to the WOA 2013 data in the northern Indian Ocean (Fig. 5).

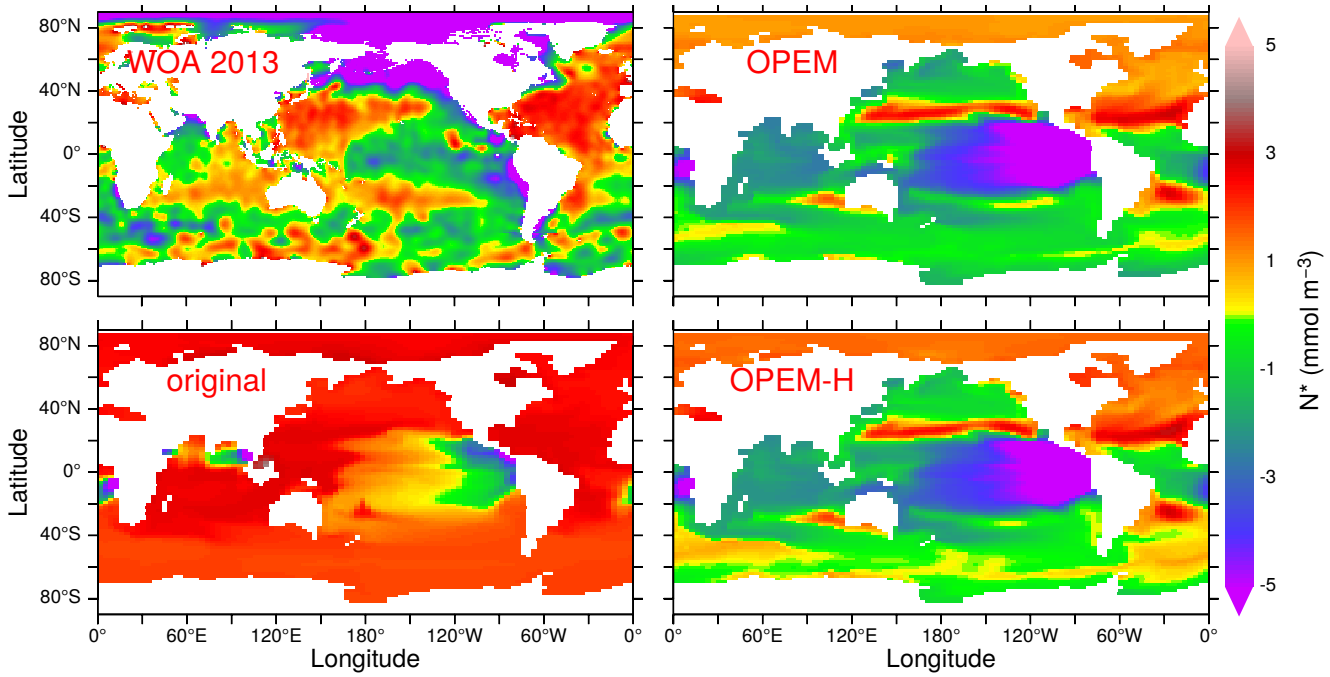

Figure 5. Annually-averaged distribution of N* in the upper 50 m in the WOA 2013 climatology and in the original, OPEM, and OPEM-H UVic simulations. Global averages for the upper 50 m are −0.4 mmol m^{-3} for the WOA 2013 and 1.8, −1.3, and −1.1 mmol m^{-3} for the original, OPEM, and OPEM-H simulations, respectively.

Interestingly, these differences cannot be seen in the O_2 distribution at 300 m, the depth of the OMZs, which is very similar in the Indian Ocean and eastern tropical Pacific among all our UVic simulations (Fig. 6), indicating that the carbon export and subsequent remineralization is very similar as well. The main differences in O_2 distribution are that O_2 is slightly higher in the Arctic Ocean and slightly lower in the equatorial Pacific and northern North Pacific in both OPEM and OPEM-H compared to the original ~~version~~ UVic (Fig. 6).

The OPEM simulations allow for a variable C:N ratio in detritus leaving the surface layers and reveal C:N ratios higher than the canonical value of 6.625 mol C (mol N)$^{-1}$, which is also the stoichiometry of zooplankton, almost everywhere between 40°S and 40°N in OPEM and OPEM-H (Fig. 7). ~~Thus, even~~ Even though detritus C:N is lower in the Bay of Bengal than in the remainder of the Indian Ocean in both OPEM simulations, this feature cannot explain the lower denitrification compared to the original UVic in this area, since the C:N ratio, which determines the O_2 demand for the remineralisation of sinking detritus, remains above the original UVic value of 6.625 mol C (mol N)$^{-1}$ ~~and determines the O_2 demand for the remineralisation of~~

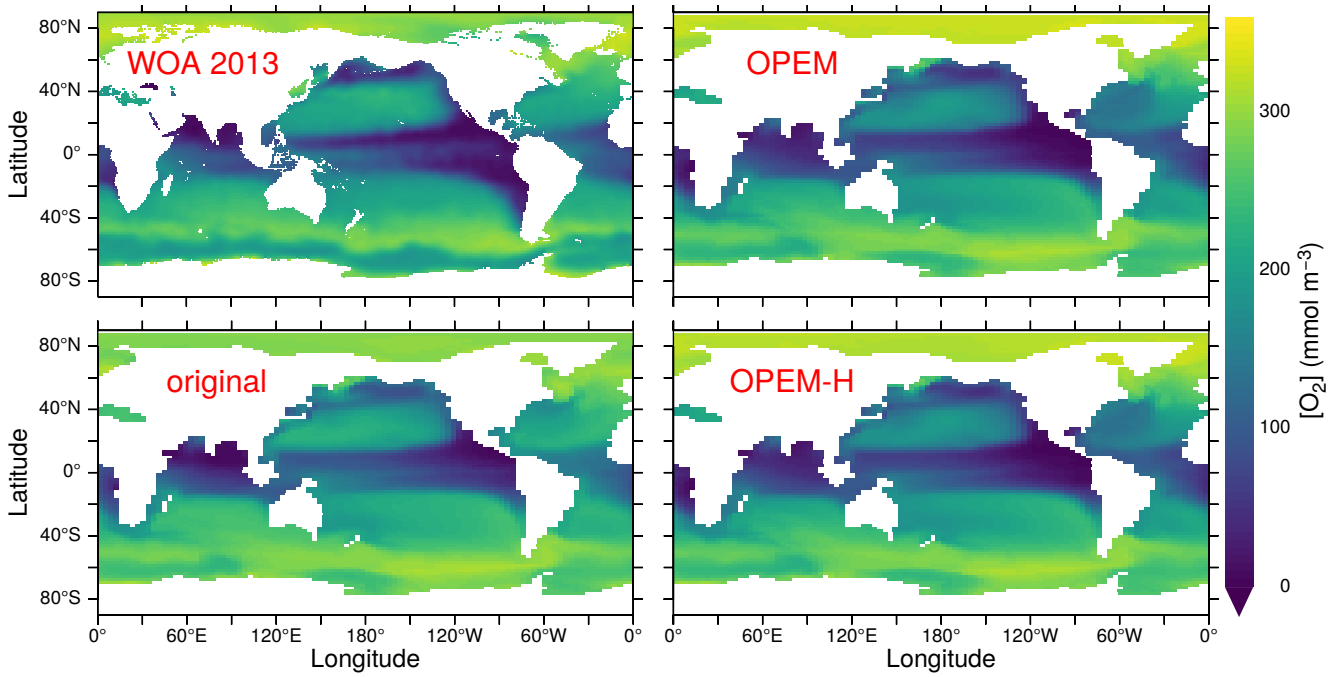

Figure 6. Annually-averaged distribution of O_2 concentration at 300 m in the WOA 2013 climatology and in the original, OPEM, and OPEM-H UVic simulations.

~~sinking detritus.~~. Rather, the lack of denitrification in the Indian Ocean in OPEM and OPEM-H (Fig. 13 bottom) appears to result simply from the reduced C export in this area compared to the original UVic (Fig. 12).

Another interesting feature of the OPEM and OPEM-H simulations is their ability to reproduce, at least qualitatively, the gradient of DIN:DIP ratios in the deep ocean (Fig. 8). The WOA 2013 data indicate relatively high DIN:DIP in the deep North Atlantic, decreasing towards the Southern, Indian, and Pacific Oceans. This gradient is very weak (and reversed) in the original UVic model (Fig. 8). Also, not all simulations in our OPEM and OPEM-H ensembles can reproduce this gradient, whereas other models without variable stoichiometry can (e.g., Kriest and Oschlies, 2015). Thus, reproducing the deep DIN:DIP distribution appears to require ~~the combination of decoupled C, N, and P with a suitable parameter set~~mostly a suitable model calibration. Note that deep-water N:P ratios are systematically higher in OPEM-H compared to OPEM, because of the elevated N* values in OPEM-H in high-latitude surface waters that feed the deep ocean interior (Fig. 5). We interpret the surface N* distribution outside the deep-water formation regions as a consequence, rather than a cause the of deep-ocean nutrient distributions, however.

3.2 Chlorophyll~~and~~, primary production, and autotrophic biomass

Chlorophyll concentrations are generally more evenly distributed in OPEM and OPEM-H, which agrees better with the MODIS Aqua (level 3) satellite estimates (Hu et al., 2012) than the original UVic model, which also overestimates chlorophyll in the

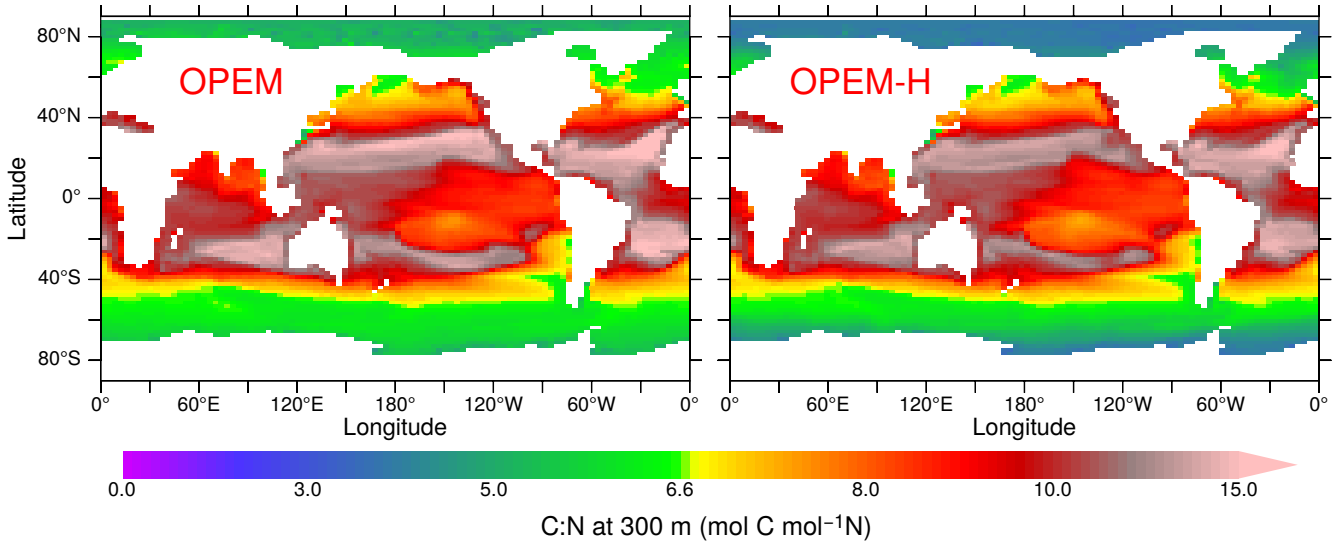

Figure 7. Annually-averaged C:N ratio of detritus at 300 m in the OPEM and OPEM-H simulations. The colour bar is centered at 6.625 mol C (mol N)$^{-1}$, which is the C:N ratio of zooplankton in all our UVic simulations.

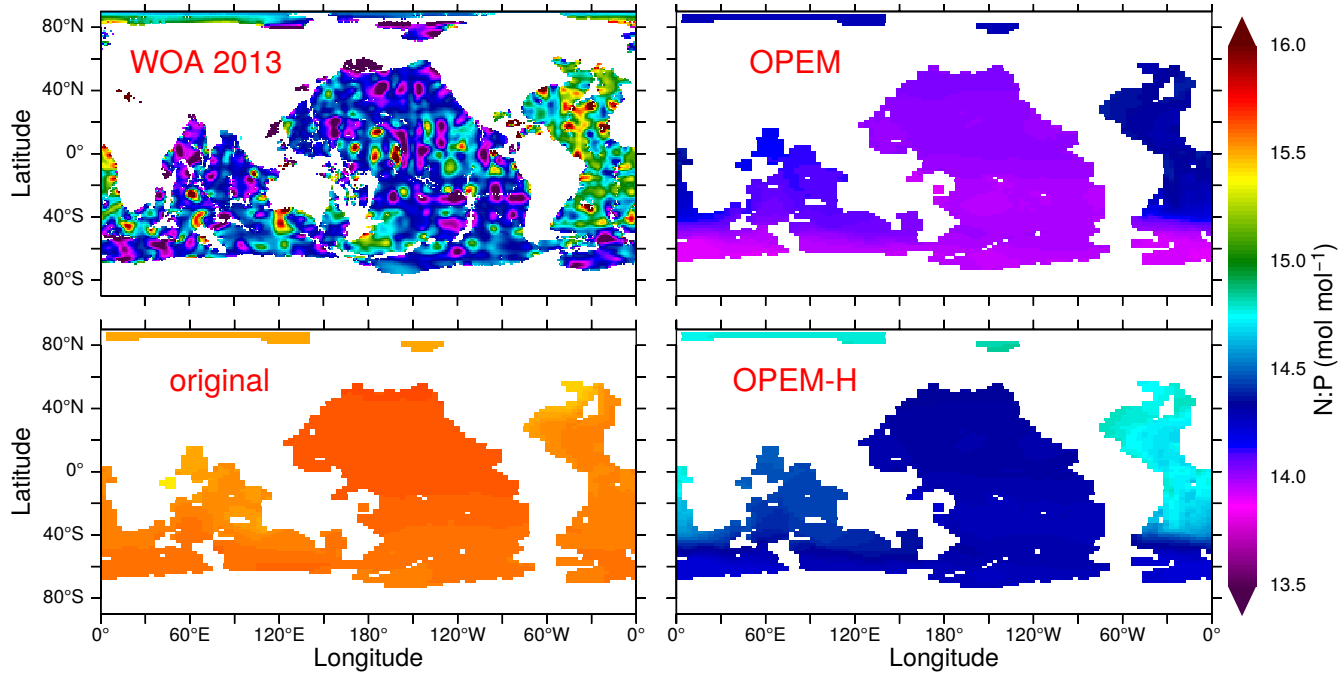

Figure 8. Distribution of DIN:DIP in the deep ocean (at 3200 m) in the WOA 2013 climatology and in the original, OPEM, and OPEM-H UVic simulations.

tropics and the Indian Ocean more pronouncedly. Only the OPEM-H simulation predicts reasonably high chlorophyll in the Arctic Ocean compared to the satellite estimates (Fig. 9). OPEM and OPEM-H apparently overestimate surface Chl in the oligotrophic subtropical gyres compared to the satellite estimate, which may be partly explained by both the inability of the satellite to detect deep chlorophyll maxima (DCM) and the coarse vertical resolution of the UVic grid. Unlike the original UVic, OPEM and OPEM-H have variable Chl:C ratios leading to pronounced DCM in the second layer (not shown). The surface layer in the UVic grid is 50 m thick, i.e., much thicker than the surface mixed layer in the typically strongly stratified oligotrophic subtropical gyres. Thus, the model underestimates light and overestimates nutrient supply to the surface in these regions, both of which tend to raise the Chl:C ratio (Pahlow et al., 2013), so that some of the high predicted surface Chl concentrations can be understood as the manifestation of an unresolved DCM within UVic's surface layer. As discussed below, however, part of the high Chl prediction also reflects an overestimation of autotrophic biomass (POC).

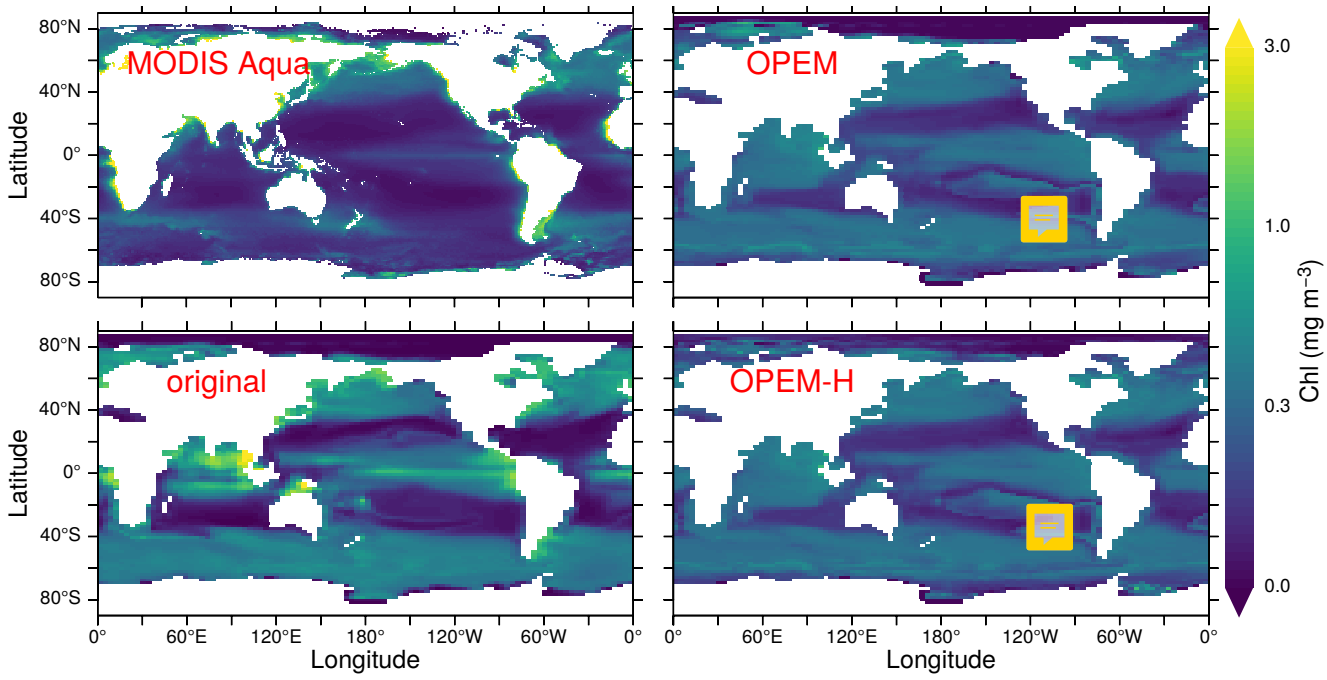

Figure 9. Annually averaged distribution of surface Chl estimated from MODIS Aqua (level 3) data for 2002 – 2019, and predicted from the original, OPEM, and OPEM-H UVic simulations. The MODIS Aqua averages in the top-left panel treat missing data as 0. Chl is calculated assuming Chl:N = 1.59 g mol^{-1} (Oschlies et al., 2000) for the original UVic model. Note that the surface layer is 50 m thick in UVic, whereas the satellite estimate is for the upper ∼20 m.

Global net primary production is defined here as

$$\mathrm{NPP} = (\mu_{\mathrm{phy}} - \lambda_{\mathrm{phy}}) \cdot C_{\mathrm{phy}} + (\mu_{\mathrm{dia}} - \lambda_{\mathrm{dia}}) \cdot C_{\mathrm{dia}} \tag{8}$$

where μ is the net relative growth rate and λ the leakage rate representing fast remineralisation in UVic. NPP in OPEM is the same as in OPEM-H (88.0 Pg C yr^{-1}) and is much higher than the estimate from Westberry et al. (2008) of 52 Pg C yr^{-1}, which in

turn exceeds that in the original UVic model (44.3 Pg C yr^{-1}). The NPP for the original UVic is lower than previously published (55 Pg C yr^{-1}, Nickelsen et al., 2015) because we include λ_{phy} in Eq. (8). The global averages predicted by the OPEM and OPEM-H simulations are slightly higher than the range of predictions from ocean color- and model-based estimates reported by Carr et al. (2006). NPP is much more evenly distributed in OPEM and OPEM-H than in the original UVic model, but the carbon-based productivity model (CbPM) (Westberry et al., 2008) predicts an even more uniform distribution (Fig. 10). The original configuration clearly underestimates NPP in the oligotrophic gyres, whereas OPEM and OPEM-H overestimate NPP in the tropical ocean. The high predicted NPP in OPEM and OPEM-H is apparently linked to an overestimate in autotrophic biomass (Fig. 11). The 50 m thick surface layer in the UVic grid implies an overestimate of nutrient supply under stratified conditions, which could, in combination with the relatively high surface autotrophic POC, explain the high NPP estimates in tropical and subtropical areas in Fig. 10.

~~Another~~

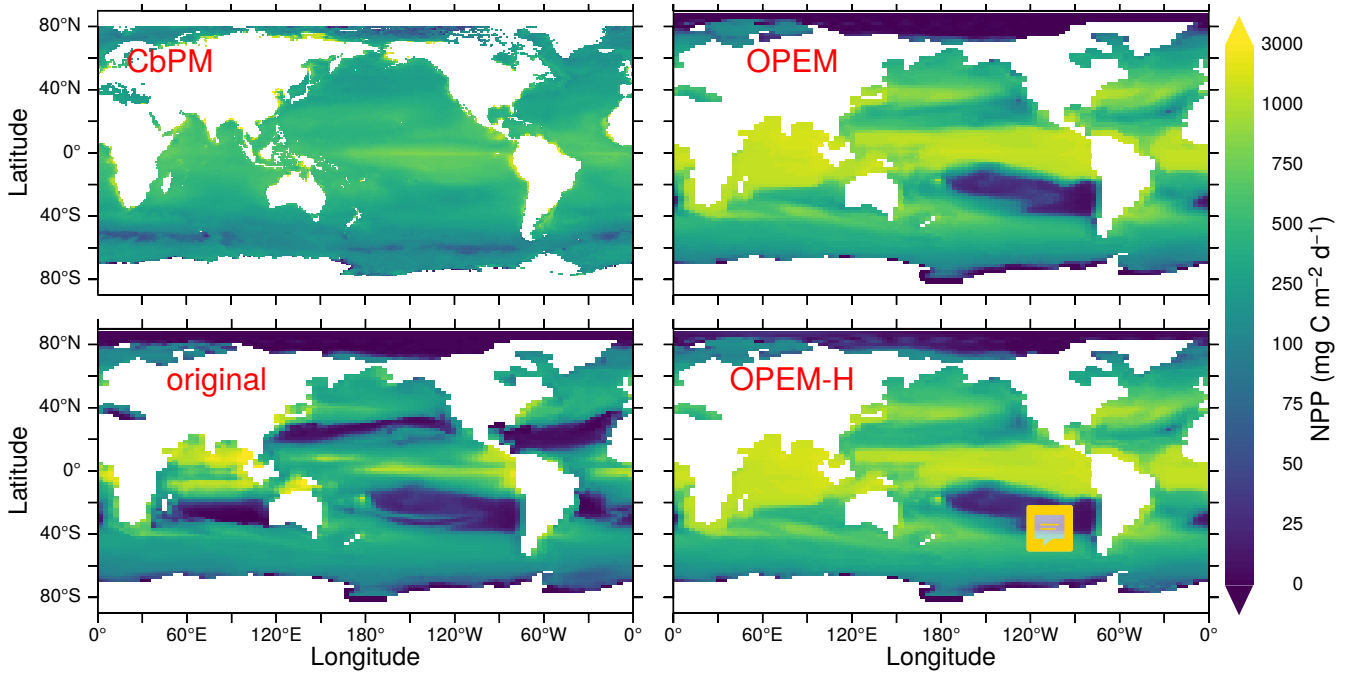

Figure 10. Annually-averaged distribution of vertically-integrated net primary production (NPP) estimated from satellite data via the C-based productivity model (CbPM) and predicted from the original, OPEM, and OPEM-H UVic simulations. The satellite-based CbPM estimate is the average for 2012–1018 (Westberry et al., 2008) with missing data treated as 0.

A possible explanation for the discrepancy between the OPEM and CbPM predictions may be that we do not include light affinity (α) among the list of parameters to be calibrated, because this parameter showed relatively little effect during our preliminary sensitivity analysis used to select sensitive model parameters. However, Arteaga et al. (2016) found that simple adaptive equations for α and A_0, meant to represent adaptation to nutrient or light limitation, greatly improved predicted Chl:C

compared to constant α and A_0 as applied in the present study. The use of constant parameters means that the OPEM and OPEM-H represent physiological flexibility as observed within species, but do not consider variations in plankton community composition.

Comparing the patterns in NPP and surface autotrophic POC (Figs. 10 and 11) suggests a spatial correlation between deviations in these two quantities (Fig. 11, lower left). Thus, some of the NPP overestimate could result from an overestimate in POC: The predicted NPP in both OPEM and OPEM-H is 1.7 times the CbPM estimate in Fig. 10 and the average surface autotrophic POC in OPEM and OPEM-H is 1.4 and 1.7 times that of the satellite-based CbPM estimate in Fig. 11. We interpret this as indicating that the growth rates of the primary producers may be relatively well represented by their optimality-based formulation, but the model behaviour might benefit from improvements in the representation of top-down control. While the growth of the primary producers is defined by the optimality-based formulation of phytoplankton introduced here, mortality is only partly determined by the optimal current-feeding model employed to describe zooplankton behaviour. A large part of phytoplankton mortality is still due to the mortality terms of the original UVic. The importance of top-down control becomes apparent from the result that autotrophic POC is much greater than the zooplankton feeding threshold throughout most of the World ocean in OPEM and OPEM-H (contours in the right panels of Fig. 11). Thus, the feeding threshold itself appears to be reasonable compared to the satellite-derive autotrophic POC, but our zooplankton somehow fails to exert sufficient top-down control when food availability is high.

Net community production (NCP) is spatially more evenly distributed in OPEM and OPEM-H than in the original UVic model. Both the more evenly distribution and the subsequently higher global total NCP are much closer to the satellite-based estimate of Li and Cassar (2016) than the original UVic model, except in the Indian Ocean (Fig. 12). The relatively low NPP in the original UVic model appears to be connected to a correspondingly low NCP (9.3 $\mathrm{Pg\,C\,yr^{-1}}$), which is close to previous model predictions (clustering around 10 $\mathrm{Pg\,C\,yr^{-1}}$, Laws et al., 2000; Dunne et al., 2005; DeVries and Weber, 2017). The high (overestimated) NPP in OPEM and OPEM-H is associated with much higher NCP predictions (12.9 and 13.0 $\mathrm{Pg\,C\,yr^{-1}}$, respectively), which are much closer to the satellite-based estimate of 13.5 $\mathrm{Pg\,C\,yr^{-1}}$ (Fig. 12) based on Li and Cassar (2016).

3.3 N_2 fixation and diazotrophs

N_2 fixation rates are shown in Fig. 13. Unfortunately, our model simulations differ most strongly in the Indian Ocean, for which no data exist in the MAREDAT database of Luo et al. (2012). One of the problems we face regarding N_2 fixation is that our UVic simulations do not include benthic denitrification and hence miss the dominant oceanic fixed-N loss term (e.g., Gruber, 2004; Wang et al., 2019). Since we have run the models into steady state, N_2 fixation must balance denitrification, which in our case occurs only in the water-column. Thus, our UVic simulations cannot be expected to generate realistic global rates of N_2 fixation unless water-column denitrification is strongly overestimated. Accordingly, our predicted N_2 fixation rates (53.9 $\mathrm{Tg\,N\,yr^{-1}}$ in the original UVic, 71.2 $\mathrm{Tg\,N\,yr^{-1}}$ in OPEM, and 69.4 $\mathrm{Tg\,N\,yr^{-1}}$ in OPEM-H, Fig. 13) are much closer to current estimates of water-column denitrification than total N_2 fixation ($\approx$ 70 vs. $\approx$ 160 $\mathrm{Tg\,N\,yr^{-1}}$, Wang et al., 2019). Another major difference is the much larger relative contribution of northern-hemisphere N_2 fixation in OPEM and OPEM-H compared to the original UVic. The North Atlantic contributes only 4 % in the original UVic, but the 23 % and 24 % contributions in

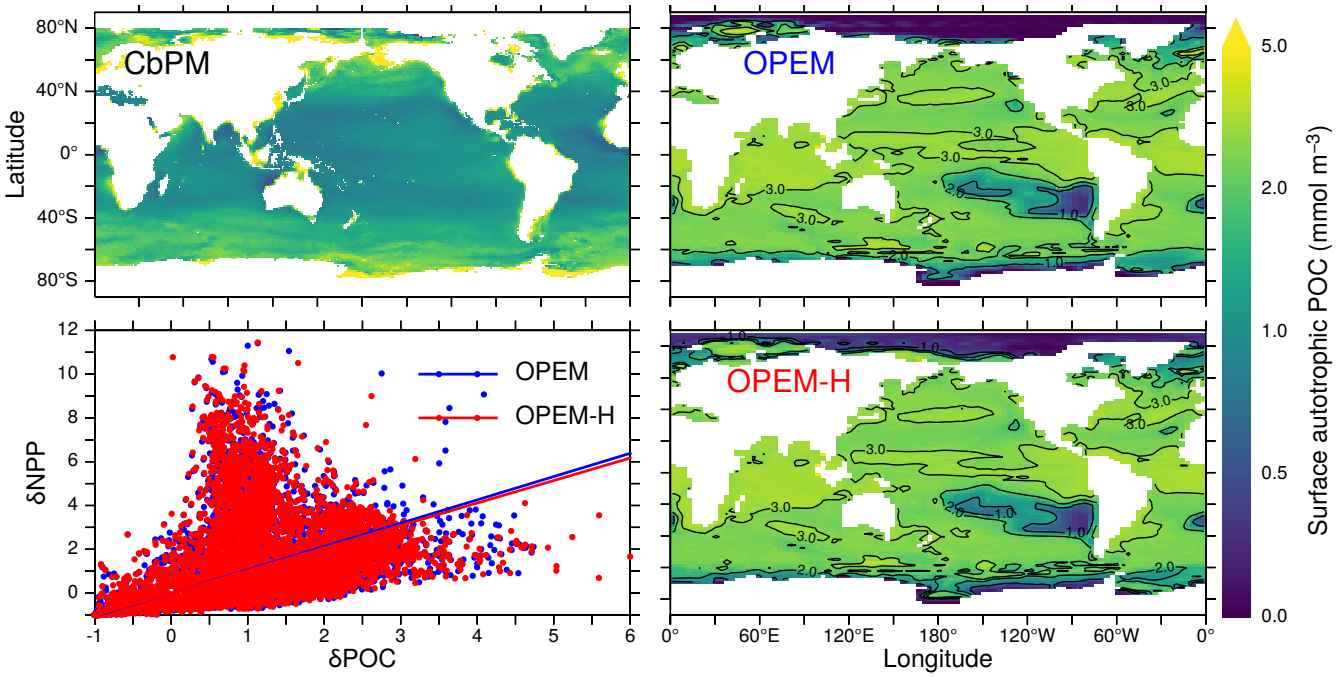

Figure 11. Annually-averaged distribution of ~~vertically-integrated net primary production~~ surface autotrophic particulate organic carbon (~~NPP~~POC) estimated from satellite data via the C-based productivity model (CbPM) and predicted from the ~~original,~~ OPEM ~~,~~ and OPEM-H UVic simulations. The contours in the right panels indicate multiples of the zooplankton feeding threshold (Π_{th}, Eq. C17), i.e. a value of 1 means that effective autotrophic POC (defined as $\phi_{phy}C_{phy} + \phi_{dia}C_{dia}$) is equal to Π_{th}. The lower left panel illustrates the relation between relative errors in vertically-integrated NPP and surface autotrophic POC (δNPP and δPOC, respectively) with respect to the CbPM data. The relative errors δx are defined as $\delta x = x_{model}/x_{CbPM} - 1$. The solid lines show the regressions forced through the origin. The slopes of these lines are 1.064 ± 0.059 ($R^2 = 0.05$, OPEM) and 1.028 ± 0.024 ($R^2 = 0.25$, OPEM-H). The satellite-based CbPM estimate is the average for ~~2012–1018~~ 1998–2007 (Westberry et al., 2008) with missing data treated as 0.

OPEM and OPEM-H, respectively, are closer to the observation-based estimate of 23 % reported by Landolfi et al. (2018), for the data from Luo et al. (2012), than any other model mentioned there.

Both OPEM and OPEM-H predict less N_2 fixation than the original UVic model in the Indian Ocean, which explains (at least partly) the differences in N* there (Fig. 5). OPEM and OPEM-H have no N_2 fixation in the northern Indian Ocean, which is an area of intense diazotrophy in the original UVic, owing the presence of diazotrophs in the original UVic and their absence in OPEM and OPEM-H in this region (Fig. 15). Other models, for example the one of Monteiro et al. (2011) also produce high rates of N_2 fixation in the northern Indian Ocean, similar to the distribution simulated by the original UVic. In contrast, Löscher et al. (2019) recently found no evidence for significant N_2 fixation in the Bay of Bengal. Whether the qualitative change towards very little N_2 fixation also in other parts of the Indian Ocean, as simulated by both OPEM and OPEM-H, is a qualitative improvement in the representation of N_2 fixation by biogeochemical ocean models, remains to be seen. OPEM-H

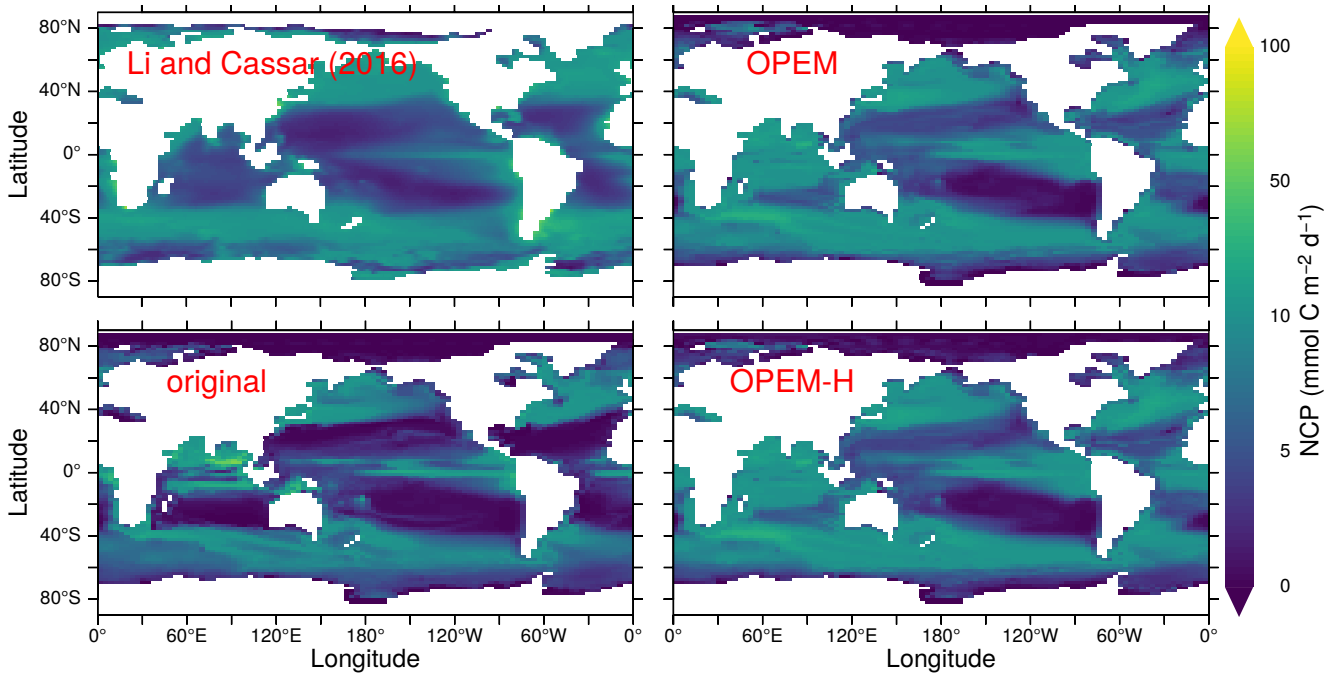

Figure 12. Annually-averaged distribution of net community production (NCP) in the upper 100 m. Global oceanic NCP is 13.5 Pg C yr^{-1} for the satellite-based estimate from Li and Cassar (2016) and 9.3, 12.9, and 13.0 Pg C yr^{-1} for the original, OPEM, and OPEM-H simulations, respectively. The data from Li and Cassar (2016) are 1997–2010 averages of their genetic-programming results for SeaWiFS, aggregated into a monthly climatology on the UVic grid and then temporally averaged with missing data treated as 0.

predicts a wider geographical range for N_2 fixation than the other UVic configurations, owing to Houlton's 2008 temperature function for diazotrophy, now occurring in a few spots north of 40°N (Fig. 13). Mulholland et al. (2019) recently reported high rates for the east coast of North America. The effect of the lower temperature function of Houlton et al. (2008) compared to the UVic temperature function for diazotrophs at high temperatures appears to be rather small, but may be the main reason for the slightly lower global N_2 fixation in OPEM-H compared to OPEM. Thus, widening the temperature range of N_2 fixation as in OPEM-H could well be a prerequisite for a more realistic representation of diazotrophy.

Comparing the distributions of simulated N* and N_2 fixation reveals a positive relation with N_2 fixation, which occurs mostly in regions with N* > 0 (Fig. 13). This pattern is very different from that in the analysis of Deutsch et al. (2007), who assumed a high PO_4^{3-} demand of diazotrophs, whereas our model does not make this assumption and actually predicts that N_2 fixation can greatly increase the competitive ability of diazotrophs at low PO_4^{3-} concentrations (Pahlow et al., 2013). Thus, in our models the rise in N* due to N_2 fixation does not destroy the niche of the diazotrophs but rather creates an environment in which their ability to utilise very low PO_4^{3-} concentrations allows them to persist. This ability derives from the absence of N limitation in the original UVic, and from the additional N allocation towards P uptake in OPEM and OPEM-H.

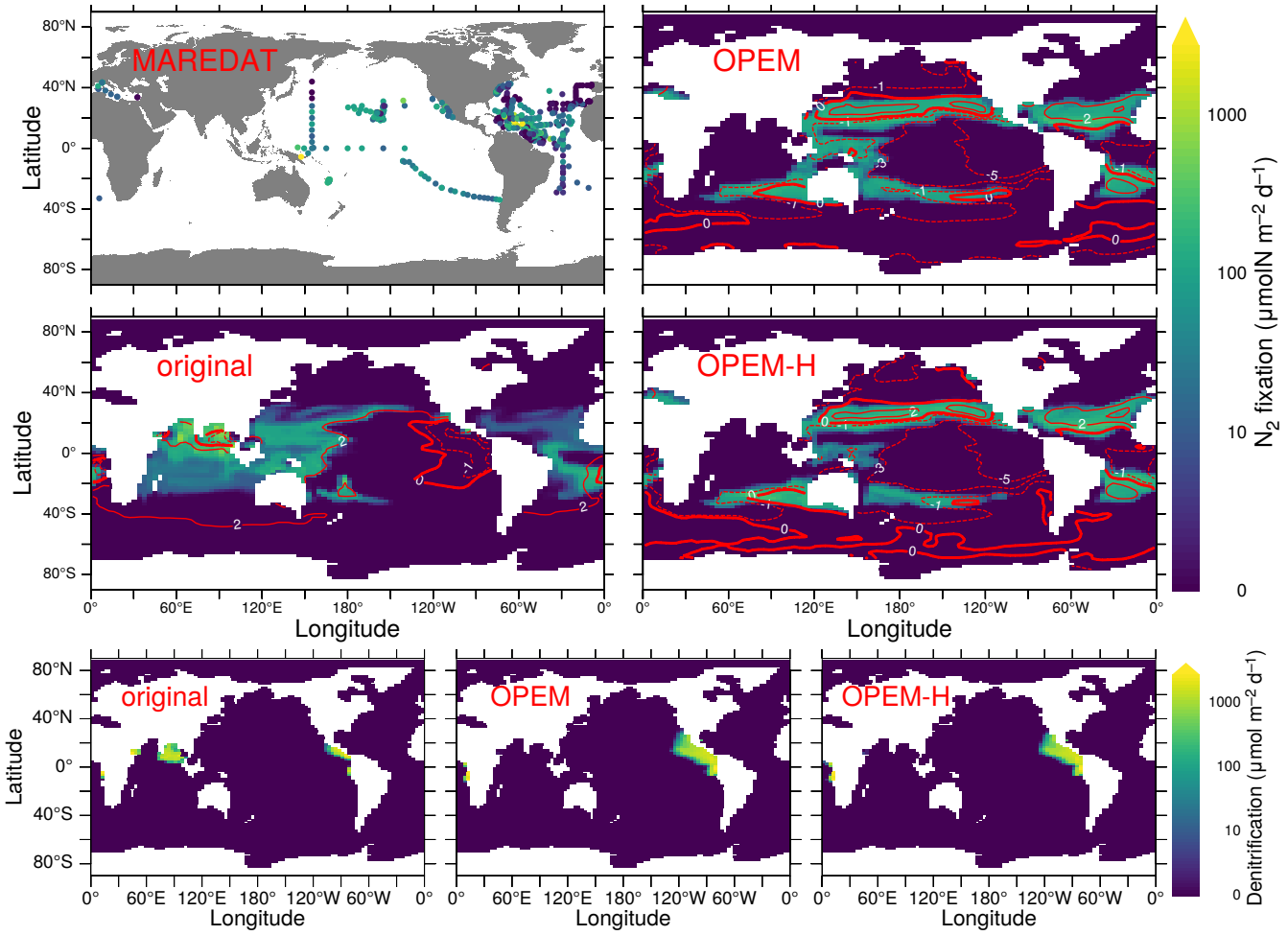

Figure 13. Top 4 panels: Annually-averaged and vertically-integrated rate of N_2 fixation in MAREDAT and the original UVic, OPEM, and OPEM-H simulations. Bottom 3 panels: Annually-averaged and vertically-integrated rate of denitrification. Global oceanic N_2 fixation (same as global denitrification in these spun-up steady-state simulations) is 53.9, 71.2, and 69.4 Tg N yr^{-1} for the original UVic, OPEM and OPEM-H, respectively. Overlaid red contours indicate surface N*. The MAREDAT data are total N_2-fixation rates from Luo et al. (2012).

~~The high competitive ability of diazotrophs can be visualised in the pattern of NO_3^-/PO_4^{3-} vs. $[PO_4^{3-}]$, where N_2 fixation can occur under high NO_3^-/PO_4^{3-} ration only when $[PO_4^{3-}]$ is low in OPEM and OPEM-H (Fig. 14). Accordingly,~~ Pahlow et al. (2013) suggested that the coexistence of ordinary and diazotrophic phytoplankton should result in a roughly inverse relation between NO_3^-/PO_4^{3-} and $[PO_4^{3-}]$, ~~which is indeed exhibited by~~ owing to the high competitive ability of diazotrophs under low NO_3^- and in particular PO_4^{3-} concentrations. This inverse relation implies that N_2 fixation can occur under high NO_3^-/PO_4^{3-} ratios only when $[PO_4^{3-}]$ is low, and is indeed observed in data from WOCE section A05 in the subtropical North Atlantic (Millero et al., 2000) ~~. The pattern of NO_3^-/PO_4^{3-} vs. $[PO_4^{3-}]$ in~~ and predicted by

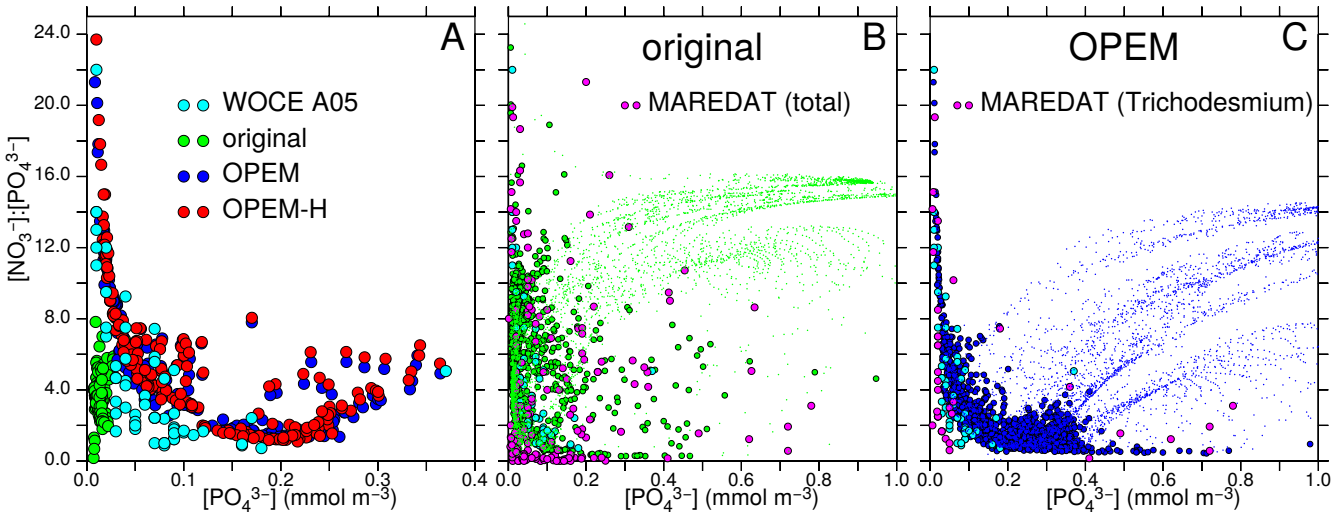

Figure 14. Patterns of surface NO_3^-/PO_4^{3-} vs. PO_4^{3-}. A Data from WOCE section A05 (Millero et al., 2000, along 24.5°N across the North Atlantic,) and results for 10°N–30°N in the North Atlantic from the original, OPEM and OPEM-H configurations. B and C Global patterns for the surface layer where $PO_4^{3-} \leq 1\,\mathrm{mmol\,m^{-3}}$ (dots), with green and blue disks highlighting results where N_2 fixation occurs in the original and OPEM simulations, respectively. The light-blue disks in B and C are the WOCE data from panel A. MAREDAT data are for locations with positive total (panel B) and *Trichodesmium* (panel C) N_2 fixation rates from Luo et al. (2012).

OPEM and OPEM-H~~in this region approximately matches that in WOCE section A05, whereas the pattern is very different in the original UVic~~, but not the original UVic, for the same region (Fig. 14A). The patterns for the global surface ocean reveal a similar inverse relation for the original UVic, albeit much less constrained than for OPEM (Fig. 14B, C). In ~~both~~ all cases, the patterns for locations with N_2 fixation are very different from those for all regions (green and blue dots in Fig. 14B, C). Whereas the pattern for the original UVic appears more similar to the pattern in the data from Luo et al. (2012) corresponding to total N_2 fixation, except where both NO_3^- and PO_4^{3-} are very low (Fig. 14B), the pattern in OPEM is closer to that where N_2 fixation by *Trichodesmium* occurs (Fig. 14C). Thus, the representation of diazotrophy still appears to warrant further investigation. While none of our UVic configurations can explain N_2 fixation occurring at very low NO_3^- and PO_4^{3-} concentrations (Fig. 14B), the physiology of N_2 fixation clearly has a strong influence on NO_3^-/PO_4^{3-} and hence N* patterns~~. Thus, the representation of diazotrophy still appears to warrant further investigation.~~, as revealed, in particular, for the clear relation between NO_3^-/PO_4^{3-} and $[PO_4^{3-}]$ for *Trichodesmium* in OPEM and observations (Fig. 14C).

Contrary to the original UVic model, we do not apply any explicit growth-rate reduction to the diazotrophs in our OPEM simulations, but we assign a lower nutrient affinity and a higher Fe half-saturation concentration to diazotrophs ($k_{\mathrm{Fe,\,dia}} > k_{\mathrm{Fe,\,phy}}$, whereas $k_{\mathrm{Fe,\,dia}} < k_{\mathrm{Fe,\,phy}}$ in the original UVic), and the model calibration yielded a higher ~~values~~ value of the prey-capture coefficients for diazotrophs ~~(Table 2, see also Chien et al. , 2019).~~ (Table 2, see also Part II, Chien et al., 2020). Both OPEM and OPEM-H have a similar phytoplankton biomass and distribution (Fig. 15). ~~Phytoplankton~~ Phytoplankton biomass

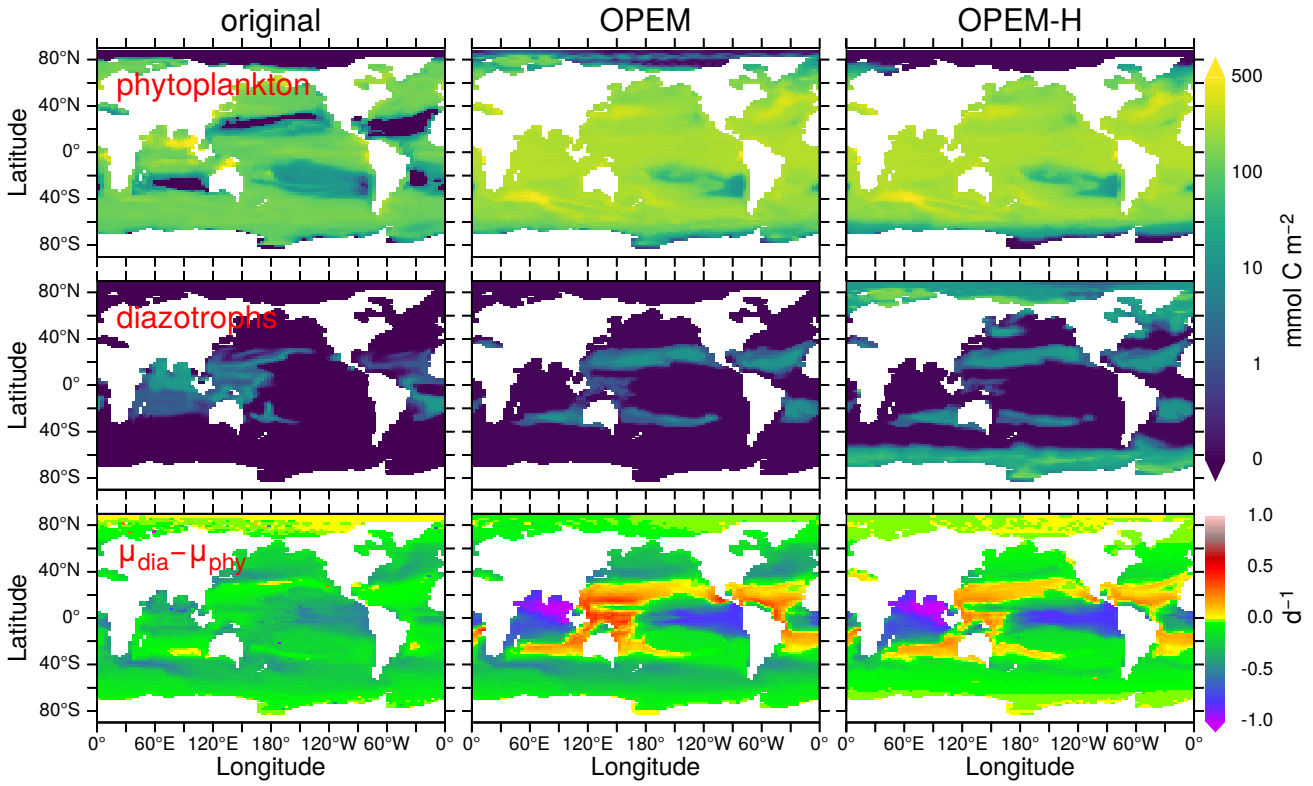

Figure 15. Vertically-integrated and temporally-averaged phytoplankton (top) and diazotroph biomass (centre) and difference between diazotroph and phytoplankton net relative growth rates (bottom), in the original, OPEM, and OPEM-H UVic simulations. Note that the positive growth-rate differences for the original UVic in the Arctic are spurious as they result from $\mu_{\mathrm{dia}} = 0\,\mathrm{d}^{-1}$ and $\mu_{\mathrm{phy}} < 0\,\mathrm{d}^{-1}$

(not Chl, see Fig. 9) is much more evenly distributed and the integrated biomass is about 2.3 times as large as in the original UVic model.

Diazotrophs are implemented as facultative and their biomass is distributed very differently in all three UVic simulations (Fig. 15). In the original UVic and OPEM, the diazotroph distribution roughly matches that of N_2 fixation, whereas prominent diazotroph biomass appears at high latitudes, even in the Arctic and Antarctic Oceans, in OPEM-H, mostly unassociated with N_2 fixation (~~cf.~~ see also Fig. 13). In fact, non-N_2 fixing diazotrophs are responsible for the improved representation of Chl, NPP, and NCP in the Arctic when compared to satellite-based estimates (Figs. 9–12) in OPEM-H, but also for the somewhat higher N* values at high latitudes compared to OPEM (Fig. 5).

The main reason why the facultative diazotrophs can populate the high latitudes in OPEM-H is their higher ~~α (~~light affinity ($\alpha = 0.5$ compared to $0.4\,\mathrm{m^2\,mol\,C\,W^{-1}\,(g\,Chl)^{-1}\,d^{-1}}$ for ordinary phytoplankton), which can overwhelm the effect of the much higher food preference for diazotrophs (compare ϕ_{dia} and ϕ_{phy}, Table 2) under light-limited conditions. A high α for diazotrophs was also obtained by Pahlow et al. (2013). In these areas, characterised by low light and high inorganic nutrient availability,

the advantage of a higher α more than compensates for the lower nutrient affinity (A_0) and higher N demand (Q_0^N) of the diazotrophs. Our interpretation of this behaviour is that the ~~OPEM models' diazotroph compartment~~ diazotroph compartment in OPEM-H actually represents two functional groups, one occurring in low latitudes, representing what we usually associate with facultative diazotrophs, and one occurring at high latitudes, representing non-N_2 fixing species adapted to low light and long periods of darkness. The (facultative) diazotrophs occur mostly where their realised net relative growth ~~rates exceed those~~ rate exceeds that of ordinary phytoplankton ($\Delta\mu > 0$, $\Delta\mu = \mu_{dia} - \mu_{phy}$) for OPEM and OPEM-H, but not for the original UVic (Fig. 13). The main reason for this discrepancy in the orignal UVic is the much lower food preference for diazotrophs (0.1) compared to ordinary phytoplankton (0.3) in this configuration, which partly decouples the competitive balance between the two autotrophic groups from $\Delta\mu$.

While the occurrence of diazotrophs in the Arctic appears helpful in view of high-latitude NPP, they are also responsible for the overestimation of N* there (Fig. 5), owing to their high N:P ratios. The C:N:P of ordinary phytoplankton in the Arctic (not shown) is close to Redfield proportions in OPEM, but this simulation fails to generate any appreciable NPP there. Although it might also be possible to explain the low N* in the Arctic with a high N:P ratio in Arctic zooplankton, we are not aware of any indication of this. Hence, phytoplankton in the Arctic appears to have a low N:P ratio and cannot be represented by our facultative diazotrophs. Low phytoplankton N:P utilisation ratios in the Arctic have been reported by, e.g., Mills et al. (2015), who also inferred high rates of benthic denitrification there. Since we have no benthic denitrification and almost no N_2 fixation in our UVic simulations, it is clear that the stoichiometric imbalance between phytoplankton and zooplankton strongly affect surface N* in the Arctic. Thus, the most likely explanation of the low Arctic N* may be the combination of benthic denitrification and phytoplankton communities dominated by species with high light affinity and a low N subsistence quota.

3.4 C:N:P ratios

Simulated ~~log-normally averaged particulate~~ log-averaged particulate (i.e. the sum of phytoplankton, diazotrophs, zooplankton, detritus) C:N and C:P ratios of both OPEM and OPEM-H are well above the canonical Redfield ratios (C:N = 6.625 mol mol^{-1} and C:P = 106 mol mol^{-1}, Table 3) in the topmost two layers. Both simulations tend to overestimate C:N ratios in the surface layer and underestimate C:P compared to observations compiled by Martiny et al. (2014), though not as much as the uniform Redfield C:P ratio employed in the original UVic model. While the data indicate increasing C:P with depth, it is lower in the second compared to the first layer in OPEM and OPEM-H (Table 3). The increasing C:P in the data may be indicative of preferential remineralisation of P relative to C and N (e.g., Letscher and Moore, 2015), which is absent in the current UVic configurations. The decline of ~~the~~ C:N and C:P with depth in UVic is the result of primary production with lower light and greater nutrient availability in the second layer. This effect may well be too strong in UVic, owing to its coarse vertical resolution, enforcing a homogeneous vertical distribution of all biological tracers within the upper 50 m.

The latitudinal patterns of the particulate C:N and C:P ratios are shown in Fig. 16. Interestingly, the simulated C:N ratios are closer to the observations in the southern hemisphere, while the simulated C:P ratios match better in the northern hemisphere. C:N ratios in the surface layer appear too high throughout, whereas those in the second layer are a lot closer to the observations, whereas C:P ratios seem to match similarly in both layers (Table 3 and Fig. 16).

Table 3. ~~Log-normally averaged~~ Log-averaged C:N and C:P ratios for the depth ranges of the upper two layers in the UVic model.

	Martiny et al. (2014)		OPEM		OPEM-H	
	C:N	C:P	C:N	C:P	C:N	C:P
$0-50\,\mathrm{m}$	7.6	148	10.0	136	9.7	133
$50-130\,\mathrm{m}$	7.4	165	7.7	125	7.4	122

Patterns of C:N ratios mirror the relation between light and nutrient limitation in our OPEM simulations, with high C:N ratios indicating strong nutrient limitation, which is also generally observed in phytoplankton culture experiments (Pahlow et al., 2013). Thus, one possible explanation for the too high particulate C:N ratios in the surface layer could be that too little nutrients reach the surface ocean at subtropical northern latitudes. This is consistent with too low rates of NPP being predicted around 20°N (Fig. 10), where the overestimation in surface C:N ratios is strongest (Fig. 16). The lower C:N ratios at high latitudes (60°S and 60°N) in OPEM-H reflect the dominance of (non-N_2 fixing) diazotrophs there in this simulation.

~~The~~ The relatively high C:N ~~and C:P ratios of~~ ratios throughout most the surface layer also largely explains the lower export efficiency, as indicated by the much higher NPP estimate (Fig. 10) relative to NCP (Fig. 12) in OPEM and OPEM-H compared to the original UVic. Since the average particulate C:N and C:P ratios are much greater in OPEM and OPEM-H than the (Redfield) C:N and C:P ratios of the zooplankton, the excess C is released in dissolved form (as CO_2) by the zooplankton according to Eq. (C15). Thus, consumption of particles with elevated C:N and/or C:P relative to the zooplankton lowers the export efficiency. While particulate C:P agrees much better with the observations than C:N, it is still on average well above the (Redfield) C:P ratio of the zooplankton, which implies that a better match of surface particulate C:N alone might not reconcile the relative magnitudes of NPP and NCP in OPEM and OPEM-H with the satellite-derived estimates. Both the high surface C:N and low P:C in mid-latitude regions might result from the underestimation of N_2 fixation, owing to the lack of benthic denitrification. Enhanced N_2 fixation would add fixed N to the surface ocean, partly releasing phytoplankton from N limitation and intensifying P limitation, and could thus bring C:N and C:P ratios closer to the observations. Further promising approaches in this respect may be the consideration of preferential remineralisation, which could allow enhanced N assimilation due to additional P availability, or allowing for variable stoichiometry in zooplankton (e.g., Talmy et al., 2014).

The C:N and C:P ratios of sinking particles (detritus) in OPEM and OPEM-H are greater than those of total particulate matter ~~, because a major source of detritus in UVic is zooplankton egestion. Since zooplankton have a~~ (Fig. 7), because the C:N:P ratio of zooplankton is 106:16:1 but that of its food is larger~~, zooplankton respire and egest~~. Zooplankton respire the excess C in the food, ~~part of which hence ends up in the detritus pool (Fig. 7).~~ thereby reducing the average particulate C:N:P, whereas the detritus pool is fed not only by zooplankton egestion but also by the phytoplankton and diazotroph mortality terms with relatively high C:N:P ratios. The magnitude of this effect is modulated by the zooplankton assimilation efficiency (E_{zoo}) as this determines the fraction of particulate egestion. In regions with high $E_{\mathrm{zoo}} \approx 1$ (Fig. 17), almost no particles are egested, whereas for $E_{\mathrm{zoo}} \approx 0.5$ about half of the ingested food ~~(plus excess C)~~ is lost to detritus. The relatively low assimilation efficiencies in the Arctic between 90°E and 120°W in OPEM-H ~~results~~ compared to OPEM in Fig. 17 result from the availability of food, as

this OPEM-H is the only simulation with any appreciable NPP (Fig. 10) and hence primary-producer biomass in this region (Fig. 15), and E_{zoo} is inversely related to ingestion in OPEM and OPEM-H. Food availability exceeds the zooplankton feeding threshold in this region only for OPEM-H (contours in Fig. 17).

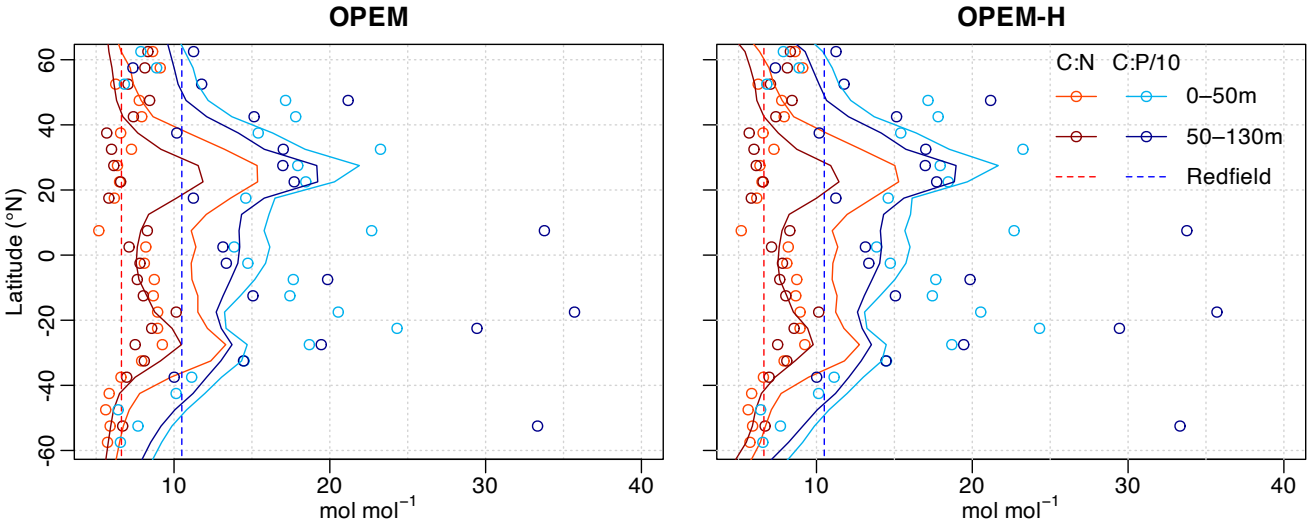

Figure 16. Zonally-averaged particulate C:N and C:P ratios for the depth ranges of the two topmost layers of UVic for 5° latitude bands. Lines are predictions from the OPEM and OPEM-H simulations and circles represent data from Martiny et al. (2014). POC < 0.01 mmol m^{-3}, PON < 1 µmol m^{-3}, and POP < 0.1 µmol m^{-3} were removed from the observations prior to calculating the ratios. Observed ratios were mapped onto the UVic grid by taking the median of all available data for each grid cell, and then log-normal zonal averages log-averages calculated.

4 Conclusions

The above description of the model behaviour highlights some of the improvements of our optimality-based (OPEM, OPEM-H) compared to the original biogeochemistry in the UVic model. Some of these may also be possible with the original UVic with improved parameters, e.g., the deep-ocean N:P distribution (Fig. 8) or a better global NCP (Fig. 12), as these vary strongly among our different parameter sets tested during the calibration process of OPEM and OPEM-H (Chien et al., 2019). (Chien et al., 2020). Others are simply impossible to reach with a fixed-stoichiometry model, e.g., the distribution of C:N and C:P ratios in particulate matter (Fig. 16). Apparently, our optimality-based biology has a certain internal rigidity (Krishna et al., 2019), preventing us from tuning the OPEM simulations so that, e.g., global NPP, NCP, and N_2-fixation distributions can simultaneously be reproduced very well with the same parameter settings. We thus try to use the resulting, and often systematic, model-data discrepancies in the behaviour of OPEM and OPEM-H as a magnifying glass on model deficiencies to identify avenues for future biogeochemical model development.

A similar difference in low-latitude NPP pattern as between the CbPM and OPEM predictions can be seen on the Ocean Productivity website (O'Malley, 2017) as resulting from the use of a polynomial (Behrenfeld and Falkowski, 1997) vs. an exponential (Eppley, 1972) temperature function, as also applied in the UVic model. The CbPM does not have a direct temperature dependence and Taucher and Oschlies (2011) found that omission of direct temperature effects on biotic processes did not reduce the ability of the UVic model to reproduce observed tracer distributions. Mechanistically, temperature effects might well be subdued under light-limiting conditions, since photochemical reactions are less temperature sensitive than most other biochemical processes. The wider temperature range for diazotrophy in OPEM-H allows for N_2 fixation north of 40°N, which ~~have~~ has been observed recently in the western North Atlantic (Mulholland et al., 2019). Therefore, investigating temperature effects could be a promising approach towards more realistic NPP and N_2-fixation rates.

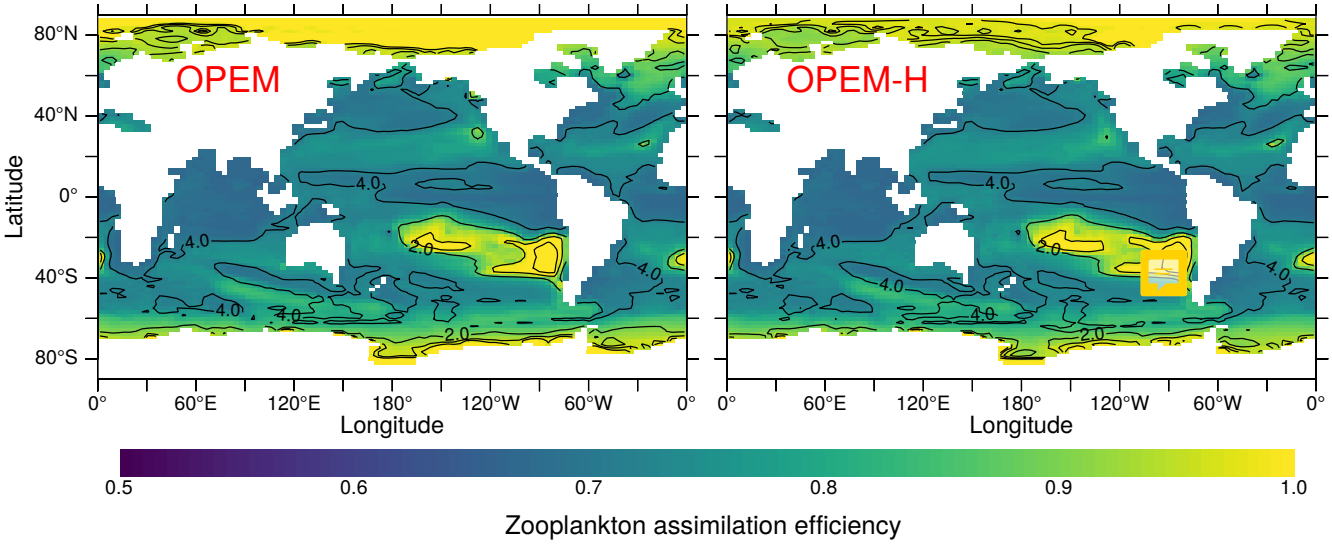

Figure 17. Annually-averaged zooplankton assimilation efficiency in the surface layer in the OPEM and OPEM-H simulations. The contours (at levels 0.5, 1, 2, 4) indicate effective food concentration (Π^C, Eq. 4) as multiples of the feeding threshold (Π_{th}, Eq. C17).

Environmental constraints on diazotrophy in our UVic simulations suffer from the absence of benthic denitrification, as mentioned above. In addition, preferential P remineralisation could be important for a better representation of N_2 fixation (Monteiro and Follows, 2012). For example, Fernández-Castro et al. (2016) found that preferential P remineralisation is essential for reproducing observed N_2 fixation rates at BATS, particularly when atmospheric deposition of fixed N is also considered. Thus, preferential P remineralisation may not only be important for improving the vertical distribution of particulate C:P (Fig. 16) but also for the simulation of diazotrophy. According to Fernández-Castro et al. (2016), this phenomenon could also be a prerequisite for realistically accounting for the effects of atmospheric deposition of nutrients into the surface ocean.

The similarity in the spatial patterns of NPP and surface autotrophic POC, also as they compare to satellite-derived estimates suggests that the growth of primary producers might be relatively well described but further developments in the representation

of top-down control by zooplankton, but also by higher trophic levels or viruses, may be another promising route towards a better resolution of plankton biogeochemical processes.

Besides temperature and top-down effects, the distributions of NPP and particulate C:N ratios are also strongly affected by light and nutrient affinity (model parameters α and A_0). The use of fixed settings in these parameters may be responsible for both overestimating NPP at low latitudes (Fig. 10) and preventing ordinary phytoplankton from growing in the Arctic Ocean (Fig. 15), as indicated by the growth of facultative (but mostly non-N_2 fixing) diazotrophs there in the OPEM-H simulation. The biotic compartments of the OPEM configurations have been shown to match the observed behaviour of at least some phytoplankton and zooplankton species (Pahlow and Prowe, 2010; Pahlow et al., 2013). Thus, the failure to obtain a better fit to the observed NPP distribution may reflect a certain rigidity, brought about by attempting to represent plankton communities by a globally uniform parameter set, i.e., one and the same combination of one phytoplankton, one diazotroph, and one zooplankton species. As mentioned above, Arteaga et al. (2016) achieved a strong improvement in model behaviour by replacing α and A_0 with a trade-off represented by opposite linear functions of light and nutrient limitation. Since our cost function does not appear to be very sensitive to α, we interpret these findings as indicating that the regional variability of α may be more important for the model behaviour than ~~the global average of α~~its global average. Similar formulations could be introduced, e.g., to represent species sorting (Norberg, 2004; Smith et al., 2016), possibly responsible for regional and local variations in α and A_0. Whether variations in these two parameters suffice, e.g., to explain the low N* in the Arctic, remains to be seen. The approach might have to be extended to further parameters for a more realistic representation of different phytoplankton and zooplankton communities (Prowe et al., 2018; Su et al., 2018). Nevertheless, it is clear from Fig. 5 that N* in the surface ocean is very sensitive to plankton physiology (subsistence quotas), which could greatly complicate inferring regional balances of N_2 fixation and denitrification from N* or similar quantities (e.g., Mills et al., 2015).

Code availability. The University of Victoria Earth System Climate Model version 2.9 is available at http://www.climate.uvic.ca/model/. The code for the Original Model and OPEM is available at https://dx.doi.org/10.3289/SW_1_2020. The instructions needed to reproduce the model results described in this article are in the supplemental material.

Appendix A: Bug fixes applied to all configurations

UVic has already contained code intended to reduce the occurrence of negative concentrations by setting all sink terms to 0 once a concentration drops below a certain threshold. ~~Thus~~ This mechanism was made partly ineffective, however, by passing positive values to the biogeochemical subroutine (`npzd_src`), even when the actual tracer concentration was negative, so that the negative concentration was not detected, or too late, and sink terms could still apply. This was corrected by passing the actual tracer values to the `npzd_src` subroutine.

The dynamic Fe model (Nickelsen et al., 2015) injects atmospheric Fe deposition directly into the surface layer, which we consider as a bug as this bypasses the surface-flux mechanism built into UVic. Correcting this bug also reduces the occurrence of negative Fe concentrations.

Appendix B: Preventing negative concentrations in OPEM

One of the main problems for implementing our variable-stoichiometry formulation in UVic's finite-difference code is the occurrence of negative concentrations in UVic. Negative concentrations occur predominantly as a result of the semi-implicit vertical mixing scheme when applied to steep vertical gradients (with smaller contributions arising from advection, the explicit isopycnal mixing scheme, and high-latitude filtering), as revealed by detailed inspection of the model's behaviour. Since the vertical gradients related to the biotic tracers in OPEM are generally much steeper, at least in the upper 3 layers of the ocean grid, negative concentrations can become much larger and more widespread in OPEM than in the original UVic. Inside its biogeochemical module, UVic deals with negative concentrations by preventing, at every time step and in every grid box, any fluxes out of negative tracer compartments, as mentioned above. UVic also applies a flux-corrected central-differencing scheme for tracer advection (flux-corrected transport, FCT, applied here also in the vertical) in order to prevent generation of negative concentrations. Negative concentrations are also generated in the main biogeochemical module of UVic (subroutine npzd_src), owing to the long time-steps (we use 0.5 times the physical time step of 30 h and, if this would generate negative tracer concentrations, subcycle with 0.25 times the physical time step) and the Euler scheme used for calculating the sources-minus-sinks terms.

For many cases (parameter settings), phytoplankton and/or diazotrophs can end up negative everywhere in OPEM, compromising our calibration procedure, which depends on the reliability of simultaneous evaluation of simulation ensembles (see Section 2.4 and Part II, Chien et al., 2020). We have addressed the problem in OPEM by limiting the biological tracer fluxes of the sub-cycled biological time step at every grid box, so that not more than 90 % of any tracer is removed within any grid box during one time step. In order to counter the generation of negative concentrations by advection and vertical mixing, we also modify the physical transport of all particulate tracers and dissolved iron as follows: The sources-minus-sinks terms of the biogeochemical module are applied before calculating advective and diffusive fluxes, so that diffusion is the only remaining source of negative concentrations. In all cases where the sum of all diffusive fluxes ($\mathcal{D}$) would remove more of a tracer than is present in a grid cell after applying advective fluxes ($\mathcal{T}$), we calculate a correction factor, $f_\mathcal{D} = -\mathcal{T}/(\mathcal{D} \times \Delta t)$, where Δt is the time step, which is then multiplied with all outward diffusive fluxes to ensure a non-negative tracer concentration. This flux limitation does not affect tracer conservation. Since limiting the flux out of one grid cell reduces the flux into the neighbouring cell, this procedure is applied recursively until non-negative concentrations are guaranteed everywhere. Whenever high-latitude filtering (Kvale et al., 2017) results in negative concentrations, we multiply positive changes $\Delta\mathcal{T}^+$ by a factor $f_\mathrm{filt} = \sum_{\mathcal{T}_\mathrm{filt} \le 0.1\mathcal{T}} (0.1\mathcal{T} - \mathcal{T}_\mathrm{filt}) / \sum \Delta\mathcal{T}^+$ and hence allow filtering-induced reductions by at most 90 %, where $\mathcal{T}_\mathrm{filt}$ is the (possibly negative) result of the high-latitude filter.

Appendix C: Optimality-based process descriptions

C1 Phytoplankton and diazotrophs

Please note that we omit the subscripts phy and dia in this subsection.

C1.1 Optimal growth regulation.

Our optimality-based formulations use allocation factors to allocate energy and other resources between light harvesting and nutrient acquisition at each grid point and time step, such that net growth of phytoplankton is maximised. The rates of net relative growth (μ), nutrient uptake (V^{N} and V^{P}), and N_2 fixation (F^{N}) in the OGM (optimal-growth model) are given by the optimality-based chain-model of Pahlow et al. (2013), modified here to allow for temperature dependence and Fe limitation and to avoid out-growing the P subsistence quota during transition towards P limitation. Net relative growth rate is the difference between C fixation (V^{C}) and the sum of respiration (R) and extra dissolved inorganic C (DIC) release (r_{DIC}, see below) to prevent outgrowing the P subsistence quota. The chain model idea is based on the roles of N and P in a phytoplankton cell, where P is mainly needed for N assimilation and N drives all other biochemical rates (Ågren, 2004), including growth. Thus, the optimal regulation can be described in terms of two conceptual levels, with the lower level consisting of the nutrient-uptake apparatus and the chloroplast, and the upper level being the whole cell. Within the nutrient-uptake apparatus, cellular N is allocated between N and P uptake so as to maximise N assimilation (see Section C1.2 below). Since the role of P is restricted to the nutrient-uptake apparatus in this model, we can ignore P in the formulation of the optimal allocation scheme at the whole-cell level:

$$\mu = V^{\mathrm{C}} - R - r_{\mathrm{DIC}} = V^{\mathrm{C}} - R^{\mathrm{Chl}} - \zeta^{\mathrm{N}} V^{\mathrm{N}} - r_{\mathrm{DIC}}, \qquad R = R^{\mathrm{Chl}} + \zeta^{\mathrm{N}} V^{\mathrm{N}} \tag{C1}$$

$$V^{\mathrm{C}} = L_{\mathrm{day}} \cdot V_0^{\mathrm{C}}(T) \cdot f_{\mathrm{C}} \cdot S_I, \qquad R^{\mathrm{Chl}} = [L_{\mathrm{day}} V_0^{\mathrm{C}}(T) \cdot \overline{S}_{\mathrm{I}} + f(T) \cdot R_{\mathrm{M}}^{\mathrm{Chl}}] \cdot \zeta^{\mathrm{Chl}} \cdot \theta \tag{C2}$$

We collect all N-independent gain and loss terms in μ^*,

$$\mu^* = L_{\mathrm{day}} \cdot V_0^{\mathrm{C}}(T) \cdot \overline{S}_{\mathrm{I}} \cdot (1 - \zeta^{\mathrm{Chl}} \hat{\theta}) - f(T) \cdot R_{\mathrm{M}}^{\mathrm{Chl}} \cdot \zeta^{\mathrm{Chl}} \cdot \hat{\theta}, \qquad \hat{\theta} = \frac{\mathrm{Chl{:}C}}{f_{\mathrm{C}}} \tag{C3}$$

$$\Rightarrow \quad \mu = f_{\mathrm{C}} \cdot \mu^* - f_{\mathrm{V}} \cdot \zeta^{\mathrm{N}} \cdot \widehat{V}^{\mathrm{N}} - r_{\mathrm{DIC}}, \qquad f_{\mathrm{C}} = 1 - \frac{1}{2}\frac{Q_0^{\mathrm{N}}}{Q^{\mathrm{N}}} - f_{\mathrm{V}}, \quad f_{\mathrm{V}} = \frac{1}{2}\frac{Q_0^{\mathrm{N}}}{Q^{\mathrm{N}}} - \zeta^{\mathrm{N}} \cdot (Q^{\mathrm{N}} - Q_0^{\mathrm{N}}) \tag{C4}$$

where the allocation factors f_{C} and f_{V} ensure optimal allocation of cellular N between C fixation and nutrient uptake, respectively (see Pahlow et al., 2013, for derivation), $f(T)$ is temperature dependence, L_{day} is day length, V_0^{C} the temperature- and Fe-dependent maximum potential rate for C processing, α the light-absorption coefficient (light affinity), $\hat{\theta}$ the Chl:C ratio of the chloroplast, I irradiance, ζ^{Chl} and ζ^{N} the costs of Chl synthesis and N assimilation, R^{Chl} the cost of Chl synthesis and maintenance, $R_{\mathrm{M}}^{\mathrm{Chl}}$ the cost of Chl maintenance, and $\overline{S}_{\mathrm{I}}$ the depth- and time-averaged light saturation of the photosynthetic

apparatus. $\overline{S}_{\mathrm{I}}$ is calculated assuming a triangular light cycle and constant light attenuation within a grid cell:

$$\overline{S}_{\mathrm{I}} = \frac{1}{\Delta z}\int_0^1\int_0^{\Delta z} 1-\mathrm{e}^{-\alpha^*\cdot I(z)\cdot x}\mathrm{d}z\mathrm{d}x, \qquad I(z)=I_0\mathrm{e}^{-\epsilon z}, \qquad \alpha^*=\frac{\alpha\hat{\theta}}{V_0^{\mathrm{C}}(T)} \tag{C5}$$

$$= 1-\frac{\mathrm{Ei}(-2\alpha^*I_0)-\mathrm{Ei}[-2\alpha^*I(\Delta z)]}{\epsilon\cdot\Delta z}-\frac{(1-\mathrm{e}^{-2\alpha^*I(\Delta z)})/I(\Delta z)-(1-\mathrm{e}^{-2\alpha^*I_0})/I_0}{2\alpha^*\cdot\epsilon\cdot\Delta z} \tag{C6}$$

where I_0 and $I(\Delta z)$ are the mean daytime light intensities at the top and bottom of the current grid cell of height Δz, ϵ is the light-attenuation coefficient, Ei is the exponential-integral function, and the factor 2 converts the mean to the maximum irradiance in the triangular light cycle. As in the original UVic code, we assume that $\epsilon \propto \mathrm{N_{phy}}+\mathrm{N_{dia}}+$absorption by seawater, since chlorophyll is not a tracer. Eqs. (C5) and (C6) apply only for $I > I_{\min}$, where $I_{\min}=\zeta^{\mathrm{Chl}}R_{\mathrm{M}}^{\mathrm{Chl}}f(T)/(\alpha L_{\mathrm{day}})$ is the minimum light intensity for photosynthesis (see Pahlow et al., 2013). Thus, for $I_0 > I_{\min} > I(\Delta z)$, (C6) is applied to the part of the grid-cell where $I > I_{\min}$ and then multiplied with $\Delta z^*/\Delta z$, where $I(\Delta z^*)=I_{\min}$. In effect, this means that $\overline{S}_{\mathrm{I}} > 0$ occurs only in the upper 240 m (the top 3 layers) of the ~~Uvic~~ UVic grid.

C1.2 Optimal uptake kinetics.

DIN and DIP uptake and $\mathrm{N_2}$ fixation are defined as products of allocation factors, setting the size of the respective cellular compartment, and the rate of uptake normalized to the size of that compartment ($\widehat{V}$). $\widehat{V}$ is defined in Eq. C8 via optimal uptake kinetics (Pahlow, 2005; Smith et al., 2009). The size of the nutrient-uptake compartment, responsible for DIN and DIP uptake and $\mathrm{N_2}$ fixation, contains fraction f_{V} of the cellular N resources, of which fraction f_{N} is available for DIN uptake, leaving $f_{\mathrm{V}}(1-f_{\mathrm{N}})$ for DIP uptake:

$$V^{\mathrm{N}}=f_{\mathrm{V}}f_{\mathrm{N}}(1-f_{\mathrm{F}})\widehat{V}^{\mathrm{N}}, \qquad V^{\mathrm{P}}=f_{\mathrm{V}}(1-f_{\mathrm{N}})\widehat{V}^{\mathrm{P}}, \qquad F^{\mathrm{N}}=f_{\mathrm{V}}f_{\mathrm{N}}f_{\mathrm{F}}F_0^{\mathrm{N}}(T)\left(1-\frac{Q_0^{\mathrm{P}}}{Q^{\mathrm{P}}}\right) \tag{C7}$$

$$\widehat{V}^{\mathrm{N}}=\left(\sqrt{\frac{1}{V_{\max}^{\mathrm{N}}}}+\sqrt{\frac{1}{A_0\,\mathrm{DIN}}}\right)^{-2}, \qquad \widehat{V}^{\mathrm{P}}=\left(\sqrt{\frac{1}{V_0^{\mathrm{P}}(T)}}+\sqrt{\frac{1}{A_0\,\mathrm{DIP}}}\right)^{-2}, \qquad V_{\max}^{\mathrm{N}}=V_0^{\mathrm{N}}(T)\left(1-\frac{Q_0^{\mathrm{P}}}{Q^{\mathrm{P}}}\right) \tag{C8}$$

$$f_{\mathrm{N}}=\frac{1}{1+\sqrt{\frac{Q_0^{\mathrm{P}}}{Q^{\mathrm{P}}}\frac{V_0^{\mathrm{N}}(T)}{\widehat{V}^{\mathrm{P}}}\left(\frac{\widehat{V}^{\mathrm{N}}}{V_{\max}^{\mathrm{N}}}\right)^{1.5}}}, \qquad f_{\mathrm{F}}=\begin{cases}1 & \text{if} \quad V^{\mathrm{N}}(f_{\mathrm{F}}=0) < F^{\mathrm{N}}(f_{\mathrm{F}}=1)\\ 0 & \text{if} \quad V^{\mathrm{N}}(f_{\mathrm{F}}=0) \geq F^{\mathrm{N}}(f_{\mathrm{F}}=1)\end{cases} \tag{C9}$$

where A_0 is nutrient affinity and f_{F} the allocation for $\mathrm{N_2}$ fixation within the nutrient-uptake compartment. The allocation factor f_{F} is implemented as a switch, so that the facultative diazotrophs either fix $\mathrm{N_2}$ or utilize DIN (see Pahlow et al., 2013, for derivation). The dependence of $V_{\max}$ and F^{N} on Q^{P} introduces a chain of limitations, where the P quota limits N uptake and N limits all other processes. Extra DIC release (r_{DIC}) during transition towards severe P limitation prevents outgrowing of the P subsistence quota (Q_0^{P}):

$$r_{\mathrm{DIC}}=\max\left[(V^{\mathrm{C}}-R)\frac{Q_0^{\mathrm{P}}}{Q^{\mathrm{P}}}-\frac{V^{\mathrm{P}}}{Q_0^{\mathrm{P}}},0\right]\cdot\max\left(2-\frac{Q^{\mathrm{P}}}{Q_0^{\mathrm{P}}},0\right) \tag{C10}$$

where the first term limits r_{DIC} to conditions of declining Q^{P} and the second term states that $r_{\mathrm{DIC}} > 0$ occurs only for $Q^{\mathrm{P}} < 2Q^{\mathrm{P}}_0$. Eq. (C10) is an admittedly rather arbitrary measure to stabilise the OGM, but it did result in reasonable rates of DOC production in a previous study (Fernández-Castro et al., 2016).

C1.3 Temperature and Fe limitation

Temperature and Fe limitation are implemented by

$$V_0^{\mathrm{C}}(T) = V_0^{\mathrm{N}}(T) = f_p(T) \cdot S_{\mathrm{Fe}} \cdot V_0, \qquad V_0^{\mathrm{P}}(T) = f_p(T) \cdot V_0, \qquad F_0^{\mathrm{N}}(T) = f_{\mathrm{nfix}}(T) \cdot S_{\mathrm{Fe}} \cdot F_0 \qquad p \in \{\mathrm{phy}, \mathrm{dia}\} \tag{C11}$$

$$\lambda_{\mathrm{phy}} = \lambda_{0,\mathrm{phy}} \cdot f_{\mathrm{phy}}(T) \qquad M_{\mathrm{dia}} = M_{0,\mathrm{dia}} \cdot f_{\mathrm{dia}}(T) \tag{C12}$$

where V_0 is the potential-rate parameter, F_0 the potential rate of N_2 fixation, $f_p(T)$ the group-specific temperature dependence of nutrient uptake and photosynthesis, $f_{\mathrm{dia}}(T)$ the temperature dependence of N_2 fixation and S_{Fe} the Fe limitation term.

C2 Zooplankton

Net growth (μ_{zoo}) is described in terms of total ($\mathcal{A}_{\mathrm{t}}$, see Eq. C18 below) and foraging activity ($\mathcal{A}_{\mathrm{f}}$), and corrected for r_{Q}:

$$\mu_{\mathrm{zoo}} = (E_{\mathrm{zoo}} \cdot g_{\mathrm{zoo}} - R^*_{\mathrm{zoo}}) \cdot r_{\mathrm{Q}}, \qquad g_{\mathrm{zoo}} = \mathcal{A}_{\mathrm{f}} \cdot S_{\mathrm{g}}, \quad S_{\mathrm{g}} = 1 - \exp\left(-\Pi^{\mathrm{C}}\right) \tag{C13}$$

$$E_{\mathrm{zoo}} = E_{\max}\left[1 - \exp\left(\frac{\mathcal{A}_{\mathrm{t}}}{\mathcal{A}_{\mathrm{f}}} - \beta - \frac{\mathcal{A}_{\mathrm{t}}}{\mathcal{A}_{\mathrm{f}}}\right)\right], \qquad X^{\mathrm{C}}_{\mathrm{zoo}} = g_{\mathrm{zoo}}(1 - E_{\mathrm{zoo}}) \cdot \mathrm{C}_{\mathrm{zoo}}, \quad X^{n}_{\mathrm{zoo}} = R^{n}_{\mathrm{zoo}} \cdot \frac{X^{\mathrm{C}}_{\mathrm{zoo}}}{R^{\mathrm{C}}_{\mathrm{zoo}}} \tag{C14}$$

$$R^*_{\mathrm{zoo}} = c_{\mathrm{a}} \cdot E_{\mathrm{zoo}} \cdot g_{\mathrm{zoo}} + c_{\mathrm{f}} \cdot \mathcal{A}_{\mathrm{f}} + f_{\mathrm{zoo}}(T) \cdot R^{\mathrm{M}}_{\mathrm{zoo}}, \qquad R^{\mathrm{C}}_{\mathrm{zoo}} = (E_{\mathrm{zoo}} \cdot g_{\mathrm{zoo}} - \mu_{\mathrm{zoo}}) \cdot \mathrm{C}_{\mathrm{zoo}} \tag{C15}$$

$$R^{n}_{\mathrm{zoo}} = \frac{g_{\mathrm{zoo}} \cdot \mathrm{C}_{\mathrm{zoo}} \cdot \dfrac{\Pi^{n}}{\Pi^{\mathrm{C}}} - \mu_{\mathrm{zoo}} \cdot n_{\mathrm{zoo}}}{1 + \dfrac{X^{\mathrm{C}}_{\mathrm{zoo}}}{R^{\mathrm{C}}_{\mathrm{zoo}}}}, \quad n \in \{\mathrm{N}, \mathrm{P}\} \tag{C16}$$

where $\mathrm{C}_{\mathrm{zoo}} = 6.625 \cdot \mathrm{N}_{\mathrm{zoo}}$ and $\mathrm{N}_{\mathrm{zoo}}$ are zooplankton POC and PON, μ_{zoo} net relative growth rate, $G^{\mathrm{N}}_{\mathrm{zoo}}$ predation on zooplankton, M_{zoo} (quadratic) mortality, $Q^{\mathrm{N}}_{\mathrm{zoo}}$ N:C ratio, g_{zoo} relative ingestion rate, E_{zoo} and $E_{\max}$ actual and maximal assimilation efficiency, $X^{\mathrm{C}}_{\mathrm{zoo}}$ egestion, R^*_{zoo} and $R^{\mathrm{C}}_{\mathrm{zoo}}$ minimal (uncorrected for r_{Q}) and actual respiration, R^{n}_{zoo} metabolic N and P losses, β digestion coefficient, c_{a} and c_{f} cost of assimilation and foraging coefficients, and $R^{\mathrm{M}}_{\mathrm{zoo}}$ maintenance respiration. The same relation between dissolved and particulate losses applies for N and P as for C in (C16). Eqs. (C13)–(C15) define the benefits (g_{zoo}) and costs (E_{zoo} and R^*_{zoo}) of foraging, whence the optimal foraging activity is obtained as

$$\mathcal{A}_{\mathrm{f}} = \begin{cases} \dfrac{\mathcal{A}_{\mathrm{t}}}{-1 - W_{-1}\left(\left[\dfrac{c_{\mathrm{f}}}{S_{\mathrm{g}} E_{\max}(1 - c_{\mathrm{a}})} - 1\right] \mathrm{e}^{-(1+\beta)}\right)} & \text{if } \Pi^{\mathrm{C}} > \Pi_{\mathrm{th}} \\ 0 & \text{if } \Pi^{\mathrm{C}} \le \Pi_{\mathrm{th}} \end{cases}, \qquad \Pi_{\mathrm{th}} = \ln \frac{1}{1 - \dfrac{c_{\mathrm{f}}}{E_{\max}(1 - c_{\mathrm{a}})}} \tag{C17}$$

where W_{-1} is Lambert's W-function and Π_{th} is the feeding threshold. $\mathcal{A}_{\text{t}}$ is a function of the maximal ingestion rate ($g_{\max}$) and temperature:

$$\mathcal{A}_{\text{t}} = g_{\max} \cdot f_{\text{zoo}}(T) \left\{ -1 - W_{-1} \left(\left[\frac{c_{\text{f}}}{E_{\max}(1 - c_{\text{a}})} - 1 \right] \text{e}^{-(1+\beta)} \right) \right\} \tag{C18}$$

The predation rates for individual prey types are

$$G_p^{\text{C}} = \frac{\phi_p \text{C}_p}{\Pi^{\text{C}}} \cdot g_{\text{zoo}} \cdot \text{C}_{\text{zoo}}, \qquad \text{C}_{\text{zoo}} = \frac{\text{N}_{\text{zoo}}}{Q_{\text{zoo}}^{\text{N}}}, \qquad G_p^{\text{N}} = G_p^{\text{C}} \cdot Q_p^{\text{N}}, \qquad G_p^{\text{P}} = G_p^{\text{C}} \cdot Q_p^{\text{P}}, \qquad p \in \{\text{phy, dia, det, zoo}\} \tag{C19}$$

Eqs. (4) and (C13)–(C16) stipulate that most of the excess C, N, or P rejected to maintain homeostasis is released in dissolved inorganic form (~~cf.~~ see Eqs. C13 and C15). This is because the actual growth rate μ_{zoo} is obtained as the product of r_{Q} and the potential growth rate, i.e., that obtained for food with the same stoichiometry as the zooplankton in Eq. (C13), and respiration $R_{\text{zoo}}^{\text{C}}$ is then derived from μ_{zoo} in Eq. (C15), whereas egestion $X_{\text{zoo}}^{\text{C}}$ is not affected by r_{Q} in Eq. (C13). Since the relation of dissolved and particulate N and P losses follows that for C (X_{zoo}^{n} in Eq. C13), a stoichiometric imbalance between zooplankton and its food increases dissolved losses for N and P as well.

Author contributions. L. Arteaga and M. Pahlow implemented the optimality-based formulations in the UVic. M. Pahlow and C.-T. Chien performed the ensemble solutions and selected the reference simulations. All authors contributed to the manuscript text.

Competing interests. The authors declare that they have no conflict of interest.

Acknowledgements. We wish to thank K. Meissner for very helpful advice during the model implementation, W. Koeve for documenting many of UVic's preprocessor options, and I. Kriest and C. Somes for examining the deep-ocean DIN:DIP gradients in their model simulations. The manuscript has benefitted strongly from the reviews by D. Talmy, E. Zakem, and an anonymous referee. M. Pahlow was supported by Deutsche Forschungsgemeinschaft (DFG) by the SFB754 (Sonderforschungsbereich 754 "Climate-Biogeochemistry Interactions in the Tropical Ocean", www.sfb754.de) and as part of the Priority Programme 1704 (DynaTrait). M. Pahlow and C.-T. Chien were supported by the BMBF-funded project PalMod. L. Arteaga was partially supported by the 2014 miniproposal award from the Integrated School of Ocean Sciences (ISOS) Kiel, and by NASA under award NNX17AI73G.

References

Ågren, G. I.: The C : N : P stoichiometry of autotrophs – theory and observations, Ecol. Lett., 7, 185–191, https://doi.org/10.1111/j.1461-0248.2004.00567.x, 2004.

Anderson, L. A. and Sarmiento, J. L.: Redfield ratios of remineralization determined by nutrient data analysis, Global Biogeochem. Cycles, 8, 65–80, https://doi.org/10.1029/93GB03318, 1994.

Arora, V. K., Katavouta, A., Williams, R. G., Jones, C. D., Brovkin, V., Friedlingstein, P., Schwinger, J., Bopp, L., Boucher, O., Cadule, P., and et al.: Carbon-concentration and carbon-climate feedbacks in CMIP6 models, and their comparison to CMIP5 models, Biogeosciences Discuss., https://doi.org/10.5194/bg-2019-473, 2019.

Arteaga, L., Pahlow, M., and Oschlies, A.: Global patterns of phytoplankton nutrient and light colimitation inferred from an optimality-based model, Global Biogeochem. Cycles, 28, https://doi.org/10.1002/2013GB004668, 2014.

Arteaga, L., Pahlow, M., and Oschlies, A.: Modelled Chl:C ratio and derived estimates of phytoplankton carbon biomass and its contribution to total particulate organic carbon in the global surface ocean, Global Biogeochem. Cycles, 30, https://doi.org/10.1002/2016GB005458, 2016.

Behrenfeld, M. J. and Falkowski, P. G.: Photosynthetic rates derived from satellite-based chlorophyll concentration, Limnol. Oceanogr., 42, 1–20, https://doi.org/10.4319/lo.1997.42.1.0001, 1997.

Bopp, L., Resplandy, L., Orr, J. C., Doney, S. C., Dunne, J. P., Gehlen, M., Halloran, P., Heinze, C., Ilyina, T., Seferian, R., Tjiputra, J., and Vichi, M.: Multiple stressors of ocean ecosystems in the 21st century: projections with CMIP5 models, Biogeosciences, 10, 6225–6245, https://doi.org/10.5194/bg-10-6225-2013, 2013.

Carr, M.-E., Friedrichs, M. A., Schmeltz, M., Noguchi Aita, M., Antoine, D., Arrigo, K. R., Asanuma, I., Aumont, O., Barber, R., Behrenfeld, M., et al.: A comparison of global estimates of marine primary production from ocean color, Deep-Sea Res. II, 53, 741–770, https://doi.org/10.1016/j.dsr2.2006.01.028, 2006.

Chen, B. and Smith, S. L.: Optimality-based approach for computationally efficient modeling of phytoplankton growth, chlorophyll-to-carbon, and nitrogen-to-carbon ratios, Ecol. Model., 385, 197–212, https://doi.org/10.1016/j.ecolmodel.2018.08.001, 2018.

Chien, C.-T., Pahlow, M., Schartau, M., and Oschlies, A.: Optimality-Based Non-Redfield Plankton-Ecosystem Model (OPEMv1.0) in the UVic-ESCM 2.9. Part II: Sensitivity Analysis and Model Calibration, Geosci. Model Dev. Discuss., 2020, https://doi.org/10.5194/gmd-2019-324, 2020.

Danabasoglu, G., Lamarque, J., Bacmeister, J., Bailey, D. A., DuVivier, A. K., Edwards, J., Emmons, L. K., Fasullo, J., Garcia, R., Gettelman, A., and et al.: The Community Earth System Model Version 2 (CESM2), J. Adv. Model. Earth Syst., 12, https://doi.org/10.1029/2019ms001916, 2020.

Deutsch, C., Sarmiento, J. L., Sigman, D. M., Gruber, N., and Dunne, J. P.: Spatial coupling of nitrogen inputs and losses in the ocean, Nature, 445, 163–167, https://doi.org/10.1038/nature05392, 2007.

DeVries, T. and Weber, T.: The export and fate of organic matter in the ocean: New constraints from combining satellite and oceanographic tracer observations, Global Biogeochem. Cycles, 31, 535–555, https://doi.org/10.1002/2016GB005551, 2017.

DeVries, T., Deutsch, C., Primeau, F., Chang, B., and Devol, A.: Global rates of water-column denitrification derived from nitrogen gas measurements, Nature Geosci., 5, 547–550, https://doi.org/10.1038/ngeo1515, 2012.

Dunne, J. P., Armstrong, R. A., Gnanadesikan, A., and Sarmiento, J. L.: Empirical and mechanistic models for the particle export ratio, Global Biogeochem. Cycles, 19, GB4026, https://doi.org/10.1029/2004GB002390, 2005.

Dunne, J. P., John, J. G., Adcroft, A. J., Griffies, S. M., Hallberg, R. W., Shevliakova, E., Stouffer, R. J., Cooke, W., Dunne, K. A., Harrison, M. J., and et al.: GFDL's ESM2 Global Coupled Climate–Carbon Earth System Models. Part I: Physical Formulation and Baseline Simulation Characteristics, J. Clim., 25, 6646–6665, https://doi.org/10.1175/jcli-d-11-00560.1, 2012.

Eby, M., Zickfeld, K., Montenegro, A., Archer, D., Meissner, K. J., and Weaver, A. J.: Lifetime of Anthropogenic Climate Change: Millennial Time Scales of Potential CO_2 and Surface Temperature Perturbations, J. Clim., 22, 2501–2511, https://doi.org/10.1175/2008JCLI2554.1, 2009.

Eby, M., Weaver, A. J., Alexander, K., Zickfeld, K., Abe-Ouchi, A., Cimatoribus, A. A., Crespin, E., Drijfhout, S. S., Edwards, N. R., Eliseev, A. V., Feulner, G., Fichefet, T., Forest, C. E., Goosse, H., Holden, P. B., Joos, F., Kawamiya, M., Kicklighter, D., Kienert, H., Matsumoto, K., Mokhov, I. I., Monier, E., Olsen, S. M., Pedersen, J. O. P., Perrette, M., Philippon-Berthier, G., Ridgwell, A., Schlosser, A., von Deimling, T. S., Shaffer, G., Smith, R. S., Spahni, R., Sokolov, A. P., Steinacher, M., Tachiiri, K., Tokos, K., Yoshimori, M., Zeng, N., and Zhao, F.: Historical and idealized climate model experiments: an intercomparison of Earth system models of intermediate complexity, Clim. Past, 9, 1111–1140, https://doi.org/10.5194/cp-9-1111-2013, 2013.

Eppley, R. W.: Temperature and phytoplankton growth in the sea, Fish. Bull., 70, 1063–1085, 1972.

Fernández-Castro, B., Pahlow, M., Mouriño-Carballido, B., Marañón, E., and Oschlies, A.: Optimality-based *Trichodesmium* Diazotrophy in the North Atlantic Subtropical Gyre, J. Plankton Res., 38, 946–963, https://doi.org/10.1093/plankt/fbw047, 2016.

Garcia, H. E., Locarnini, R. A., Boyer, T. P., Antonov, J. I., Mishonov, A. V., Baranova, O. K., Zweng, M. M., Reagan, J. R., and Johnson, D. R.: Dissolved Oxygen, Apparent Oxygen Utilization, and Oxygen Saturation, in: World Ocean Atlas 2013, edited by Levitus, S., vol. 3, NOAA Atlas NESDIS 75, https://doi.org/http://www.nodc.noaa.gov/OC5/indprod.html, 2013a.

Garcia, H. E., Locarnini, R. A., Boyer, T. P., Antonov, J. I., Mishonov, A. V., Baranova, O. K., Zweng, M. M., Reagan, J. R., and Johnson, D. R.: Dissolved Inorganic Nutrients (phosphate, nitrate, silicate), in: World Ocean Atlas 2013, edited by Levitus, S., vol. 4, NOAA Atlas NESDIS 76, https://doi.org/http://www.nodc.noaa.gov/OC5/indprod.html, 2013b.

Getzlaff, J. and Dietze, H.: Effects of increased isopycnal diffusivity mimicking the unresolved equatorial intermediate current system in an earth system climate model, Geophys. Res. Lett., 40, 2166–2170, https://doi.org/10.1002/grl.50419, 2013.

Gismervik, I.: Numerical and functional responses of choreo- and oligotrich planktonic ciliates, Aquat. Microb. Ecol., 40, 163–173, https://doi.org/10.3354/ame040163, 2005.

Gruber, N.: The dynamics of the marine nitrogen cycle and its influence on atmospheric CO_2 variations, in: The Ocean Carbon Cycle and Climate, edited by Follows, M. and Oguz, T., pp. 97–148, Kluwer, 2004.

Gruber, N. and Sarmiento, J. L.: Global Patterns of marine nitrogen fixation and denitrification, Global Biogeochem. Cycles, 11, 235–266, https://doi.org/10.1029/97GB00077, 1997.

Holling, C. S. and Buckingham, S.: A behavioral model of predator-prey functional responses, Behav. Sci., 21, 183–195, https://doi.org/10.1002/bs.3830210305, 1976.

Houlton, B. Z., Wang, Y.-P., Vitousek, P. M., and Field, C. B.: A unifying framework for dinitrogen fixation in the terrestrial biosphere, Nature, 454, 327–330, https://doi.org/10.1038/nature07028, 2008.

Hu, C., Lee, Z., and Franz, B.: Chlorophyll a algorithms for oligotrophic oceans: A novel approach based on three-band reflectance difference, J. Geophys. Res. Oceans, 117, https://doi.org/10.1029/2011jc007395, 2012.

Hülse, D., Arndt, S., Wilson, J. D., Munhoven, G., and Ridgwell, A.: Understanding the causes and consequences of past marine carbon cycling variability through models, Earth Sci. Rev., 171, 349–382, https://doi.org/10.1016/j.earscirev.2017.06.004, 2017.

IPCC: Climate Change 2013: The Physical Science Basis. Contribution of Working Group I to the Fifth Assessment Report of the Intergovernmental Panel on Climate Change, Cambridge, 2013.

Keller, D. P., Oschlies, A., and Eby, M.: A new marine ecosystem model for the University of Victoria Earth System Climate Model, Geosci. Model Dev., 5, 1195–1220, https://doi.org/10.5194/gmd-5-1195-2012, 2012.

Keller, D. P., Lenton, A., Scott, V., Vaughan, N. E., Bauer, N., Ji, D., Jones, C. D., Kravitz, B., Muri, H., and Zickfeld, K.: The Carbon Dioxide Removal Model Intercomparison Project (CDRMIP): rationale and experimental protocol for CMIP6, Geosci. Model Dev., 11, 1133–1160, https://doi.org/10.5194/gmd-11-1133-2018, 2018.

Key, R., Olsen, A., van Heuven, S., Lauvset, S. K., Velo, A., Lin, X., Schirnick, C., Kozyr, A., Tanhua, T., Hoppema, M., Jutterström, S., Steinfeldt, R., Jeansson, E., Ishi, M., Perez, F. F., and Suzuki, T.: Global Ocean Data Analysis Project, Version 2 (GLODAPv2), ORNL/CDIAC-162, NDP-P093, Carbon Dioxide Information Analysis Center, Oak Ridge National Laboratory, US Department of Energy, https://doi.org/10.3334/CDIAC/OTG.NDP093_GLODAPv2, 2015.

Kiørboe, T., Møhlenberg, F., and Hamburger, K.: Bioenergetics of the planktonic copepod *Acartia tonsa*: relation between feeding, egg production and respiration, and composition of specific dynamic action, Mar. Ecol. Prog. Ser., 26, 85–97, https://doi.org/10.3354/meps026085, 1985.

Klausmeier, C. A., Litchman, E., Daufresne, T., and Levin, S. A.: Phytoplankton stoichiometry, Ecol. Res., 23, 479–485, https://doi.org/10.1007/s11284-008-0470-8, 2008.

Kriest, I.: Calibration of a simple and a complex model of global marine biogeochemistry, Biogeosciences, 14, 4965–4984, https://doi.org/10.5194/bg-14-4965-2017, 2017.

Kriest, I. and Oschlies, A.: MOPS-1.0: towards a model for the regulation of the global oceanic nitrogen budget by marine biogeochemical processes, Geosci. Model Dev., 8, 2929–2957, https://doi.org/10.5194/gmd-8-2929-2015, 2015.

Krishna, S., Pahlow, M., and Schartau, M.: Comparison of two carbon-nitrogen regulatory models calibrated with mesocosm data, Ecol. Model., 411, 108711, https://doi.org/10.1016/j.ecolmodel.2019.05.016, 2019.

Kvale, K. F., Khatiwala, S., Dietze, H., Kriest, I., and Oschlies, A.: Evaluation of the Transport Matrix Method for simulation of ocean biogeochemical tracers, Geosci. Model Dev., 10, 2425–2445, https://doi.org/10.5194/gmd-10-2425-2017, 2017.

Kwiatkowski, L., Aumont, O., Bopp, L., and Ciais, P.: The Impact of Variable Phytoplankton Stoichiometry on Projections of Primary Production, Food Quality, and Carbon Uptake in the Global Ocean, Global Biogeochem. Cycles, 32, https://doi.org/10.1002/2017gb005799, 2018.

Landolfi, A., Dietze, H., Koeve, W., and Oschlies, A.: Overlooked runaway feedback in the marine nitrogen cycle: the vicious cycle, Biogeosciences, 10, 1351–1363, https://doi.org/10.5194/bg-10-1351-2013, 2013.

Landolfi, A., Kaehler, P., Koeve, W., and Oschlies, A.: Global Marine N_2 Fixation Estimates: From Observations to Models, Front. Microbiol., 9, 2112, https://doi.org/10.3389/fmicb.2018.02112, 2018.

Laufkötter, C., Vogt, M., Gruber, N., Aita-Noguchi, M., Aumont, O., Bopp, L., Buitenhuis, E., Doney, S. C., Dunne, J., Hashioka, T., Hauck, J., Hirata, T., John, J., Quéré, C. L., Lima, I. D., Nakano, H., Seferian, R., Totterdell, I., Vichi, M., and Völker, C.: Drivers and uncertainties of future global marine primary production in marine ecosystem models, Biogeosciences, 12, 6955–6984, https://doi.org/10.5194/bg-12-6955-2015, 2015.

Lauvset, S. K., Key, R. M., Olsen, A., van Heuven, S., Velo, A., Lin, X., Schirnick, C., Kozyr, A., Tanhua, T., Hoppema, M., Jutterström, S., Steinfeldt, R., Jeansson, E., Ishii, M., Pérez, F. F., Suzuki, T., and Watelet, S.: A new global interior ocean mapped climatology: the $1^\circ \times 1^\circ$ GLODAP version 2, Earth Syst. Sci. Data, 8, 325–340, https://doi.org/10.5194/essd-8-325-2016, 2016.

Laws, E. A., Falkowski, P. G., Walker O. Smith, J., Ducklow, H., and McCarthy, J. J.: Temperature effects on export production in the open ocean, Global Biogeochem. Cycles, 14, 1231–1246, https://doi.org/10.1029/1999GB001229, 2000.

Lessard, E. J. and Murrell, M. C.: Microzooplankton herbivory and phytoplankton growth in the northwestern Sargasso Sea, Aquat. Microb. Ecol., 16, 173–188, https://doi.org/10.3354/ame016173, 1998.

Letscher, R. T. and Moore, J. K.: Preferential remineralization of dissolved organic phosphorus and non-Redfield DOM dynamics in the global ocean: Impacts on marine productivity, nitrogen fixation, and carbon export, Global Biogeochem. Cycles, 29, 2014GB004904, https://doi.org/10.1002/2014GB004904, 2015.

Li, Z. and Cassar, N.: Satellite estimates of net community production based on O_2/Ar observations and comparison to other estimates, Global Biogeochem. Cycles, 30, 2015GB005314, https://doi.org/10.1002/2015GB005314, 2016.

Löptien, U. and Dietze, H.: Effects of parameter indeterminacy in pelagic biogeochemical modules of Earth System Models on projections into a warming future: the scale of the problem, Global Biogeochem. Cycles, 31, https://doi.org/10.1002/2017GB005690, 2017.

Löscher, C. R., Mohr, W., Bange, H. W., and Canfield, D. E.: No nitrogen fixation in the Bay of Bengal?, Biogeosciences Discuss., 2019, 1–25, https://doi.org/10.5194/bg-2019-347, 2019.

Luo, Y.-W., Doney, S. C., Anderson, L. A., Benavides, M., Berman-Frank, I., Bode, A., Bonnet, S., Boström, K. H., Böttjer, D., Capone, D. G., Carpenter, E. J., Chen, Y. L., Church, M. J., Dore, J. E., Falcón, L. I., Fernández, A., Foster, R. A., Furuya, K., Gómez, F., Gundersen, K., Hynes, A. M., Karl, D. M., Kitajima, S., Langlois, R. J., LaRoche, J., Letelier, R. M., Marañón, E., McGillicuddy Jr., D. J., Moisander, P. H., Moore, C. M., Mouriño-Carballido, B., Mulholland, M. R., Needoba, J. A., Orcutt, K. M., Poulton, A. J., Rahav, E., Raimbault, P., Rees, A. P., Riemann, L., Shiozaki, T., Subramaniam, A., Tyrrell, T., Turk-Kubo, K. A., Varela, M., Villareal, T. A., Webb, E. A., White, A. E., Wu, J., and Zehr, J. P.: Database of diazotrophs in global ocean: abundance, biomass and nitrogen fixation rates, Earth Syst. Sci. Data, 4, 47–73, https://doi.org/10.5194/essd-4-47-2012, 2012.

Martiny, A. C., Vrugt, J. A., and Lomas, M. W.: Concentrations and ratios of particulate organic carbon, nitrogen, and phosphorus in the global ocean, Sci. Data, 1, 140048, https://doi.org/10.1038/sdata.2014.48, 2014.

Matrai, P. A. and Keller, M. D.: Total organic sulfur and dimethylsulfoniopropionate in marine phytoplankton: intracellular variations, Mar. Biol., 119, 61–68, https://doi.org/10.1007/BF00350107, 1994.

Millero, F. J., Fiol, S., Campbell, D. M., and Parilla, G.: Carbon dioxide, hydrographic, and chemical data obtained during the R/V Hespérides cruise in the Atlantic Ocean (WOCE section A5, July 14 – August 15, 1992), Carbon Dioxide Information Analysis Center, Oak Ridge National Laboratory, U.S. Department of Energy, https://doi.org/10.3334/CDIAC/otg.ndp074, 2000.

Mills, M. M., Brown, Z. W., Lowry, K. E., van Dijken, G. L., Becker, S., Pal, S., Benitez-Nelson, C. R., Downer, M. M., Strong, A. L., Swift, J. H., Pickart, R. S., and Arrigo, K. R.: Impacts of low phytoplankton NO_3^-:PO_4^{3-} utilization ratios over the Chukchi Shelf, Arctic Ocean, Deep-Sea Res. II, 118, 105–121, https://doi.org/10.1016/j.dsr2.2015.02.007, 2015.

Monteiro, F. M. and Follows, M. J.: On nitrogen fixation and preferential remineralization of phosphorus, Geophys. Res. Lett., 39, L06607, https://doi.org/10.1029/2012GL050897, 2012.

Monteiro, F. M., Dutkiewicz, S., and Follows, M. J.: Biogeographical controls on the marine nitrogen fixers, Global Biogeochem. Cycles, 25, GB2003, https://doi.org/10.1029/2010GB003902, 2011.

Mulholland, M. R., Bernhardt, P. W., Widner, B. N., Selden, C. R., Chappell, P. D., Clayton, S., Mannino, A., and Hyde, K.: High Rates of N_2 Fixation in Temperate, Western North Atlantic Coastal Waters Expand the Realm of Marine Diazotrophy, Global Biogeochem. Cycles, 33, https://doi.org/10.1029/2018gb006130, 2019.

Nickelsen, L., Keller, D. P., and Oschlies, A.: A dynamic marine iron cycle module coupled to the University of Victoria Earth System Model: the Kiel Marine Biogeochemical Model 2 for UVic 2.9, Geosci. Model Dev., 8, 1357–1381, https://doi.org/10.5194/gmd-8-1357-2015, 2015.

Niemeyer, D., Kemena, T. P., Meissner, K. J., and Oschlies, A.: A model study of warming-induced phosphorus–oxygen feedbacks in open-ocean oxygen minimum zones on millennial timescales, Earth Syst. Dynam., 8, 357–367, https://doi.org/10.5194/esd-8-357-2017, 2017.

Norberg, J.: Biodiversity and ecosystem functioning: A complex adaptive systems approach, Limnol. Oceanogr., 49, 1269–1277, https://doi.org/10.4319/lo.2004.49.4_part_2.1269, 2004.

O'Malley, R.: Ocean Productivity, http://www.science.oregonstate.edu/ocean.productivity/index.php, 2017.

Oschlies, A., Koeve, W., and Garçon, V.: An Eddy-Permitting Coupled Physical-Biological Model of the North Atlantic 2. Ecosystem Dynamics and Comparison With Satellite and JGOFS Local Studies Data, Global Biogeochem. Cycles, 14, 499–523, 2000.

Oschlies, A., Duteil, O., Getzlaff, J., Koeve, W., Landolfi, A., and Schmidtko, S.: Patterns of deoxygenation: sensitivity to natural and anthropogenic drivers, Phil. Trans. R. Soc. Lond. A, 375, 20160325, https://doi.org/10.1098/rsta.2016.0325, 2017.

Pahlow, M.: Linking chlorophyll-nutrient dynamics to the Redfield N:C ratio with a model of optimal phytoplankton growth, Mar. Ecol. Prog. Ser., 287, 33–43, https://doi.org/10.3354/meps287033, 2005.

Pahlow, M. and Prowe, A. E. F.: Model of optimal current feeding in zooplankton, Mar. Ecol. Prog. Ser., 403, 129–144, https://doi.org/10.3354/meps08466, 2010.

Pahlow, M., Dietze, H., and Oschlies, A.: Optimality-based model of phytoplankton growth and diazotrophy, Mar. Ecol. Prog. Ser., 489, 1–16, https://doi.org/10.3354/meps10449, 2013.

Park, J.-Y., Stock, C. A., Dunne, J. P., Yang, X., and Rosati, A.: Seasonal to multiannual marine ecosystem prediction with a global Earth system model, Science, 365, 284–288, https://doi.org/10.1126/science.aav6634, 2019.

Prowe, A. E. F., Visser, A. W., Andersen, K. H., Chiba, S., and Kiørboe, T.: Biogeography of zooplankton feeding strategy, Limnol. Oceanogr., 64, 661–678, https://doi.org/10.1002/lno.11067, 2018.

Smith, S. L., Yamanaka, Y., Pahlow, M., and Oschlies, A.: Optimal uptake kinetics: physiological acclimation explains the pattern of nitrate uptake by phytoplankton in the ocean, Mar. Ecol. Prog. Ser., 384, 1–12, 2009.

Smith, S. L., Pahlow, M., Merico, A., and Wirtz, K. W.: Optimality-based modeling of planktonic organisms, Limnol. Oceanogr., 56, 2080–2094, https://doi.org/10.4319/lo.2011.56.6.2080, 2011.

Smith, S. L., Pahlow, M., Merico, A., Acevedo-Trejos, E., Sasai, Y., Yoshikawa, C., Sasaoka, K., Fujiki, T., Matsumoto, K., and Honda, M. C.: Flexible phytoplankton functional type (FlexPFT) model: size-scaling of traits and optimal growth, J. Plankton Res., 38, 977–992, https://doi.org/10.1093/plankt/fbv038, 2016.

Strom, S. L.: Growth and grazing rates of the herbivorous dinoflagellate *Gymnodinium* sp. from the open subarctic Pacific Ocean, Mar. Ecol. Prog. Ser., 78, 103–113, https://doi.org/10.3354/meps078103, 1991.

Strom, S. L., Miller, C. B., and Frost, B. W.: What sets the lower limit to phytoplankton stocks in high-nitrate, low-chlorophyll regions of the open ocean?, Mar. Ecol. Prog. Ser., 193, 19–31, https://doi.org/10.3354/meps193019, 2000.

Su, B., Pahlow, M., and Prowe, F.: The role of microzooplankton trophic interactions in modelling a suite of mesocosm ecosystems, Ecol. Model., 368, 169–179, https://doi.org/10.1016/j.ecolmodel.2017.11.013, 2018.

Talmy, D., Blackford, J., Hardman-Mountford, N. J., Polimene, L., Follows, M. J., and Geider, R. J.: Flexible C : N ratio enhances metabolism of large phytoplankton when resource supply is intermittent, Biogeosciences, 11, 4881–4895, https://doi.org/10.5194/bg-11-4881-2014, 2014.

Talmy, D., Martiny, A. C., Hill, C., Hickman, A. E., and Follows, M. J.: Microzooplankton regulation of surface ocean POC:PON ratios, Global Biogeochem. Cycles, 30, 311–332, https://doi.org/10.1002/2015GB005273, 2016.

Taucher, J. and Oschlies, A.: Can we predict the direction of marine primary production change under global warming?, Geophys. Res. Lett., 38, L02603, https://doi.org/10.1029/2010GL045934, 2011.

Vichi, M., Pinardi, N., and Masina, S.: A generalized model of pelagic biogeochemistry.for the global ocean ecosystem. Part I: Theory, J. Mar. Syst., 64, 89–109, https://doi.org/10.1016/j.jmarsys.2006.03.006, 2007.

Wang, W.-L., Moore, J. K., Martiny, A. C., and Primeau, F. W.: Convergent estimates of marine nitrogen fixation, Nature, 566, 205–211, https://doi.org/10.1038/s41586-019-0911-2, 2019.

Weaver, A., Eby, M., Wiebe, E., Bitz, C., Duffy, P., Ewen, T., Fanning, A., Holland, M., MacFadyen, A., Matthews, H., Meissner, K., Saenko, O., Schmittner, A., Wang, H., and Yoshimori, M.: The UVic Earth System Climate Model: Model description, climatology, and applications to past, present and future climates, Atmos.-Ocean, 39, 361–428, https://doi.org/10.1080/07055900.2001.9649686, 2001.

Westberry, T., Behrenfeld, M. J., Siegel, D. A., and Boss, E.: Carbon-based primary productivity modeling with vertically resolved photoacclimation, Global Biogeochem. Cycles, 22, GB2024, https://doi.org/10.1029/2007GB003078, 2008.